GAS PHASE FLOW PATTERNS IN A BUBBLING COLUMN

A STUDY OF THE FLOW PATTERNS IN THE GAS PHASE OF A BUBBLING COLUMN

By

PETER MURRAY HILL, B.A.

A Thesis

Submitted to the Faculty of Graduate Studies

in Partial Fulfilment of the Requirements

for the Degree

Master of Engineering

McMaster University

December 1964

MASTER OF ENGINEERING (1964) McMaster University
(Chemical Engineering) Hamilton, Ontario.

TITLE: A Study of the Flow Patterns in the Gas Phase of a Bubbling Column.

AUTHOR: Peter Murray Hill, B.A. (University of Cambridge)

SUPERVISOR: Professor C. M. Crowe

NUMBER OF PAGES: viii, 138

SCOPE AND CONTENTS: The gas phase flow patterns in a bubbling column were investigated, using tracer methods to establish the residence time distribution. An analogue computer obtained the moments of this distribution directly. The air flow rate and column height were varied.

The results showed that as the air flow rate increased, although the voidage increased, the mean residence time decreased. Thus an increasing proportion of the gas phase behaved as a stagnant volume. The results are correlated in terms of a mixed region model.

Other work showed that an increase of liquid viscosity, or the inhibition of coalescence, affected only the stagnant volume. The rate of coalescence was investigated and an estimate of its magnitude was obtained.

Acknowledgments

The author is indebted to his supervisor, Dr. C. M. Crowe, for his help and guidance throughout this work. Financial assistance in the form of a scholarship from McMaster University is gratefully acknowledged.

He also wishes to express his thanks to the staff and the graduates of the Chemical Engineering Department for their many suggestions and advice, and to the technical staff for their assistance.

TABLE OF CONTENTS

(Note: For clarity, the main sections of the work are referred to in the text as parts, e.g. part 2; the main sections of these parts are referred to as sections, e.g. section 2.2.; the final divisions are referred to as subsections, e.g. subsection 2.2.2.)

LIST OF DIAGRAMS

LIST OF TABLES

1. Introduction

For the accurate design of process vessels, a knowledge of the flow patterns that exist within them is a necessity. In many applications it is possible to assume that the flow within the vessel behaves in one of two ideal ways, namely plug flow or completely mixed flow. This latter is also commonly referred to as backmixed flow, or continuous flow stirred tank reactor (CFSTR) flow. In this paper it will be referred to as CFSTR flow.

In an ideal plug flow reactor, it is assumed that the fluid passes through the vessel in a series of discrete "plugs", such that no mixing occurs between portions of fluid that enter the reactor at different times.

In an ideal CFSTR it is assumed that the contents of the reactor are at all times completely mixed and homogeneous.

These two ideal cases are the limiting cases - the one limit being no mixing, and the other limit being complete and instantaneous mixing - and actual practical vessels will have flow patterns that lie somewhere between them. The analysis of the performance of either of these ideal cases, whether the application be to heat transfer, mass transfer, or chemical reaction, is relatively simple and well developed, and for this reason real vessels are often designed on the basis of one of these ideal cases.

This type of design will be satisfactory only if the actual flow deviates slightly from ideality, but otherwise, for more severe deviations, unsatisfactory performance will result. It should also be noted that it is often possible to approach closely one of the types of ideal flow by suitable design.

It will therefore be apparent that the investigation of flow patterns within process vessels is an important preliminary to their good design.

In the present work, the system under study was the gas phase, held up as bubbles in a tank of liquid, and produced by bubbling the gas into the liquid through a multi-orifice plate in the floor of the tank. No external means of agitation was used and the mixing within the gas phase came only from the motion of the bubbles within the liquid and from their coalescence and break-up.

Very few two-phase systems have been studied to determine the type of mixing within one phase, and the only work comparable with the present work is that by Westerterp et al. (1) who determined the residence time distribution for the gas phase in a stirred tank, and by Moo-Young and Calderbank (3) who investigated the rise and coalescence of bubbles in a deep pool of liquid. (Details of this work, together with mention of other work in this field are given in appendix I).

In the present approach to this problem, the main

emphasis has been on tracer work to establish residence time distributions. This has been supported by photographic and other work to obtain the best overall picture of the system.

Accordingly the next (second) part of this paper is concerned with the tracer work and the results thereby obtained, together with other observations on the basic flow in the system. The third part is concerned with other work and includes the effects of other parameters on the system as determined by tracer studies, as well as investigations of the mechanism by which bubbles leave the system and the frequency of coalescence between bubbles within the system. The fourth and final part summarises the whole work and contains the conclusions that have been drawn from it.

2. Tracer Work

2.1 Use of Tracer Methods to Determine Residence Time Distributions

The flow pattern in a non-ideal system is best described in terms of various residence time distributions. These were originally proposed by Danckwerts (2) and the two most important ones are defined as follows:-

The internal age distribution I(t) of a vessel is defined such that I(t).dt is the fraction of fluid in the vessel with ages between t and t + dt. In this context the age of a discrete piece of fluid is the time that has elapsed since that piece of fluid entered the vessel.

The exit age distribution E(t) of a vessel is similarly defined such that E(t).dt is the fraction of fluid in the exit stream with ages between t and t + dt.

These distributions are frequently expressed in terms of a reduced time scale θ, which is measured in terms of the mean residence time. The mean residence time (τ) is defined as: $\frac{\text{volume in vessel actually used by flow}}{\text{volume flow rate of fluid through the vessel}}$

i.e. $\tau = \frac{V}{Q}$ and hence $\theta = \frac{t}{\tau}$ and is dimensionless. Examples of these distributions are given in figure 1.

In this study, since only the gas phase of the two-phase system is being studied, the volume of the vessel actually used by the flow is that volume of the gas phase (i.e. of the bubbles) used by the air flow.

Residence time distributions are usually determined by a tracer method, which is basically a study of the change in the output signal of the system with respect to time in response to a known input signal. In practice, the input signal is obtained by introducing tracer into the input stream as it enters the vessel, and then the subsequent tracer concentration changes which occur within the vessel, or in its exit stream, are observed.

The tracer input signals most commonly used are either a step change in the tracer concentration of the inlet stream or a short pulse of tracer into the inlet stream or into the vessel itself. Other inputs can be used such as a sinusoidal variation of tracer with time, or even a random variation of tracer with time, but in general these are only used when the frequency response of the system is being studied.

If a pulse (or delta function) input is used, the resulting change of outlet tracer concentration plotted against time is known as a C curve. It is quite easily shown that a normalised C curve (i.e. one that is plotted such that the total area under the curve is unity) is the same as the E residence time distribution function. The theoretical delta function $\delta(t)$ (i.e. the ideal pulse) is defined such that $\delta(t) = 0$ for $t \neq 0$, and $\delta(t) \to \infty$ at $t = 0$, with $\int_{-\infty}^{\infty} \delta(t)\, dt = 1$. It is thus a peak, at $t = 0$, of infinite height and infinitesimal width. This ideal pulse cannot of

course be realised in practice, but a sufficiently close approximation may be obtained.

If a step change in tracer concentration is used as the input signal, the resulting outlet tracer concentration curve is known as an F curve. It can be shown (2) that a normalised F curve is related to the I residence time distribution function by $F + I = 1$.

To illustrate these residence time distributions and curves, they are shown plotted for the two ideal types of flow system in figure 1.

In the present work a pulse was used as the tracer input signal for the following reasons:

(a) It gives directly the exit (E) residence time distribution curve and therefore the various moments of this curve are more easily obtained. This is important because the moments of the curve are the parameters most used in describing the residence time distribution.

(b) If the F curve is required it can be obtained by integration of the C curve since $F(t) = \int_0^t C(t)dt$ whereas the reverse procedure of obtaining the C curve by differentiation of the F curve would be bound to lead to large errors.

(c) In the present case, it was comparatively easy to generate a fairly accurate delta pulse by injecting a short burst of tracer gas bubbles directly into the tank.

The following section gives a brief description of the equipment used in the tracer work, and the method of its

FIGURE 1 DISTRIBUTION CURVES FOR IDEAL REACTORS

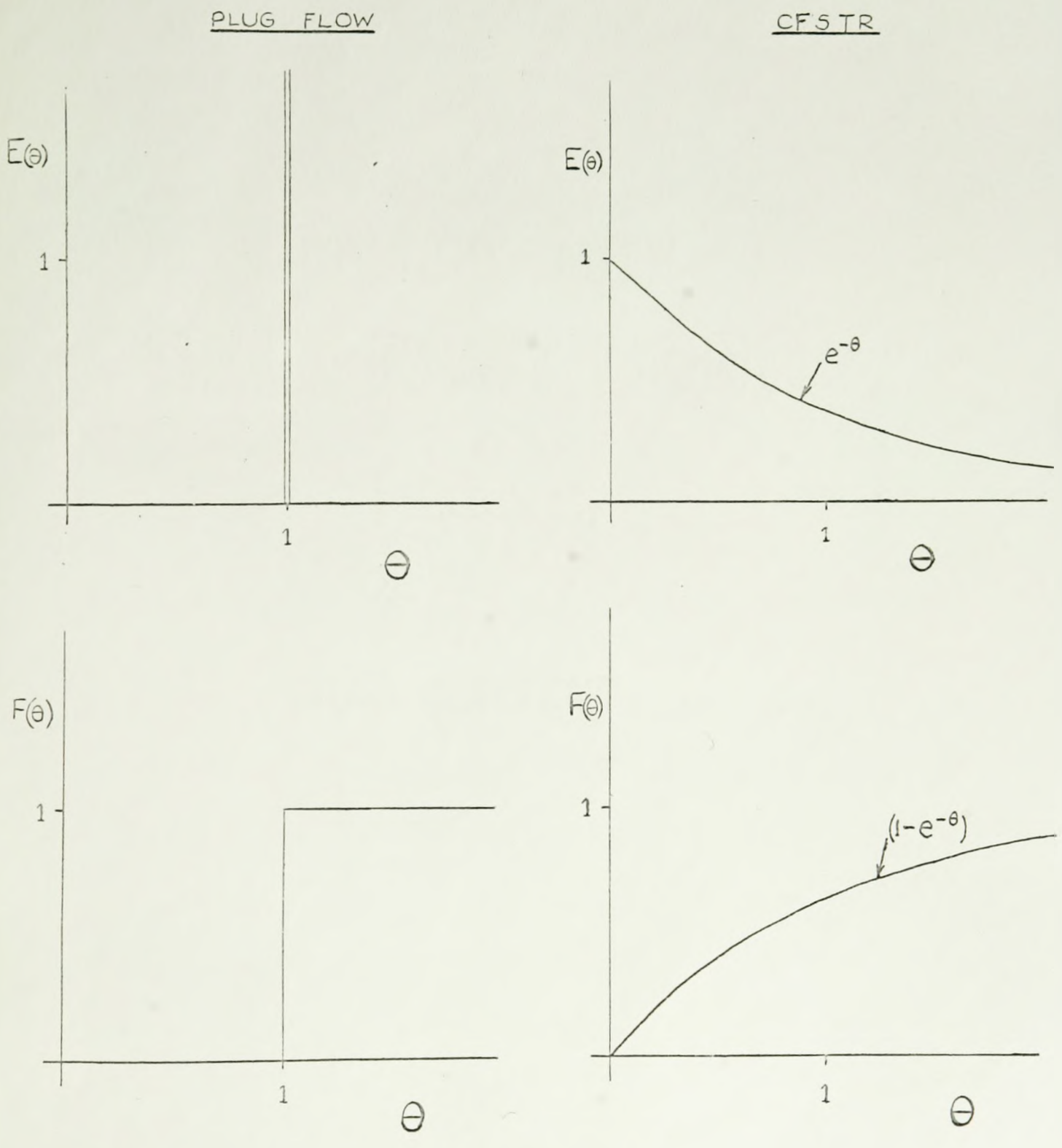

operation. Further details of the experimental work are given in Appendix II.

The results of this tracer work are given in section 2.3 which also includes a qualitative description of the system and a quantitative description in terms of the bubble size and voidage fraction. The final section in this part of the work deals with the models used to explain and interpret the results.

2.2. Experimental Work

This section is divided into two subsections dealing with the physical description of the equipment, and its method of operation, respectively.

2.2.1. Description of Equipment

The experimental tank was designed so that it would approximate the behaviour of an actual plant, and to ensure this, the dimensions were kept fairly large. For the same reason, the orifice sizes and gas chamber volume were designed to give the appropriate bubble regime. (See the end of Appendix I).

Figure 2 shows the tank in cross-section. The cylindrical wall was of lucite tube, of nominal diameter 1 foot, and could be varied in height from six inches to three feet, - six inches in six inch steps, by combining different sections. At the bottom of the liquid section was an orifice plate of duralumin, 3/8 inch thick, containing 5/64 inch diameter holes spaced on a 1 inch triangular grid, centrally symmetrical. Four of these holes were replaced by fittings and sealed off from the lower chamber, allowing column drainage or sample injection. The total number of orifice holes in the plate was 117.

Below the orifice plate was a chamber to allow the equal distribution of air to the orifice holes. This had a depth of 2 inches and an internal volume of 0.109 cu. ft.

FIGURE 2 VIEW OF TANK IN CROSS-SECTION

SCALE : APPROX. 1/4 FULL SIZE

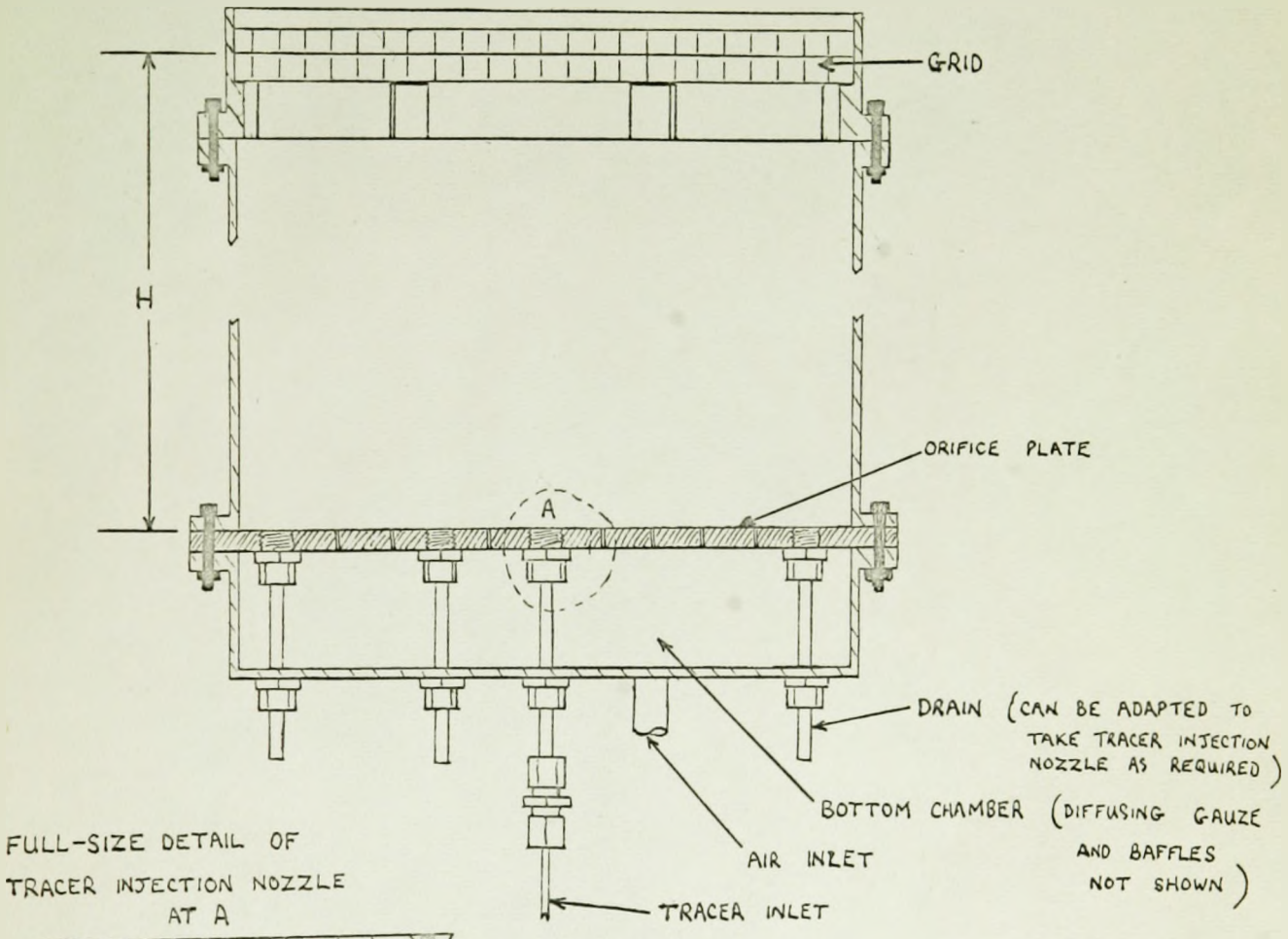

FULL-SIZE DETAIL OF TRACER INJECTION NOZZLE AT A

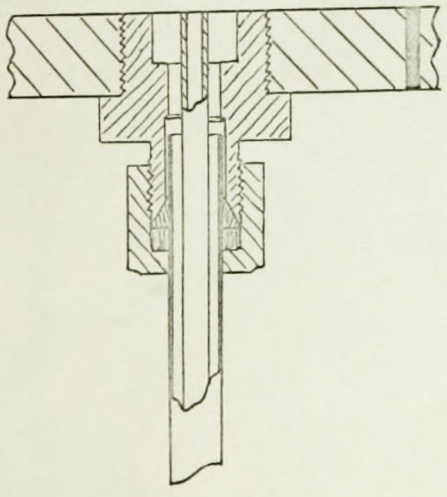

FIGURE 3

DIAGRAM OF COMPLETE EQUIPMENT

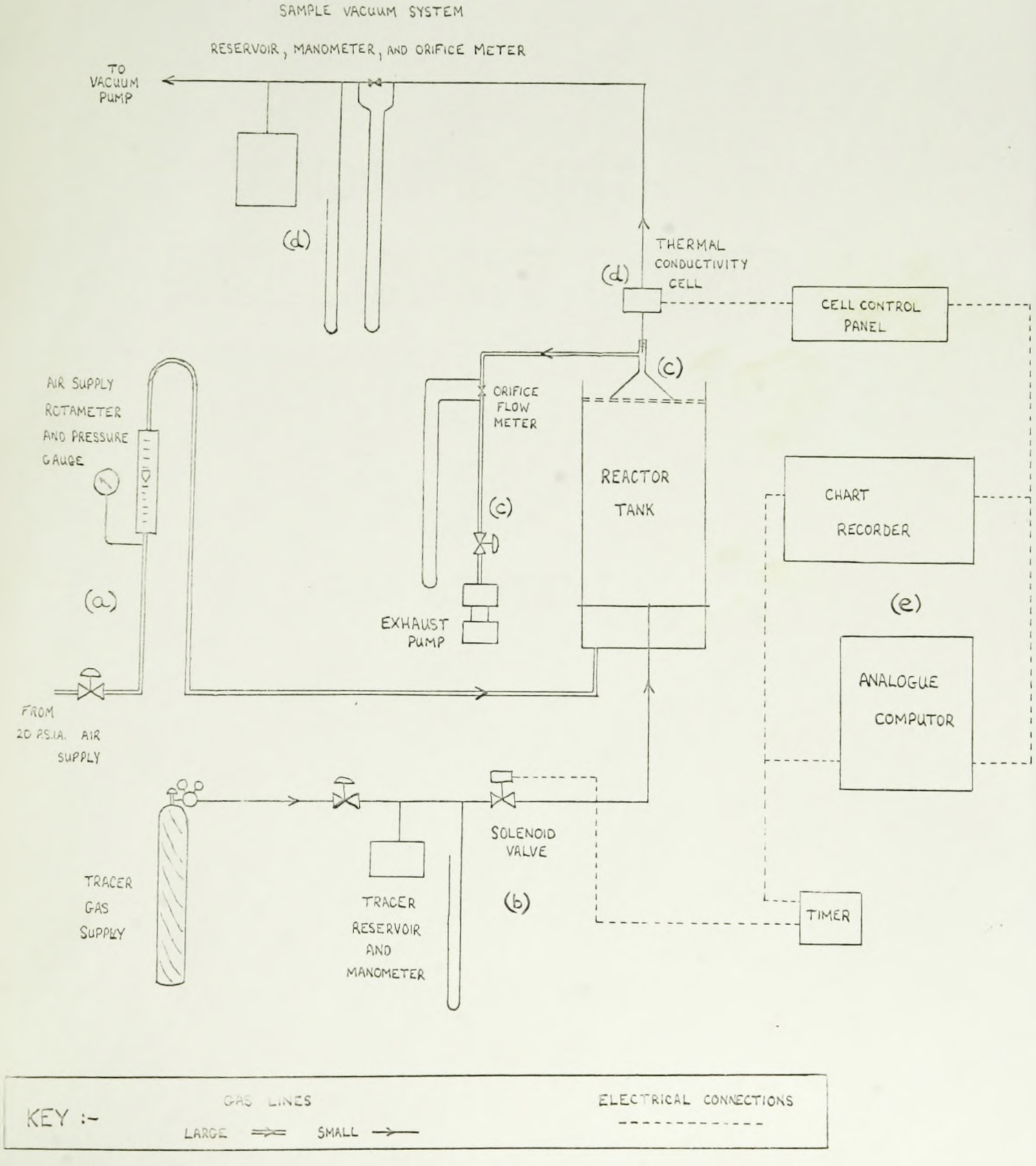

The air entered this chamber through a 5/8 inch tube and was diffused through wire mesh and baffles.

Figure 3 shows the ancillary equipment which may be conveniently split into the following parts:

(a) The air supply was taken from the laboratory 20 p.s.i.g. line via a filter. Its flow was controlled by a valve and metered by a rotameter and pressure gauge before being fed to the column.

(b) The tracer injection system consisted of a reservoir to which tracer gas could be admitted to the desired pressure as measured on a mercury manometer. From this reservoir a small gas line ran through the lower chamber of the column and terminated in a nozzle flush with the surface of the orifice plate. In this line, which was normally kept full of tracer gas, there was positioned a solenoid valve which controlled the injection of tracer gas.

The tracer gas was injected directly into the tank to ensure that the signal input to the system was a true pulse. Had the tracer gas pulse been injected into the air stream or into the lower gas chamber, diffusion and mixing of the tracer with the air in the chamber would have occurred, with the result that the input to the system itself would have no longer been a pulse. Orifices in different positions in the floor of the tank were used, without noticeable effects.

The tracer gas used for these experiments was helium because it was easily detected even at low concentrations in air by the type of detector used. A further advantage was its

virtual insolubility in water.

(c) The sampling system at the top of the column was the result of a compromise reached between the basic requirements of such a device. These were:

(i) That it should obtain a representative sample of the gas flow emerging from the whole top surface of the bubbling liquid.

(ii) That it should affect the tracer concentration change with time (i.e. the response of the system) as little as possible. Ideally the sampling system should not affect it at all, but at most a time delay could be tolerated.

(iii) That it should effectively demist the gas.

It will be seen that requirement (ii) is incompatible with (i) and (iii) which require the system to have a certain mixing volume with some form of packing, both of which would tend to give non-plug flow and subsequent distortion of the response.

The actual method used is shown in figure 4. Basically it consisted of a shallow-angled inverted cone which rested on a deep wide-mesh grid. The purpose of the grid was two-fold:

(1) it damped out the disturbance at the surface and provided a reference to keep the position of the surface consistent throughout the experimental work. The quantity of water in the tank was adjusted so that the mean position of the surface was always half way up the grid. Experiments were

FIGURE 4 DIAGRAM OF SAMPLING SYSTEM

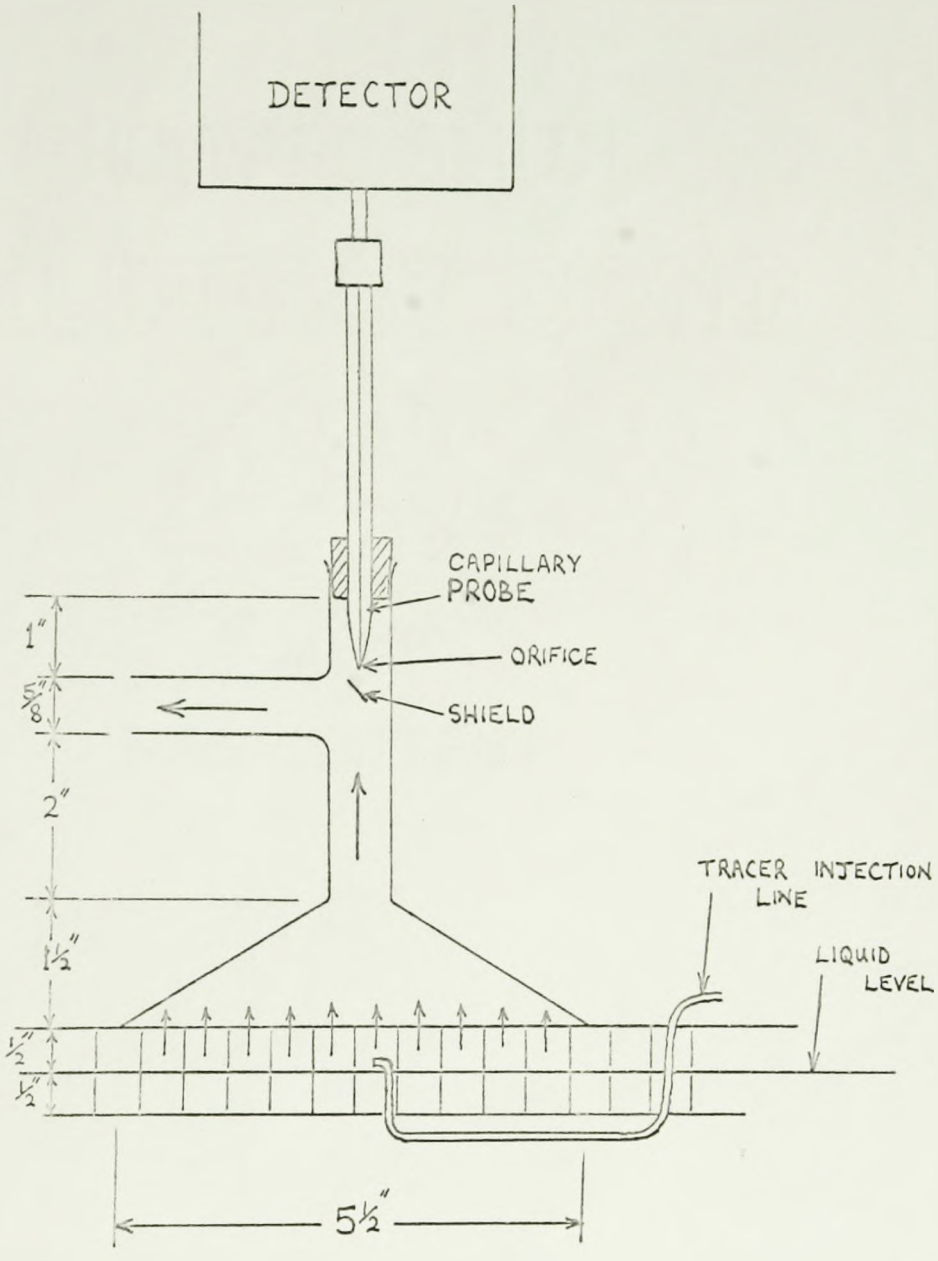

made to see if a smaller wire mesh could be used to damp out more effectively the surface waves, but this was found to affect the bursting of bubbles at the surface in such a way as to give rise to large gas hold-ups directly under the mesh.

(2) it helps to keep the air rising vertically in more uniform plug flow, once above the surface of the liquid.

The cone is shaped to give a high flow to volume ratio and effective mixing across the area sampled. This area, equivalent to the bottom opening of the cone, was one quarter of the area of cross-section of the column. Gas was sucked up through the cone and via a side arm to an orifice meter and thence to the exhaust pump. The gas flow was regulated to one quarter the total gas flow so that the superficial velocity of the gas at the base of the cone was equal to that of the gas rising in the column and hence at the base of the cone no distortion of gas streamlines should occur. The sampling probe was situated just above the side arm, out of the direct gas stream and protected from spray by a small shield. A more conventional method of demisting the gas by placing packing in the neck of the cone was only partially successful in that it worked until the packing flooded, at which point the packing became a secondary source of spray directly under the probe.

The rest of the equipment shown on Figure 3 is as follows:

(d) The detection and measurement of tracer in the

sample was accomplished by means of a hot-wire thermal conductivity bridge, operating with a reduced gas pressure of 1 p.s.i.a. The sample stream was sucked in through a capillary probe, which at its tip had an orifice giving the correct sample flow for the pressure drop across it. The stream then passed through the detection cell to an orifice meter to check the flow rate. A reservoir connected to a vacuum pump, and a vacuum manometer made up the rest of this system.

The detection cell was operated under a partial vacuum in order to attenuate, at the orifice, pressure waves originating from the bursting bubbles which otherwise were found to introduce a large amount of noise into the detector output signal.

A circuit and further details of the thermal conductivity bridge and its associated operating panel are shown in appendix II.

(e) The rest of the equipment comprised the recording and control equipment. A visual record of the response signal was displayed on a chart recorder and simultaneously an analogue computer computed and stored certain functions of the signal. (For part of the experiments a Honeywell Visicorder oscillograph was used to display both the signal and some of the computer outputs).

An electronic timer was used to control injection of the tracer and also to provide a time reference for the recorder

and the analogue computer.

Further details of the computer circuit, and typical operating conditions are given in appendix II.

2.2.2. Method of operation

Brief operating details are given below; for typical operating conditions and a set of experimental results see Appendix II, and Appendix III (f), respectively.

(a) Initially the air flow was set at the required value and the level of the bubbling liquid in the tank was adjusted so that the surface was half way up the grid on which the sampling cone rested. If the equipment had just been switched on, time had to be allowed for the hot-wire detector to come to equilibrium as indicated by absence of drift in the trace on the recorder. When this was so, the apparatus was then ready for a set of experimental runs.

(b) The sequence of operations for an experimental run was as follows:

(i) The tracer reservoir was filled to the correct pressure.

(ii) The electrical balance of the thermal conductivity bridge was checked and adjusted if necessary.

(iii) The analogue computer was switched to the initial settings, and set ready to operate.

(iv) The timer was triggered. This automatically injected a pulse by opening the solenoid valve for a set length of time, and also sent electrical signals to the recorder and the computer to indicate the time of injection.

(v) The response signal as traced on the re-

corder was observed and when it appeared that all the tracer had passed through the system, the computer was set to stop further computation and retain the stored values. The position of the cut-off point is further discussed in subsection 2.3.5.

(vi) These stored values were read from the computer and recorded with any other pertinent data.

This cycle of operations was then repeated. The total number of runs per set, depended on the consistency of the readings obtained and was usually in the range of 15-30, under constant operating conditions.

As well as this main set of runs using tracer injection at the bottom of the tank as described previously, another set of runs, either immediately preceding or following the main set, were made under identical conditions except that the tracer pulse was injected through a special nozzle placed within the grid and immediately above the surface of the bubbling liquid. This was to obtain the response under these conditions of the sampling system alone, which was required to correct the results obtained from the main set of runs.

2.3. Discussion of Results

This section contains the results not only of the tracer work, but also of photographic and other work which was performed to get more information about the system.

Accordingly the first subsection is a qualitative description of the motion of the bubbles within the tank, intended to give the reader a clearer understanding of the flow patterns in the system. The next two subsections deal with the mean bubble size and the voidage of the system, respectively.

The final two subsections discuss the results of the tracer work, firstly in terms of the shape of the residence time distribution curve, and secondly in terms of the parameters of the curve and the assumptions and theory behind the derivation of these parameters.

2.3.1. Observed Flow Patterns Within the Tank

At the lower air flow rates the general flow patterns of the bubbles could be seen quite easily with the naked eye, but at the higher air flow rates the motion was too fast and disordered to allow this. Consequently some high speed motion pictures were taken and the flow patterns and velocities determined from the bubble movement observed in "slow motion".

Figure 5 indicates the general flow of bubbles within the tank, which was of a circular pattern. Two factors contributed to this, the most important being the so-called "wall effect". Since the bubbles were not rising in an

FIGURE 5 BUBBLE FLOW REGIONS IN THE TANK

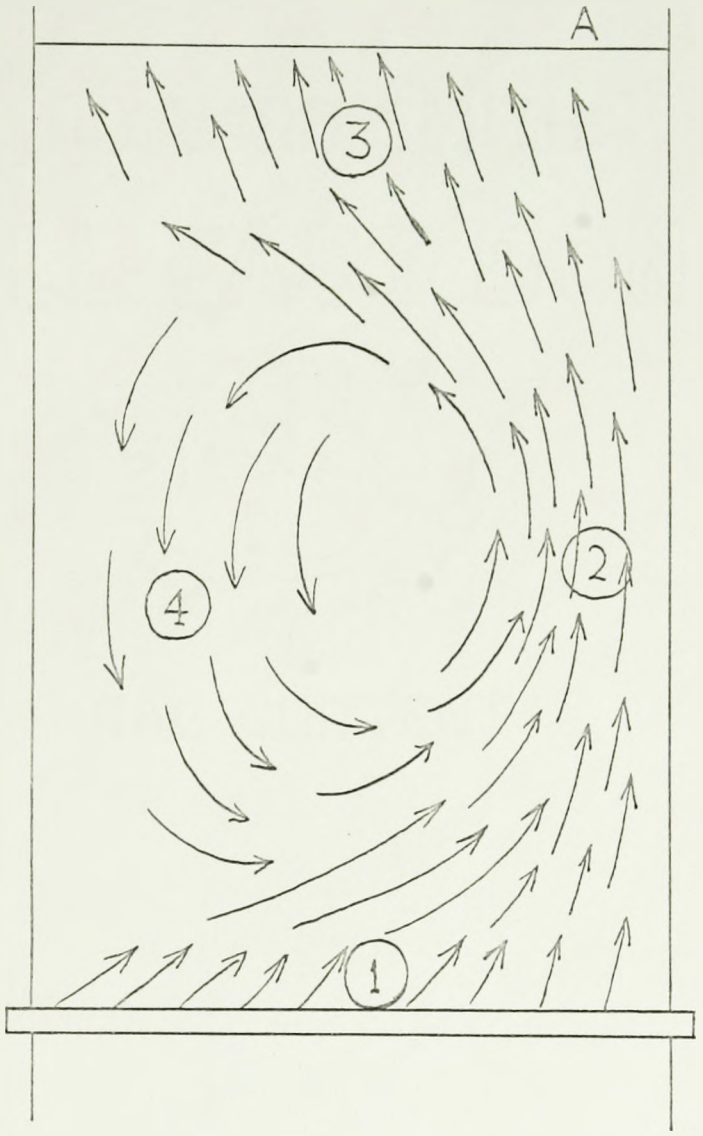

infinite medium, the liquid they carried up with them must find its way down again within the volume of the tank. It is fairly evident that the most stable flow pattern to accomplish this, and to present the least resistance to the rise of the bubbles, is that in which the bubbles rise up one side of the tank and the liquid flows down the other.

The second factor which further stabilised the pattern and maintained the direction of rotation, was that the air flow did not use all the orifices at once. (This point is further amplified in subsection 2.3.2.). This influence may be explained by supposing that initially the gas flow was through orifices distributed slightly asymmetrically, so that slightly more of them are on one side of the tank than on the other. This would tend to start the liquid in circular motion which in turn creates a slight difference in hydrostatic pressure across the plate, the pressure being greater under the descending liquid and less under the ascending liquid and bubbles. Thus, this pressure difference would favour those orifices already bubbling and perpetuate the circular motion in the plane in which it started.

In describing the flow pattern, it is convenient to split up the tank into four regions, numbered as in figure 5.

In region 1, just above the orifice plate, the liquid was moving horizontally across the plate and swept the emerging gas bubbles sideways and upwards through region 2. This liquid flow across the plate was quite rapid at higher gas flow rates and was sufficient under these conditions to break

up the bubble streams into smaller bubble fragments.

In region 2 both the liquid and the gas bubbles had high upward velocities and all the upward gas flow occurred in this region.

In region 3, the liquid had a sideways motion, being effectively "pumped" out of region 2 and continuing its circulatory motion towards region 4. The gas bubbles had a varying diagonal upward velocity, but were moving more slowly than in region 2. The voidage in this region was greater than in the others and the essential feature of this region was of gas bubbles undergoing coalescence and escape from the system.

Region 4 had the lowest proportion of gas bubbles and lower velocities than the other regions. Near the tank wall in this region the liquid was moving downwards carrying gas bubbles with it, and this motion diminished towards the centre of the tank, the quantity of gas bubbles remaining about constant but their velocities changing direction. The liquid in the centre of the tank had a slow overall circular motion but was locally disturbed by the passage of gas bubbles.

The influence of the tank height and gas flow rate on the flow patterns may be seen in figure 6 which was obtained from "slow motion" studies. The flows indicated are only approximate and show the main and more constantly recurring flows, since the actual bubble flows are erratic and transitory.

FIGURE 6 FLOW PATTERNS UNDER VARIOUS CONDITIONS

HT. : 18", AIR FLOW : 0·045 cu.ft/sec

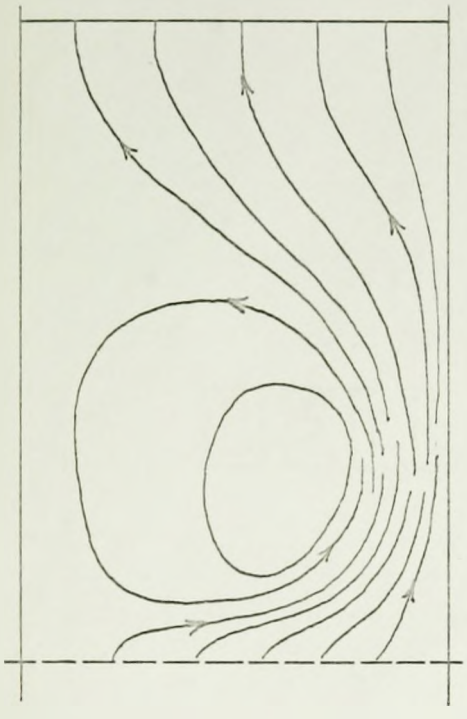

HT. : 12", AIR FLOW : 0·090 cu.ft/sec

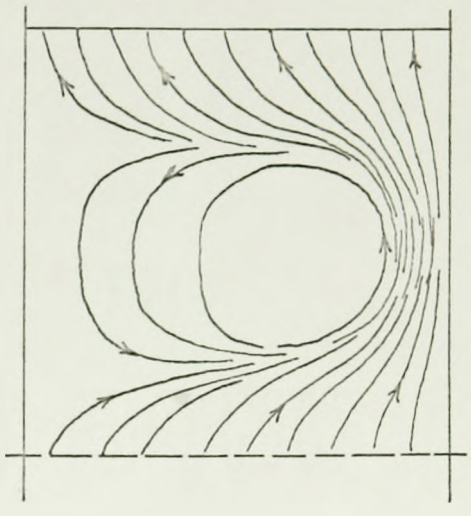

HT. : 18", AIR FLOW : 0·090 cu.ft/sec

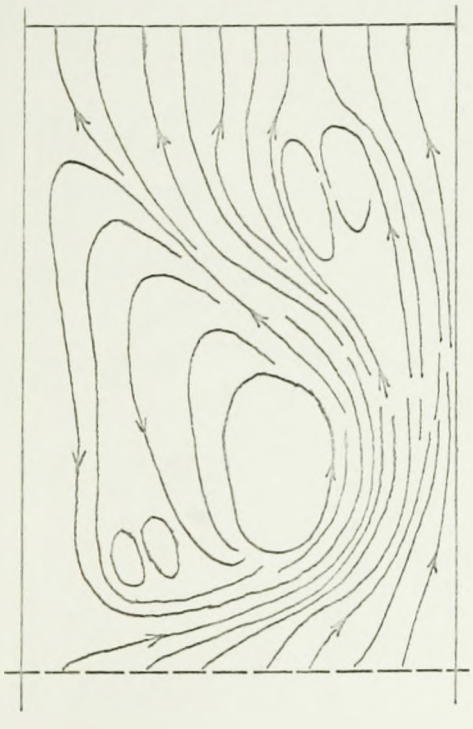

HT. : 24", AIR FLOW : 0.063 cu.ft/sec.

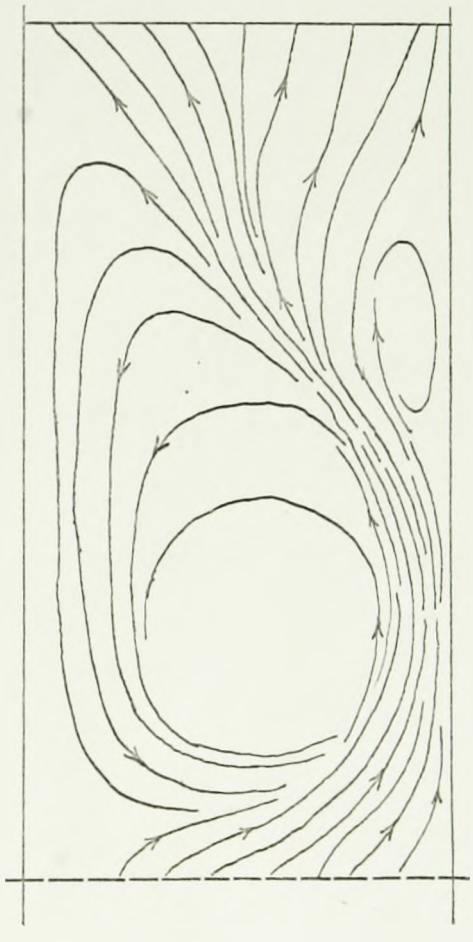

"STREAMLINES" INDICATE APPROXIMATE BUBBLE FLOW ONLY

It will be seen that the simplest patterns occurred at the lowest flow rates and tank heights. This is especially noticeable in the 1 ft. tank which appears to be of just the right dimensions to fit the "roll over" pattern favoured by the bubbles. In taller tanks this initial "roll over" occurred below the top of the tank and gave rise to more complex patterns in the upper part of the tank.

From the "slow motion" pictures it was also possible to get an estimate of the vertical bubble velocities, which were measured at various flow rates and tank heights. The results showed that there was a significant variation of upward bubble velocity, v, (in region 2) with air flow rate, ranging from about 2.4 ft./sec. to 3.4 ft./sec. over the range of air flow rates used in this work. The influence of overall tank height on this velocity was not significant.

Since the rest of the study concerns the times bubbles spend in the system, it was felt that $\frac{1}{v}$ was a more convenient variable than v itself, and hence this was used as the dependent variable in a correlation performed against $\frac{1}{Q}$.

The results, given more fully in appendix III (a), gave as a best fit:

$$\frac{1}{v} = 0.0097 \frac{1}{Q} + 0.207 \text{ (sec./ft.)} \qquad (31.1)$$

The downward bubble velocities were not measured in such detail but were observed to be about 1/4 to 1/3 of the magnitude of the upward velocities.

2.3.2. Bubble formation at the Orifices

In order to estimate the mean bubble size at the orifice plate, measurements were made at different air flow rates of (a) the number of orifices used by the gas flow, and (b) the rate of bubbling, using a stroboscopic lamp. The results for this are shown in table I.

TABLE I

Air flow rate (cu.ft./sec.)	Bubbling frequency per min.	No. of orifices used	Mean flow per orifice (cu.ft./sec.)
0.018	1160, 1170, 1120	20, 22, 22	.00086
0.027	1190, 1090, 1120	31, 32, 33, 32	.00084
0.045	1130, 920, 1000, 1260	50, 44, 49, 54	.00092
0.090	Tank too disturbed to measure accurately	c.100	.00090
Too low to measure	1080, 1010, 1110	3, 4	-

From these figures, allowing for the experimental error as indicated by the repeatability of the readings, two important results emerge:-

(a) that the rate of bubbling is independent of the gas flow rate;

(b) that the flow per orifice is constant whilst the gas flow is below the value required to bring all the available orifices into use.

Result (a) is in close agreement with work by Calderbank (4) on multiple orifices, who showed that the rate of

bubbling was independent of gas flow rate and constant at about 16 - 20 bubbles/sec., over a very wide range of gas flow rates.

Result (b) does not appear to be reported elsewhere in the literature. The constant flow rate per orifice suggests a constant pressure drop across the orifice plate and this could be checked by measuring the pressure of the lower chamber, which should be the sum of the pressure drop across the orifice plate plus the hydrostatic pressure above it. For a constant quantity of water in the tank, the hydrostatic pressure should be constant and hence changes in the lower chamber pressure are caused only by the change in pressure drop across the orifice plate. The chamber pressure was measured by connecting a manometer to the drain outlet and over the range of flow rates for which result (b) holds, it was found to be constant, indicating a constant pressure drop across the orifice plate. It is suggested that this constant pressure is that pressure required to maintain stagnant liquid in an unused orifice.

From the figures obtained it is found that the mean equivalent diameter of the bubbles initially formed is 1.36 cms. This is in exact agreement with Davidson's work (5) on single orifices, since the equivalent volume of the bubbles in this case (1.32 cc.) is within one percent of the value predicted by his correlation of bubble volume versus orifice diameter and gas flow rate (see appendix I).

It will be noted that the above results were obtained in the range of lower air flow rates. Above this range, it was found impossible to make accurate stroboscopic measurements of the bubbling frequency, mainly because the high liquid shear, horizontally across the plate, broke the bubble streams just above the orifice, stripping off a large number of small bubbles, and the subsequent motion was very disordered. At these higher flow rates, once all the orifices have come into use, the flow rate per orifice must obviously increase with increasing total air flow. However, in view of the exact correspondence in bubble size with the single orifice cases, it would seem probable that the bubbling frequency remains almost constant, as reported by Calderbank (4), and that the bubble size increases with flow as given by the empirical relationships of Davidson (5) and Leibson et al. (6) (see appendix I).

2.3.3. Total Voidage in the System

This was calculated from the increase in height of the liquid in the tank when the air flow was turned on at the specified rate. The results, expressed as a voidage fraction are shown as part of table II and also on figure 7. The voidage fraction is defined as the ratio of the volume occupied by the gas to the total volume of liquid and gas, and is usually expressed as a percentage. The exact determination of the level of the surface with the air flow on, was very difficult because of its extremely disturbed nature,

and the decimal part of the percentage given in the results cannot be justified.

As can be seen from figure 7, the voidage fraction appears to be directly proportional to the gas flow rate and a regression analysis on this assumption gave the line:

$$\text{Voidage fraction } (\%) = 104\ Q - .06$$

which is shown on the figure. The influence of column height is not obvious and although the points for the 1 ft. column appear consistently above the line, it seems more likely that the voidage fraction is independent of column height.

Also on figure 7, the results may be compared with those of Verschoor (7), who also obtained a linear relationship over this range of air flow rates. The displacement between the two lines can be attributed to a difference in mean bubble size, since in Verschoor's case a sintered glass disc was used as a gas distributor and a much smaller mean bubble size obtained. Also his column was of smaller diameter and in this case wall effects would have a greater viscous effect, slowing down the system velocities and hence giving greater voidage.

2.3.4. Shape of Residence Time Distribution Curves

A smoothed experimental curve is shown in Figure 8. In practice, noise in the system, believed to be mainly due to fluctuations in water content of the air leaving the tank, produces a far less smooth curve with many small discontinuities which are especially noticeable in the tail of the curve

FIGURE 7 VOIDAGE FRACTION VERSUS GAS FLOW RATE FOR VARIOUS TANK HEIGHTS

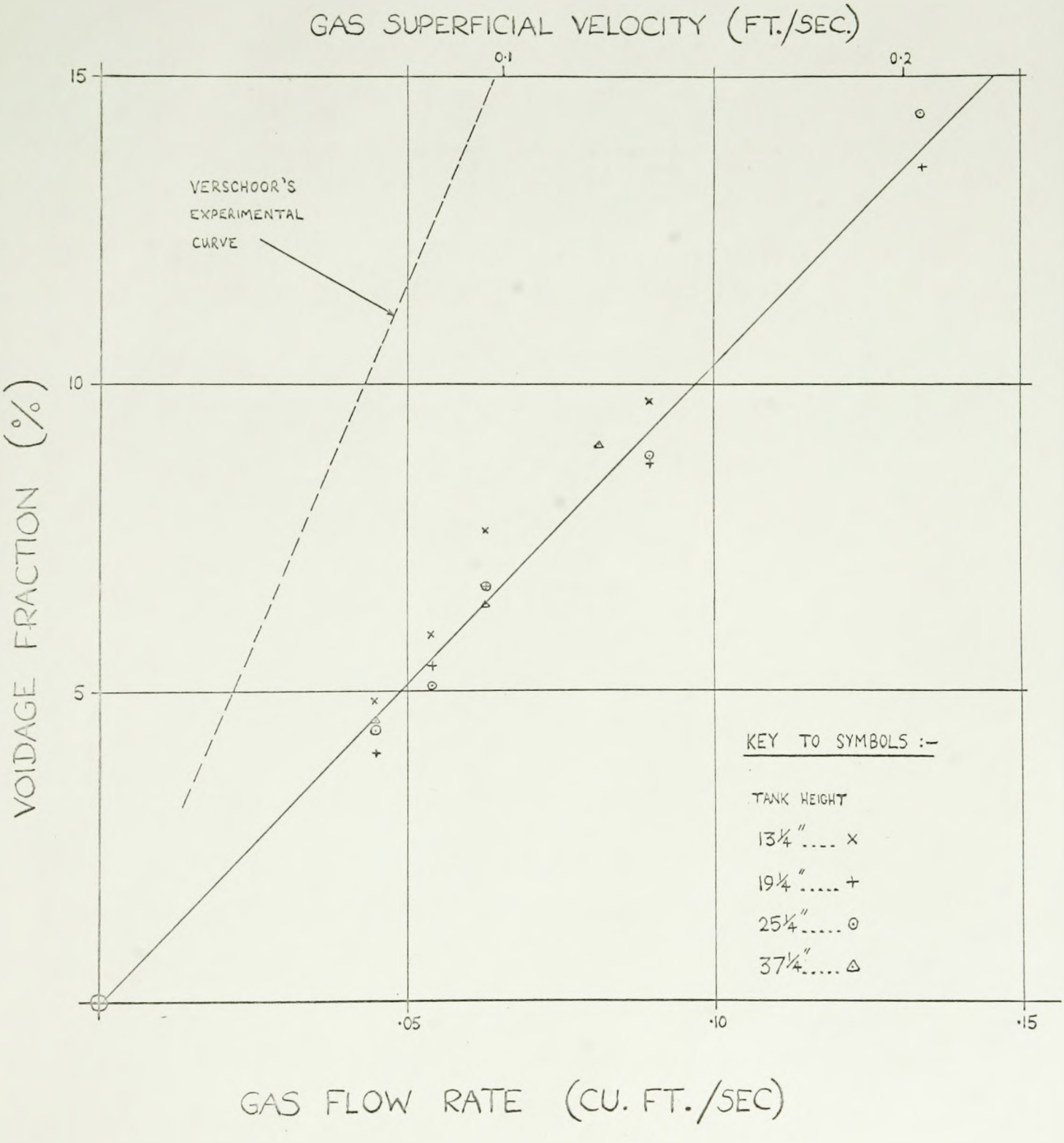

where the signal size is very small. The smoothed curve shown was obtained by superimposing 15 successive curves obtained during a run and then taking the best mean smoothed curve.

This curve, of course, represents the total response of both the reaction tank and the sampling system, and to obtain the required response of the reaction tank alone, it must be corrected for the response of the sampling system.

Other errors may also be introduced by (i) solubility effects of the tracer gas in the water, (ii) the position of the sampling system, and (iii) the fact that the pulse was not ideal. Investigations into these factors are reported in appendix III (c), (d) and (e), and showed that (i) and (ii) do not measurably affect the results, and that the corrections necessary for (iii) are included in the correction for the sampling system.

As was mentioned in section 2.2.1., the ideal sampling system, consisting of merely a time delay, could not be realised and the response of the system actually used was determined experimentally by tracer methods. The results of these experiments (see appendix III (b)) showed that the sampling system response could be represented very well by the combined response of a time delay in series with a CFSTR. The equivalent mean residence time for this CFSTR was calculated for various air flow rates and the results obtained compared well with values predicted theoretically from the dimensions of the equipment. (see appendix III (b))

FIGURE 8 RESIDENCE TIME DISTRIBUTION CURVES

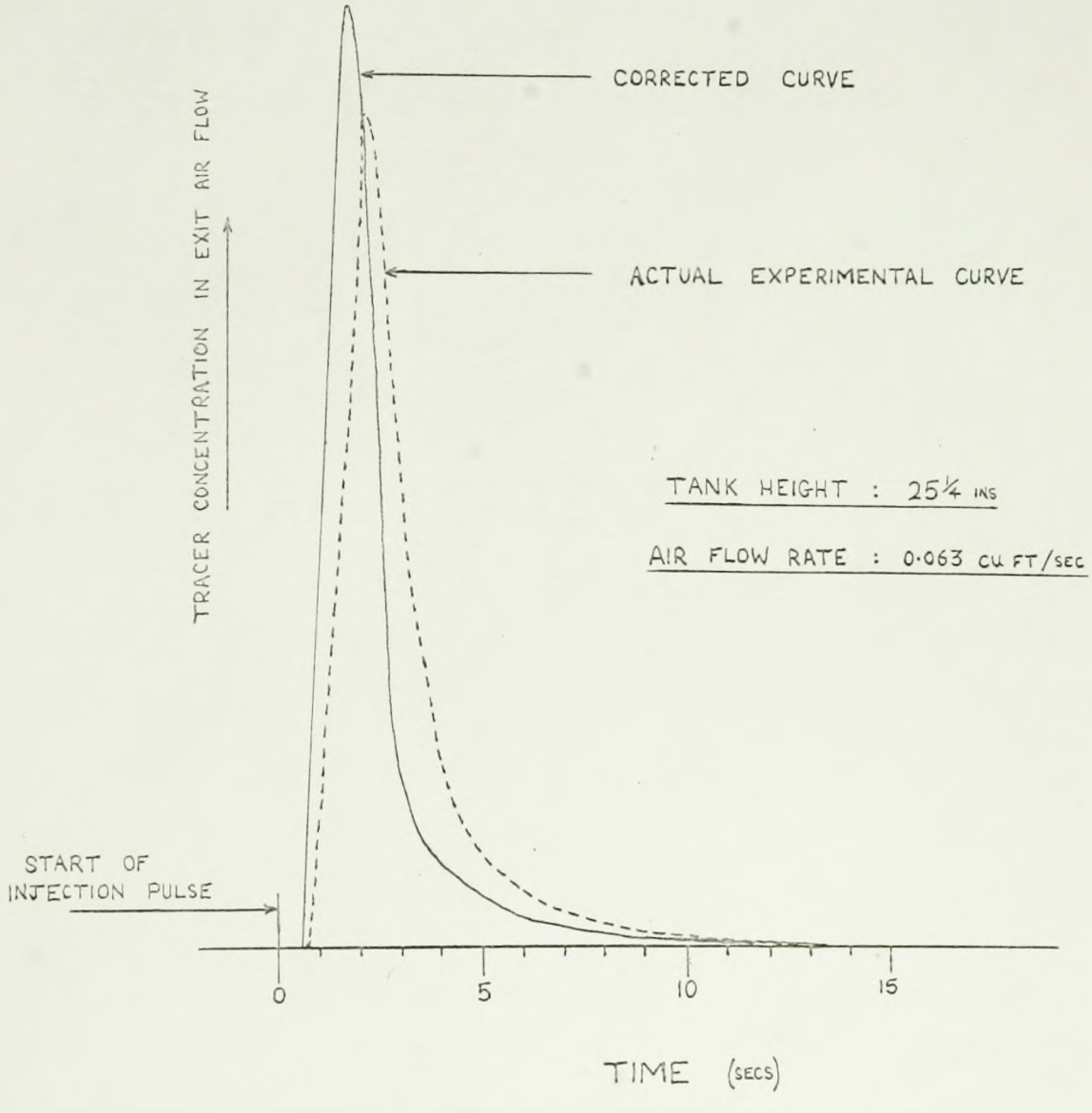

Using this representation of the response of the sampling system, the experimental curve may be corrected as follows:-

(a) The time delay may be corrected for by a shift of the curve along the time axis by an amount equal to the time delay.

(b) The CFSTR part of the response may be corrected for by the following analysis and construction, given by Westerterp et al. (1). Let the volume flow rate through the CFSTR part of the sampling system be Qs, its volume Vs and hence its mean residence time $\tau s = \frac{Vs}{Qs}$. If Ci and Co are the inlet and outlet tracer concentrations respectively, a mass balance on the tracer gives:

$$Qs.Ci = Qs.Co + Vs \frac{dCo}{dt}$$

therefore $$Ci = Co + \tau s \frac{dCo}{dt}$$

Since Co is the curve actually obtained, Ci which represents the required curve may be obtained from the following construction:

PR is the tangent to the Co curve at P.
Q is the point on the Ci curve corresponding to P on the Co curve.

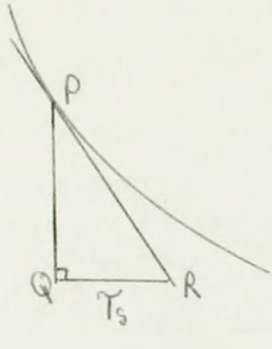

The corrected curve in figure 8 was obtained by this construction. The magnitude of this correction in terms of

the change in shape of the curve can be seen from this figure; in terms of the parameters of the curve, it is discussed in the next subsection. It will be seen that the curve consists of a sharp, comparatively high peak, with a diminishing tail. It would appear that the peak corresponds to that part of the original delta pulse input which came straight through the tank, and the tail represents the rest of the tracer which was delayed in some manner. Further analysis and interpretation of the shape of the curve is left until the section on models for the system.

Qualitatively, the effects of the air flow rate and the tank height on the shape of the curve are as follows:

An increase in air flow rate decreases the tail part of the curve and moves the peak slightly towards the origin, as predicted by the change in bubble velocity with air flow rate given in subsection 2.3.1. An increase in tank height moves the curve to the right, along the time axis, and tends to increase the tail part.

Further discussion of these effects is left until the end of the next subsection where the changes are described quantitatively in terms of parameters and may be more readily explained.

2.3.5. Derivation and Analysis of Residence Time Distribution Curve Parameters

The usual parameters for describing residence time distributions are the mean residence time (Υ), or first

moment of the distribution about the origin, and successive higher moments about this mean - the second moment about the mean being the variance (σ^2). These parameters are defined as follows:-

$$\Upsilon = \int_{-\infty}^{\infty} tC(t)dt$$

$$\sigma^2 = \int_{-\infty}^{\infty} (t-\Upsilon)^2 C(t)dt$$

It would be possible to obtain these parameters by first smoothing and correcting the experimental curves, as shown in the previous section, and then performing some form of numerical integration on the corrected curves. The disadvantages of this procedure are as follows:

(a) Original experimental curves obtained under the same conditions show considerable differences, partly inherent in the whole tracer-sampling experiment and partly due to noise, and obtaining a smoothed average curve is difficult and prone to errors.

(b) The method of correcting the curve depends on the slope of the curve and any errors in the curve tend to give magnified errors in the slope, even when the curve has been smoothed.

A much better method of obtaining the parameters of the residence time distribution for the tank alone, depends on the fact that for flow systems composed of a number of units in series, the overall mean residence time is the sum

of the individual mean residence times of each unit and likewise for the variance. (See appendix IV for a proof of this). More specifically for this case, if τ, τ_s, and τ_t, and σ^2, σ_s^2, and σ_t^2 are the mean residence times and variances of the distribution curves of the reactor tank, sampling system, and overall system, respectively; then:

$$\tau_t = \tau_s + \tau$$

$$\text{and} \quad \sigma_t^2 = \sigma_s^2 + \sigma^2$$

$$\text{hence} \quad \tau = \tau_t - \tau_s$$

$$\text{and} \quad \sigma^2 = \sigma_t^2 - \sigma_s^2$$

Thus the required parameters may be obtained from the parameters of the overall system and of the sampling system alone. These quantities can be obtained directly from the experiment.

An analogue computer was used to obtain instantaneously the moments of the tracer concentration curves about the origin of time scale (which in this case is the instant at which the injection pulse is triggered) and also their integrals with respect to time.

If f(t) represents the tracer concentration curve, and C(t) is the normalised residence time distribution curve,

$$\text{then} \quad C(t) = \frac{f(t)}{\int_{-\infty}^{\infty} f(t)dt} = \frac{f(t)}{A_1} \qquad (35.1)$$

$$\Upsilon = \int_{-\infty}^{\infty} tC(t)dt = \frac{1}{A_1}\int_{-\infty}^{\infty} tf(t)dt = \frac{A_2}{A_1} \qquad (35.2)$$

$$\overline{T^2} = \int_{-\infty}^{\infty} t^2C(t)dt = \frac{1}{A_1}\int_{-\infty}^{\infty} t^2f(t)dt = \frac{A_3}{A_1} \qquad (35.3)$$

and it can be shown that $\sigma^2 = \overline{T^2} - \Upsilon^2$

Hence Υ and σ^2 can be obtained from A_1, A_2 and A_3 which were computed directly on the analogue computer.

This was a straightforward procedure except in so far as deciding to what point in time the integrations should be carried. Since the tail of the curve is drawn out and the noise becomes quite large compared with the signal in this region, the errors due to noise become more pronounced in computing successively higher moments. In other words if the integration is carried on for too long a time, the estimated values of the mean residence time and $\overline{T^2}$ become far too large.

This problem is best solved by the concept of stagnant, or deadwater, regions as propounded by Levenspiel (8), which he defines as follows:-

"In a vessel the deadwater regions are the relatively slow moving portions of the fluid which we choose to consider to be completely stagnant. Deadwater regions contribute to

the vessel volume; however we ignore the regions in determining the various age distributions".

It is still arbitrary where the cut-off point is to be (i.e. that point beyond which the elements have residence times sufficiently large to be considered "deadwater" and ignored in the calculations), but Levenspiel (8) further notes that cut-off points in excess of twice the mean residence time give a reasonably accurate picture of a system. In the present case the cut-off point was about four times the mean residence time, which was felt to be a reasonable compromise between unduly truncating the curve and allowing possible noise to increase the estimated values of the parameters.

The results for the mean residence time and variance obtained by this method, and corrected for the influence of the sampling system, are given in Table II for various values of the air flow rate (Q) and tank height (H). The figures listed are the mean values of samples whose size is given in the last column of this table. The value quoted for the error in the mean residence time ($\pm$ 0.2 secs.), was estimated at the 95% confidence limits from the calculated variance within the samples for both the overall mean residence time and the mean residence time of the sampling system. (This calculation is given with the typical set of experimental results in appendix III (f)). The error in the variance ($\pm$ 0.6 sec.^{2}) was estimated from the above error; this is possible because

TABLE II

RESULTS OF TRACER EXPERIMENTS

COLUMN HEIGHT (INCHES)	AIR FLOW RATE (CU.FT/SEC)	M.R.T. τ (SECS)	VARIANCE σ^2 (SEC^2)	VOIDAGE FRACTION (PERCENT)	NUMBER OF READINGS IN SAMPLE
13.25	0.045	1.02	2.76	4.8	10
13.25	0.054	0.94	2.11	5.9	11
13.25	0.063	0.92	1.27	7.6	32
13.25	0.090	0.82	0.69	9.7	13
19.25	0.045	1.29	3.30	4.0	23
19.25	0.054	1.48	3.56	5.4	32
19.25	0.063	1.32	2.93	6.7	27
19.25	0.090	1.07	1.26	8.7	14
19.25	0.135	0.86	0.95	13.5	10
25.25	0.045	1.65	3.29	4.3	25
25.25	0.054	1.75	2.35	5.1	16
25.25	0.063	1.49	2.31	6.6	33
25.25	0.090	1.25	2.24	8.8	18
25.25	0.135	1.09	1.64	14.3	31
37.25	0.045	2.43	4.12	4.5	16
37.25	0.063	2.02	4.36	6.3	15
37.25	0.081	1.78	2.81	9.0	15
		$(\pm 0.2)^*$	$(\pm 0.6)^*$		

(* VALUES GIVEN ARE THE MAXIMUM ERROR FOR THE ABOVE COLUMN, AT THE 95% CONFIDENCE LIMITS)

the two parameters are derived from the same residence time distribution.

The size of the corrections necessary to allow for the sampling system is given in appendix III (b), and for the mean residence time is of much the same magnitude as the mean residence time of the tank itself. The range of these corrections is 1.2 - 1.7 secs., depending on the air flow rate. The corrections for the variance have a smaller relative magnitude and are about 1/2 to 1/4 of the corrected variance.

The mean residence time is shown on figure 9 plotted against the air flow rate, for the various tank heights used. The only interesting thing to note about these curves, apart from the overall tendency of the mean residence time to decrease with increasing air flow rate and decreasing tank height, is the limiting values of the mean residence time as $Q \rightarrow 0$. From the results presented in section 2.3.2., it is apparent that as the air flow is reduced, the number of orifices bubbling is proportionately reduced until in the limit only one or two would be bubbling. At this flow rate, the number of bubbles rising would be insufficient to move the liquid bodily, and the effect would be of bubbles rising through a stagnant liquid. Hence the mean residence time would approach a limiting value equal to the time of rise of a single bubble through the tank; this may be calculated directly from the terminal velocity of the bubble and the height of the tank. The terminal velocity of rise of a bubble of radius as calculated in section 2.3.2., (0.68 cms.) is found to be

FIGURE 9 GRAPH OF MEAN RESIDENCE TIME VERSUS GAS FLOW RATE FOR VARIOUS TANK HEIGHTS

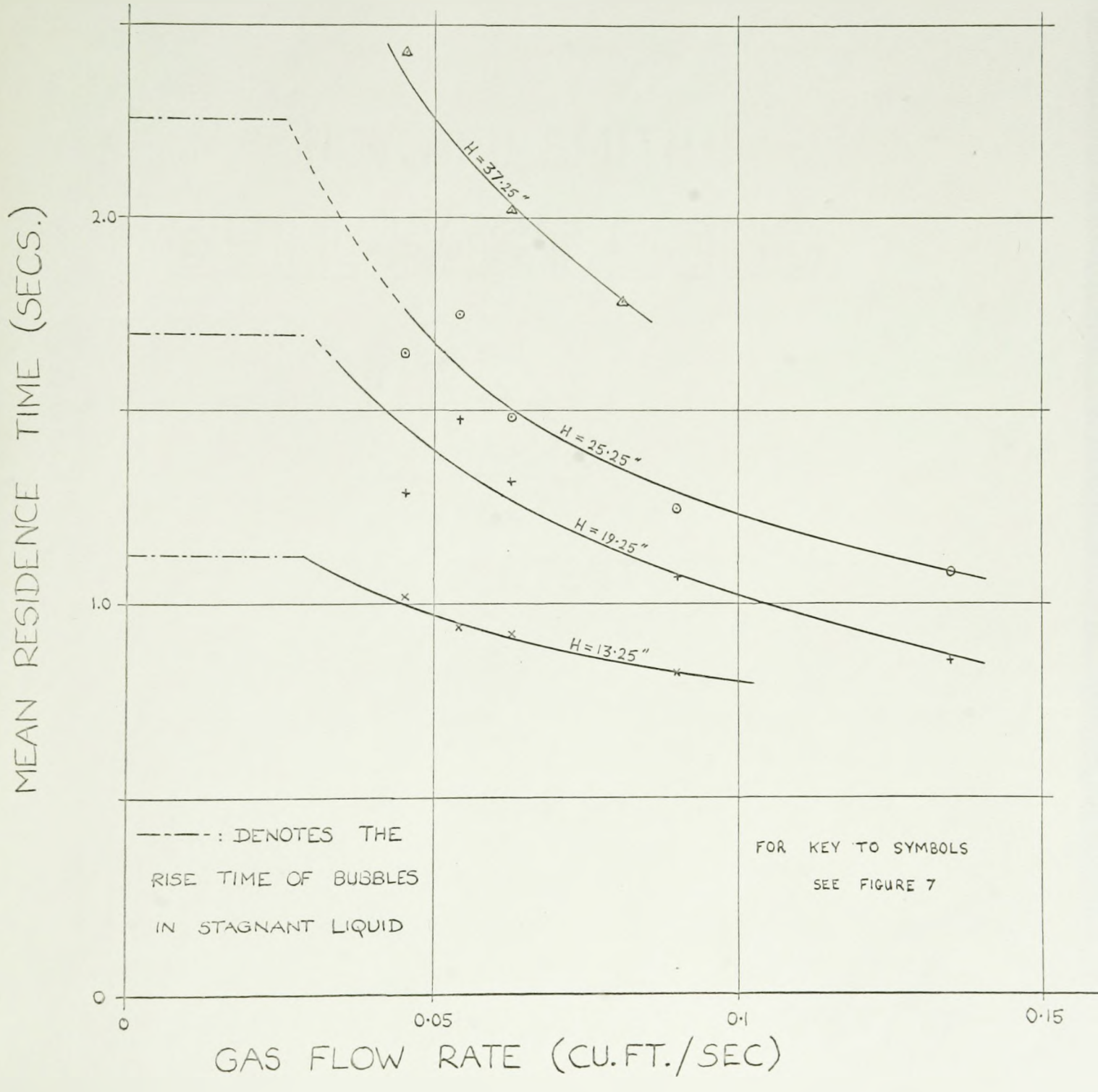

27 cms./sec. (9), and hence the times of rise for various tank heights are as indicated on figure 9 by the horizontal dashed lines. It is suggested that these lines present quite feasible terminations to the experimental curves.

If the mean residence times are plotted against the reciprocal of the air flow rate, as shown in figure 10, a linear relationship is found to exist. This linear relationship is fitted well for the higher flow rates, but it is possible that it breaks down for the lower flow rates. This can be seen in the cases of the 1-1/2 ft. and 2 ft. tanks, where there are apparently parallel deviations from the straight line. However these deviations are well within the estimated error and may be entirely coincidental.

A second graph of mean residence time versus the tank height at constant flow rate is shown in figure 11, where again it can be seen that a linear relationship exists.

The best linear relationship was obtained by multiple regression analysis on the data, and details of this are given in appendix III (g). The best fit so obtained was:

$$\gamma = 0.0187H + 0.00172 \frac{H}{Q} + 0.320 \qquad (35.4)$$

and the standard deviation for this fit was 0.3 secs. The lines derived from this expression are shown plotted on figures 10 and 11, and are seen to fit the data quite well.

The results for the variance of the residence time distributions are less accurate and show far more scatter. This is to be expected since noise in the tail of the curve

FIGURE 10 GRAPH OF MEAN RESIDENCE TIME VERSUS RECIPROCAL OF GAS FLOW RATE AT VARIOUS TANK HEIGHTS

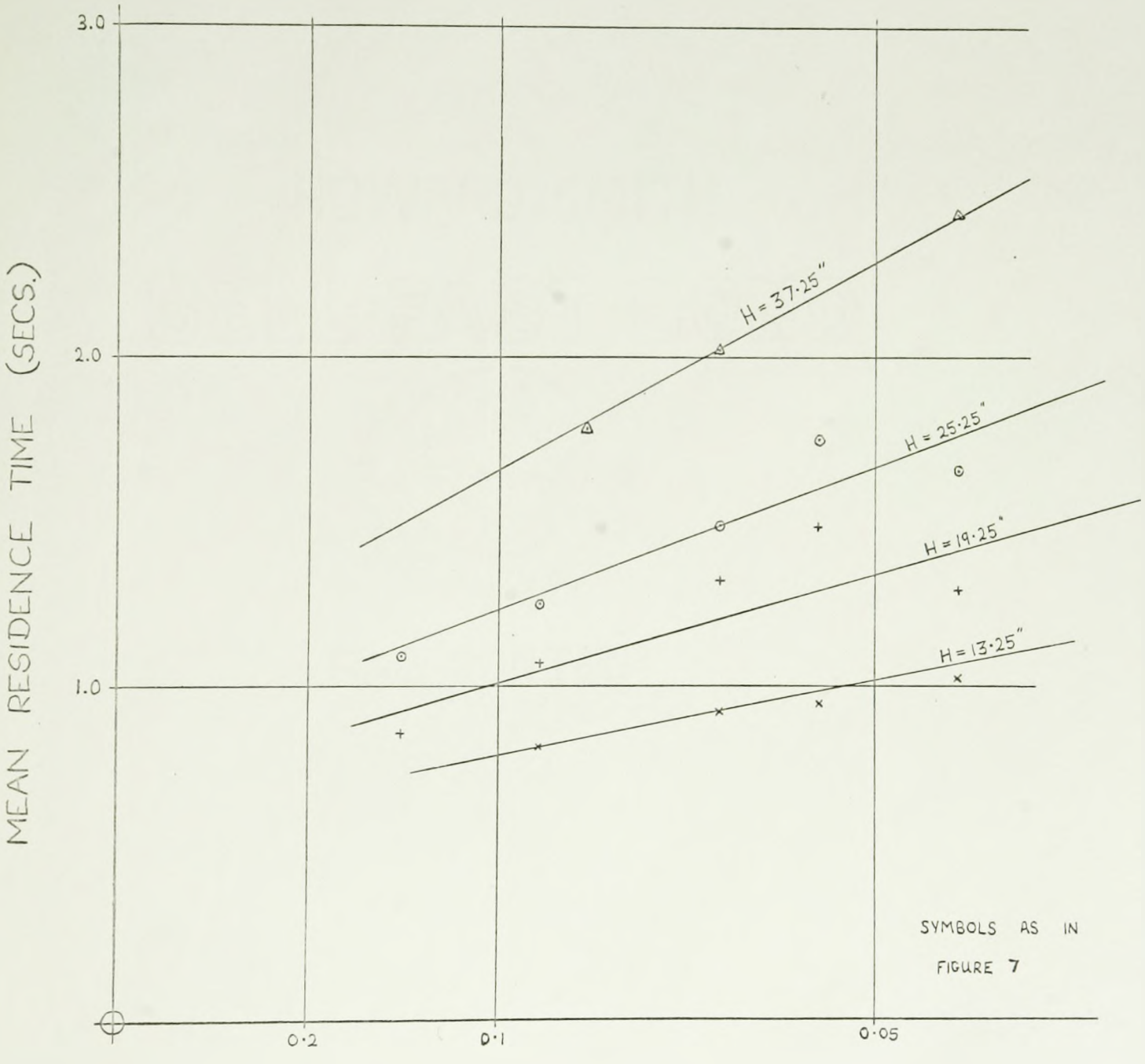

FIGURE 11 GRAPH OF MEAN RESIDENCE TIME VERSUS TANK HEIGHT FOR VARIOUS FLOW RATES

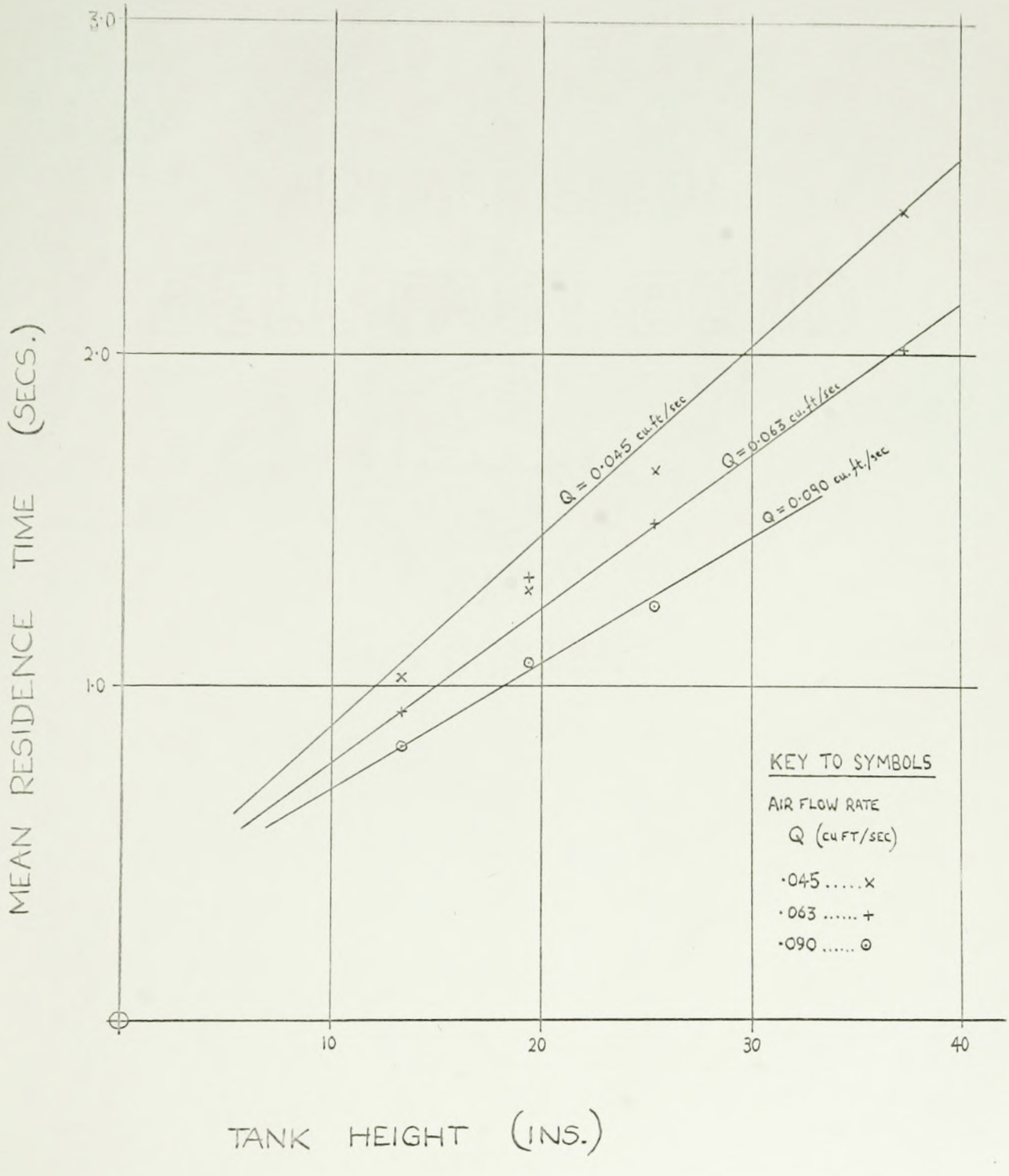

is magnified by the t^2 term in computing A_3 and hence $\overline{T^2}$. Regression analyses (see appendix III (g)) showed that the best fit could be obtained using the standard deviation, the square root of the variance, instead of the variance itself as the dependent variable. Consequently the standard deviation is shown plotted in figure 12, against the reciprocal of the air flow rate, for various constant tank heights.

As with the data for the mean residence times, a linear relation is best fitted at the higher flow rates, whereas at the lowest flow rate, the points are all significantly lower and it is possible that in this region the same linear relationship does not hold. However it must be remembered that the error due to noise in the tail of the residence time distribution curve, is greatest at low flow rates, because these conditions produce a longer tail on the curve.

For these reasons, the results at the lowest flow rate (Q = 0.045 cu. ft./sec.) were not used in the regression analysis, used to obtain the lines shown in figure 12. These lines represent the best fit for the remaining data, the equation for this being:

$$\sigma = 0.0307H + 0.0574\frac{1}{Q} - 0.0432 \qquad (35.5)$$

with a standard deviation about this line of 0.17.

An alternative fit that is nearly as good is

$$\sigma = .00223\frac{H}{Q} + 0.750 \qquad (35.6)$$

with a corresponding standard deviation about the line of 0.21.

In considering the physical meaning of these trends

FIGURE 12 GRAPH OF STANDARD DEVIATION OF RESIDENCE TIME DISTRIBUTION FUNCTION VERSUS RECIPROCAL GAS FLOW RATE AT VARIOUS TANK HEIGHTS

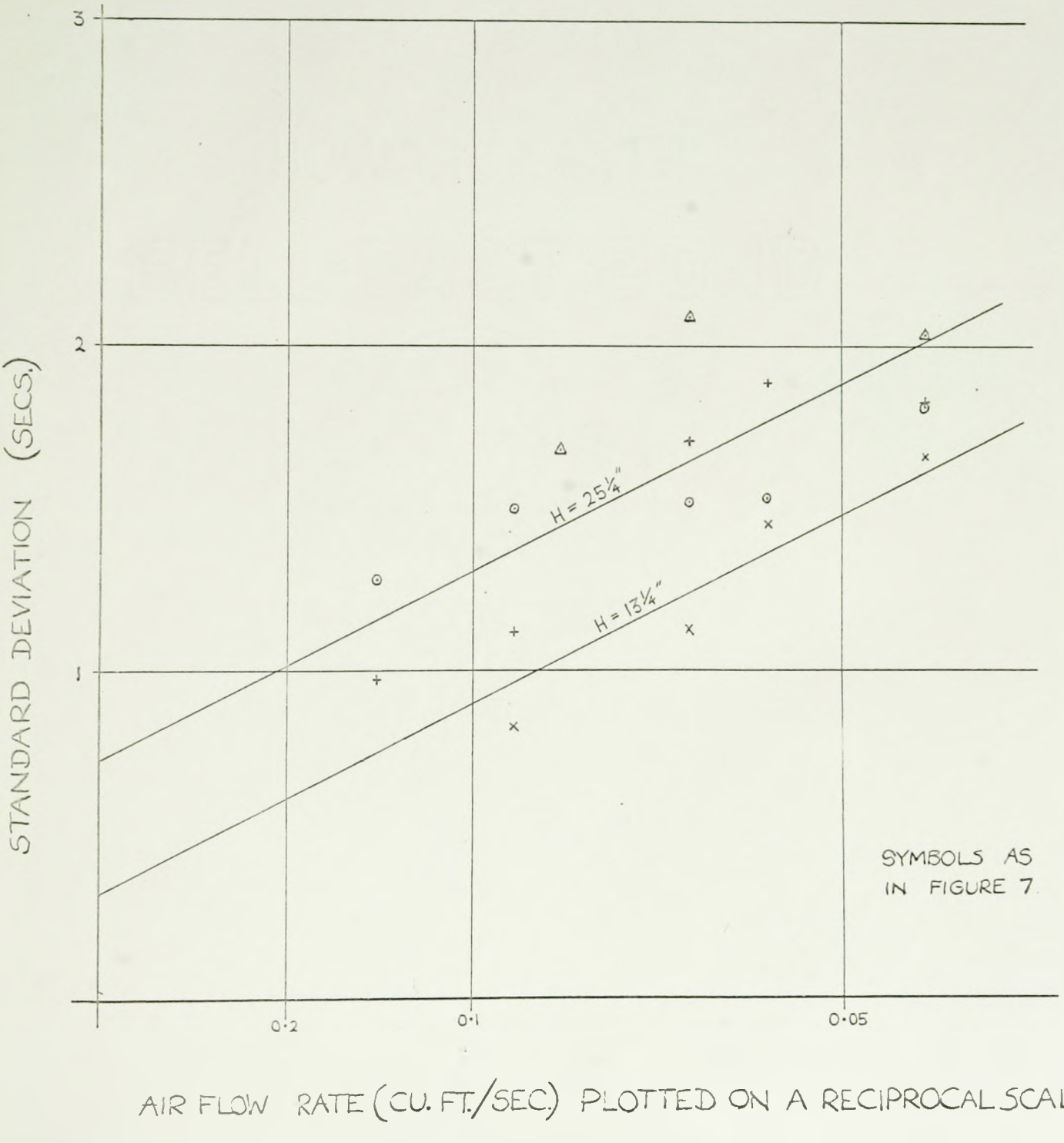

of the mean residence time and variance of the residence time distribution with changes in tank height and air flow rate, it will be convenient to first consider the behaviour of the stagnant volume, or deadwater regions.

The stagnant volume is obtained from the total voidage by subtracting the active volume, which is defined as the volume required to satisfy the mean residence time, for the actual air flow rate.

i.e. Stagnant volume = Voidage - $\Upsilon.Q$

Values for the stagnant volume obtained in this way are given as part of table III and are also shown plotted on figure 13 against the air flow rate, for the different tank heights.

It will be seen that for air flow rates below 0.063 cu. ft./ sec., the stagnant volume is essentially zero (negative values being sufficiently close to zero to lie within the estimated error limits of $\pm$ .015 cu. ft.)

Above this flowrate the stagnant volume increases rapidly; this can be accounted for by the great increase in the number of smaller bubbles, formed through the following two mechanisms:

(a) At the higher air flow rates, the motion of the liquid across the plate is much faster, because of the greater pumping effect of the bubbles, and more shearing of the bubble streams occurs, giving many smaller bubbles.

(b) As has been seen in section 2.3.2., at about this flowrate all the orifices come into use and hence the air

FIGURE 13 GRAPH OF STAGNANT VOLUMES AGAINST AIR FLOW RATE FOR VARIOUS TANK HEIGHTS

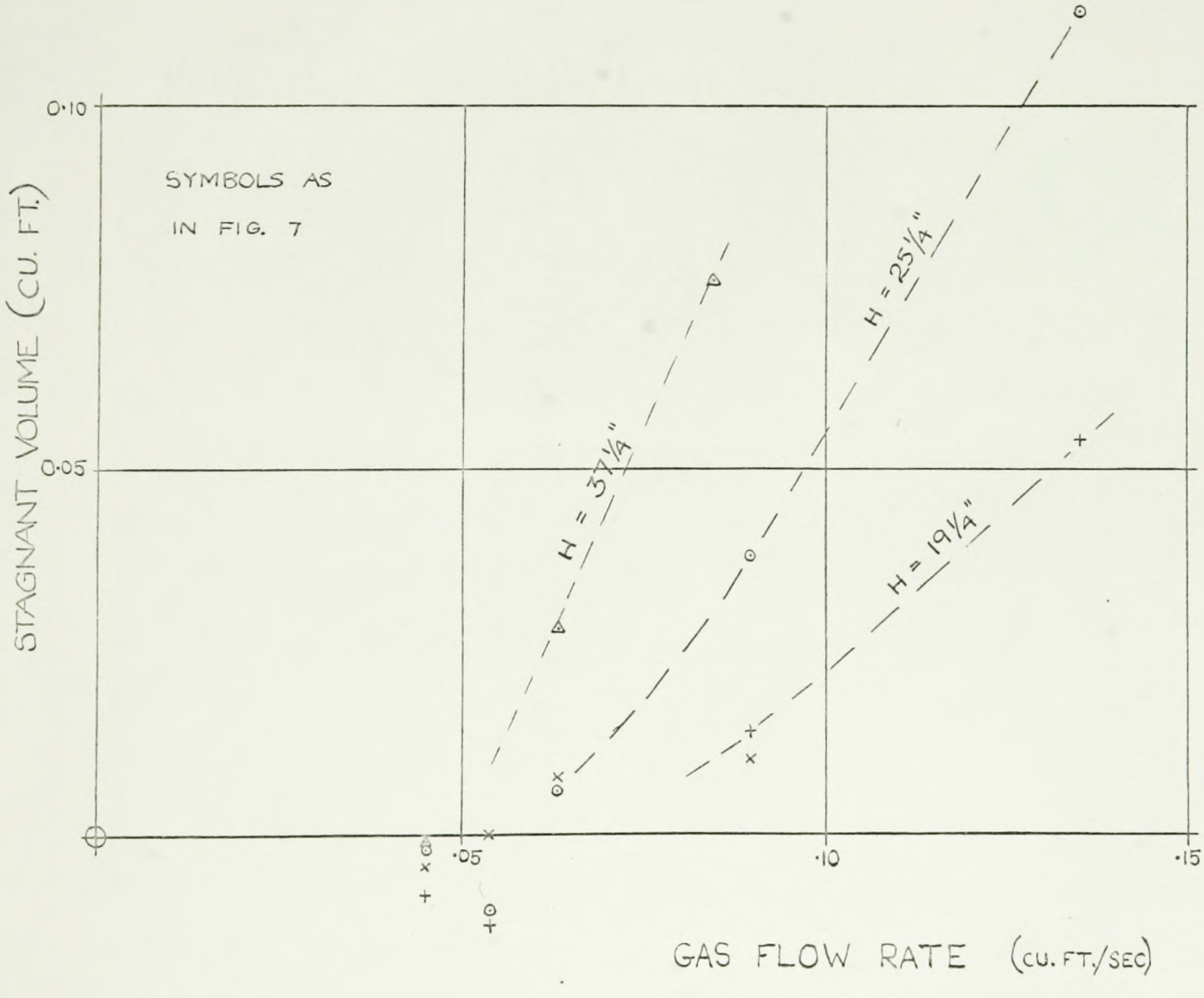

flow through each orifice increases. Thus although the original bubbles formed will be larger, their faster motion will tend to tear off small fragments which will form small bubbles.

Because of their lower terminal velocities, these small bubbles tend to be carried around with the liquid and the chance of their removal from the system by reaching the surface is less than for larger bubbles.

Another factor at high air flow rates is the greater liquid velocities in the system, which tend to sweep round and recirculate more gas bubbles of all sizes; these further add to the stagnant volume.

Therefore because of these two factors (i) more small bubbles and (ii) increased liquid velocities circulating more bubbles of all sizes, the stagnant volume increases rapidly with gas flow rate. It must be emphasised that to designate a certain part of the vessel's contents as stagnant, does not require it to be motionless; it merely requires that its retention time within the system be several times greater than the mean retention time, or expressing it in terms of probability, that its chances of removal from the system be several times less than average chance of removal from the system.

Thus the increase in voidage is due more to an increase in the stagnant volume than to an increase in the active volume. So that although the active volume increases, this increase is not sufficient to prevent the mean residence time from

decreasing, as the air flow rate increases. Physically this means that the gas flows through the tank faster with increasing gas flow and this is reflected in the higher bubble velocities. (See section 2.3.1.)

The variance, which is a rough measure of the width of the curve, decreases for much the same reason. Not only does the size of the active volume diminish the mean residence time as explained above, but also it will tend to diminish the variance which varies approximately as the reciprocal of the square of the flow rate, provided that there is no change in the flow pattern. Physically this means that the flow through the tank approaches plug flow more closely as the flow rate increases and the apparent greater mixing that can be observed is confined more to the stagnant volume than to the active volume.

2.4. Discussion and Analysis of Models Representing the System

In a process vessel where non-ideal flow occurs it is useful to derive a model for the system which adequately describes the flow patterns which occur.

The main reasons for this are:

(a) that the model can be used to predict the effects of varying the parameters of the system;

(b) that it allows generalisation of the results obtained and a convenient and quantitative comparison between different types of vessels;

and (c) that it is more easily handled when the performance of the process vessel is required for a particular application.

In general there are two types of model; the first, similar to models in other fields, is based on the fluid dynamics and physical properties of the system. The second type of model assumes the real system can be considered as a number of separate interconnected regions which behave ideally as either (i) plug flow regions, (ii) completely mixed regions (CFSTRs), (iii) completely stagnant or deadwater regions. This type of model is very flexible since a system of any complexity can be simulated by taking a sufficient number of ideal regions with suitable interconnecting flows. It is this type of composite model which will be considered here.

The disadvantage of this type of model is that since it is derived by a linear process, it can only be applied

with certainty to linear processes. This can be illustrated by a simple example of a system consisting of a CFSTR in series with a plug flow reactor. The overall residence time distribution function will be the same whether the CFSTR is first or last. Likewise the output will be the same for any linear or first-order processes that occur within them, such as a first-order reaction, since these processes only depend on the overall residence time distribution function. However, for non-linear processes or non-first order reactions, the output will depend on the sequence in which the flow passes through the vessels, so that to correctly predict the performance of the system, more information is required as to the flow pattern.

Another factor which may cause the model to incorrectly predict the performance when non-linear processes are involved, is the concept of segregation. This was originally proposed by Danckwerts (10) and is a measure of the effectiveness of the mixing process. Thus a "well mixed" tank may contain discrete fragments of fluid between which there is no mixing on a molecular scale, and which behave individually as plug flow reactors. This would still give the same residence time distribution function as for an ideal CFSTR but because of the absence of complete homogeneity would not give the same performance where non linear processes were involved.

Thus a mixed model is not uniquely defined from residence time distribution curves alone, and additional flow

information is required if the model is to correctly predict the behaviour of the system for all types of processes.

2.4.1. Derived Results for Fitting Models

The general procedure for fitting a composite model is to consider the shape of the residence time distribution curve of the whole system and consider how this shape can be synthesised from a combination of the residence time distribution curves of the ideal flow regions. (For examples of this see Levenspiel and Bischoff (8)). In addition, knowledge of the flow patterns occurring within the system may suggest the best configuration of the required flow regions and the types of interconnecting flow.

The final step is to determine the parameters of the model regions (i.e. the volumes of the respective regions and the flow rates through them) by matching the response parameters of the model to the experimentally obtained response parameters of the system.

It should be stressed that it is preferable to keep the model simple, with as few parameters as possible, and it is evident that the number of parameters in the model cannot exceed the number of experimentally obtained parameters of the system.

In the present work the available parameters are: the mean residence time, the variance, the total voidage and the measured flow velocities in the system. It is convenient to derive other quantities from these parameters and these derived quantities are shown in table III.

TABLE III

DERIVED PARAMETERS

COLUMN HEIGHT (INCHES)	AIR FLOW RATE (CU.FT/SEC)	STAGNANT VOLUME (CU.FT)	t_1 (SECS)	t_2 (SECS)	R
13.25	0.045	-0.004	0.47	0.55	3.0
13.25	0.054	0.000	0.43	0.51	2.8
13.25	0.063	0.008	0.40	0.52	2.2
13.25	0.090	0.010	0.35	0.47	1.8
19.25	0.045	-0.008	0.68	0.61	3.0
19.25	0.054	-0.012	0.62	0.86	2.2
19.25	0.063	0.001	0.58	0.74	2.3
19.25	0.090	0.014	0.51	0.56	2.0
19.25	0.135	0.054	0.45	0.41	2.4
25.25	0.045	-0.002	0.89	0.76	2.4
25.25	0.054	-0.010	0.81	0.94	1.6
25.25	0.063	0.016	0.76	0.73	2.1
25.25	0.090	0.033	0.66	0.59	2.5
25.25	0.135	0.090	0.59	0.50	2.5
37.25	0.045	0.001	1.31	1.12	1.8
37.25	0.063	0.028	1.12	0.90	2.3
37.25	0.081	0.076	1.02	0.76	2.2

The stagnant volume has already been discussed in sub-section 2.3.5. It is considered that it does not take part in the flow within the system, and when constructing the model, its position and linkage with the other regions are quite arbitrary and need not be defined.

t_1 is derived from the ascending velocity of the bubbles (v) in the system (section 2.3.1.) and is the time required for them to rise through the height of the tank.

i.e. $t_1 = H.v$

Since v is a linear function of $\frac{1}{Q}$ (see section 2.3.1.) t_1 may be represented by

$$t_1 = aH + b\frac{H}{Q} \qquad (41.1)$$

where a and b are constants.

t_2 is the difference between the mean residence time and t_1, and R is the ratio of the standard deviation of the residence time distribution, to t_2. These quantities have no exact physical significance but will be found useful in analysing the models.

2.4.2. Use of Transfer Functions

The method to be used in the following model analyses is to derive the transfer function for the model and from this obtain directly the mean residence time and the variance of the residence time distribution.

The transfer function of a system can be defined as follows:

Consider that there is an input signal (e.g. the

concentration of the input stream) to the system which is a function of time, i(t), and that the corresponding output as a function of time is o(t), and let these two functions have Laplace transforms* I(s) and O(s), respectively. Then if G(s) is the transfer function of the system;

$$O(s) = G(s).I(s)$$

Thus the transfer function may be obtained from the ratio of the Laplace transform of the output, to the Laplace transform of the input.

As examples, the transfer function of a CFSTR with a mean residence time of z is $\frac{1}{1 + zs}$ and that of a plug flow reactor with the same mean residence time is e^{-zs}.

When the transfer function refers to concentration changes, since the Laplace transform of a delta pulse is unity, it will be seen that the transfer function will be the Laplace transform of the C curve or exit residence time distribution.

The great advantage in working in terms of the transfer function is that it can be shown that for all practical cases the following relationship holds:-

The nth moment of the residence time distribution

$$= \int_{-\infty}^{\infty} t^n C(t)dt$$

---

* For a full description of the Laplace transform and its use see, for example, Churchill (11).

$$= (-1)^n \lim_{s \to 0} \frac{d^n}{ds^n} (\bar{c}(s))$$

where C(t) is the residence time distribution function and $\bar{c}(s)$ is the corresponding transfer function. The derivation of this relationship is given in appendix IV.

Thus the moments (particularly the mean residence time, and the mean square residence time, $\overline{T^2}$) can be obtained directly from the transfer function.

2.4.3. Circular Flow Model

There are two simple, composite region models which could give the shape of the experimental residence time distribution curve obtained. The first of these is based on the observed circular flow within the tank and approximates this by two plug flow reactors as shown in figure 14(a).

The full air flow Q enters at the bottom of plug flow reactor 1 and ascends with uniform velocity U. At the exit of reactor 1, a side flow qo is taken off and returns down plug flow reactor 2, with uniform velocity u. Transfer between the two reactors occurs along the whole of their length and is governed by a distribution function f(x), defined such that the quantity (dq) transferred across a small segment of depth dx, at distance x from the top of the reactor is given by: $dq = f(x)dx$

By considering small segments of each reactor, with flows and concentrations as shown in figure 14(b) a mass balance on the tracer gives the following equations:

FIGURE 14 (a) CIRCULAR FLOW MODEL DIAGRAM

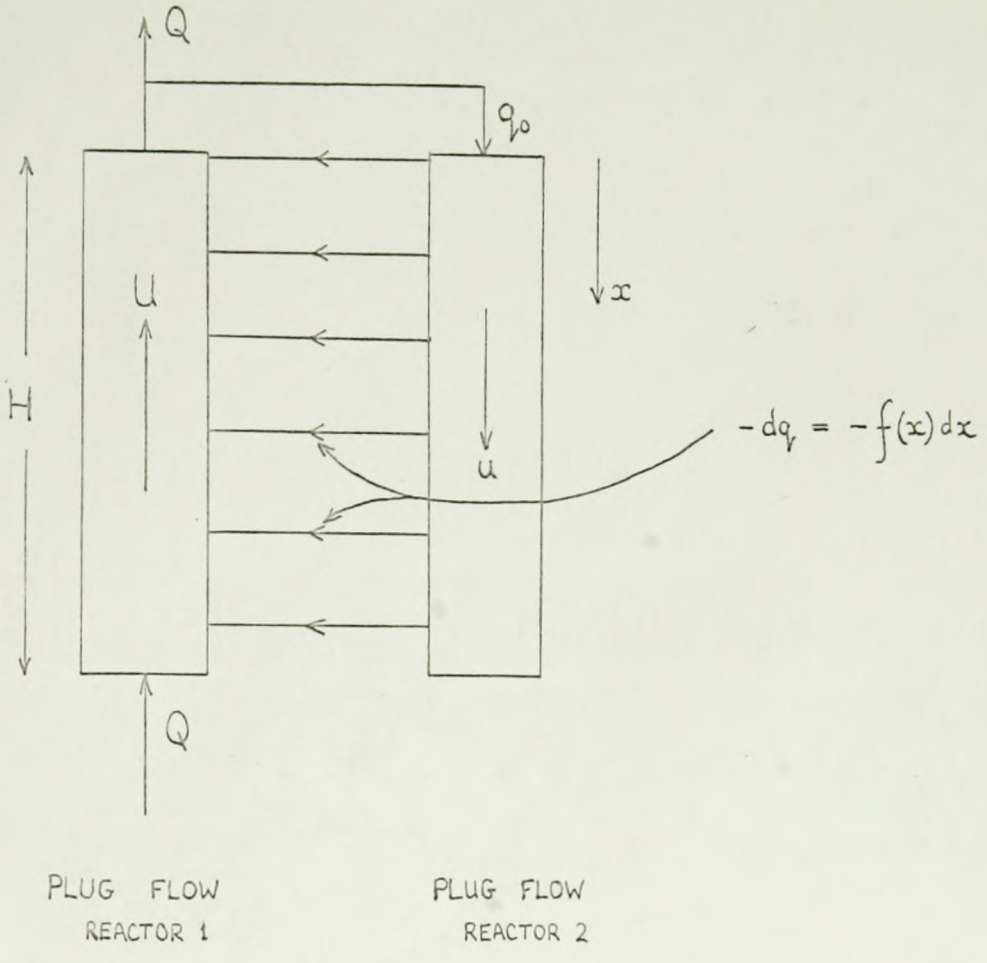

(b) MASS BALANCE SEGMENTS

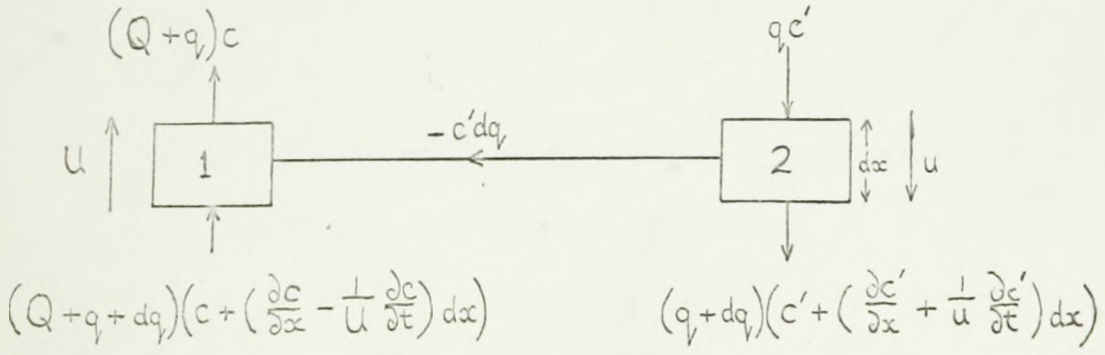

for 1 $$\frac{\partial c}{\partial x} - \frac{1}{U}\frac{\partial c}{\partial t} + \frac{c - c'}{Q + q}.\frac{dq}{dx} = 0 \qquad (43.1)$$

for 2 $$\frac{\partial c'}{\partial x} + \frac{1}{u}\frac{\partial c'}{\partial t} = 0 \qquad (43.2)$$

The boundary conditions for this system are as follows:

at $x = 0$, $c = c' = ce$, and $q = qo$;

at $x = H$, $c = co$, and $q = 0$;

at $t = 0$, $c = 0$ and $c' = 0$.

By taking Laplace transforms of c and c', denoted by $\bar{c}$ and $\overline{c'}$ respectively, equations 43.1 and 43.2 become:

$$\frac{\partial \bar{c}}{\partial x} - \frac{s}{U}.\bar{c} + \frac{\bar{c}}{Q + q}.\frac{dq}{dx} = \frac{\bar{c}'}{Q + q}.\frac{dq}{dx} \qquad (43.3)$$

and $$\frac{\partial \bar{c}'}{\partial x} + \frac{s}{u}\bar{c}' = 0 \qquad (43.4)$$

Equation 43.4 can be solved to give:

$$\bar{c}' = \overline{ce}.\exp(-sx/u)$$

Equation 43.3 can be integrated, using an integrating factor of $(Q + q).\exp(-sx/U)$, to give:

$$\bar{c}(Q + q).\exp(-sx/U) = \int \bar{c}' \frac{dq}{dx}.\exp(-sx/U).dx + \text{const} \qquad (43.6)$$

Substitution of the boundary conditions and the value of $\overline{c}'$ in equation 43.6, and subsequent rearrangement gives the transfer function:

$$\frac{\overline{ce}}{\overline{co}} = \frac{Q.\exp(-sH/U)}{(Q + qo) + \int_0^H \exp.(-sx(\frac{1}{u} + \frac{1}{U})).\frac{dq}{dx}.dx}$$

$$= \frac{F(s)}{G(s)}$$

As a check the zeroth moment of the residence time distribution

$$= \int_{-\infty}^{\infty} C(t)dt$$

$$= \lim_{s \to 0} \frac{F(s)}{G(s)}$$

$$= \frac{Q}{Q + qo - qo} = 1$$

This is the correct value.

The mean residence time and the variance may be obtained by taking the limiting values of the transfer function derivatives as explained previously and this is found to yield

$$\Upsilon = \frac{H}{U} + \frac{B}{Q} \qquad (43.9)$$

$$\text{and} \quad \sigma^{-2} = \frac{B^2}{Q^2} + \frac{C}{Q} \qquad (43.10)$$

$$\text{where} \quad B = -\left(\frac{1}{u} + \frac{1}{U}\right) \cdot \int_0^H x \frac{dq}{dx} dx \qquad (43.11)$$

$$\text{and} \quad C = \left\{ \frac{1}{u} + \frac{1}{U} \right\}^2 \int_0^H x^2 \frac{dq}{dx} \, dx \qquad (43.12)$$

These may be evaluated if a suitable expression is obtained for $\frac{dq}{dx} = f(x)$.

From the smoothness of the residence time curve, it seems probable that f(x) itself is a smooth continuous function over the range $0 \leqslant x \leqslant H$, and from observation of the flow within the tank a possible function would be:

$$f(x) = -m(H - x)^n$$

since f(x) should decrease as x increases.

By substituting this function into equations 43.11 and 43.12, and putting the values of B and C so obtained into 43.9 and 43.10, the following expressions are obtained:

$$\gamma = \frac{H}{U} + tc \cdot \frac{qo}{Q}$$

$$\sigma^2 = \frac{qo^2}{Q^2} \cdot tc^2 \left\{ 1 + \frac{2(n+2)}{n+3} \cdot \frac{Q}{qo} \right\}$$

$$\text{where} \quad tc = \left\{ \frac{1}{u} + \frac{1}{U} \right\} \cdot \frac{H}{n+2}$$

and may be considered as a measure of the circulation time.
(n is restricted such that $n \geqslant o$)
In terms of the derived parameters of the system

$$t_1 = \frac{H}{U}$$

$$\text{and hence} \quad t_2 = \frac{qo}{Q} \cdot tc$$

$$\therefore \quad R = \left\{1 + \frac{2(n+2)}{n+3} \cdot \frac{Q}{qo}\right\}^{\frac{1}{2}}$$

From experimental values of t_2, R, u and U, these expressions can be solved to give qo and n. (Here u may be assumed to be approx. 1/4 U). Solutions can best be found graphically by plotting $\frac{Q}{qo}$ as a function of n in the two cases.

However on doing this, it was found that only in a few experimental cases were there solutions that were real in n and most of the experimental results did not yield a solution. This of course is not a fundamental blow to the model since it merely suggests using a different function for $\frac{dq}{dx}$ and in fact a function of the form $f(x) = -mx^{\frac{1}{4}}$ can be fitted successfully.

A more serious fault in the model lies in the form of tc, which is directly proportional to H. Again it can be argued that this will depend on the form of the function f(x) but it has been found that for many types of function, continuous over the range $0 < x < H$, this proportionality still holds true though it has not been proved explicitly for functions in general.

This indicates that Υ itself is directly proportional to H, which is contrary to experimental findings, since the regressed expression for Υ, equation 35.4, includes a fairly large constant term:

$$\Upsilon = 0.0187H + 0.00172\frac{H}{Q} + 0.320$$

Thus although this model is useful in evaluating the experimental results in terms of the observed circular flow, and specifying the type of distribution $\frac{dq}{dx}$ must be to fit the observed results, it is felt that the agreement between the predicted and experimental forms of the expression for the mean residence time is insufficient to justify the use of this model in describing the system.

2.4.4. Analysis of Mixed Flow Model

The second type of model which could result in the observed shape of the residence time distribution is a combination of a plug flow reactor and a CFSTR arranged as shown in figure 15(a).

The way in which the curve for the model may be synthesised from the curves of the individual regions is shown in figure 15(b).

The model consists of plug flow reactor 1, with a CFSTR 2 at the exit of 1, taking in a part (q) of the exit stream, and feeding an equal amount directly back. This model would then account for the time delay, the sharp initial peak and the exponential decay towards the tail, found in the experimental curve.

This model may be compared to the actual flows in the tank, with reference to figure 5, as follows: the plug flow reactor corresponds to regions 1 and 2, and the CFSTR corresponds to region 3. The contents of region 4 may be considered as contributing to the stagnant volume.

The transfer function for the system may be synthesised much as the residence time distribution is, in figure 15(b), by considering a portion of the inflowing stream $\frac{Q - q}{Q}$ to pass only through reactor 1 and thus experience merely a time delay T_1, and the rest of the inflowing stream $\frac{q}{Q}$ to pass through 1 and 2 in series.

Thus $$G(s) = \frac{Q - q}{Q} \exp(-T_1 s) + \frac{q}{Q} \frac{1}{1 + T_2 s} \exp(-T_1 s)$$

Where $$T_1 = \frac{V_1}{Q} \quad \text{and} \quad T_2 = \frac{V_2}{q}$$

therefore $$\frac{d\,G(s)}{ds} = -T_1 \frac{Q - q}{Q} \cdot \exp(-T_1 s)$$

$$-T_1 \frac{q}{Q} \frac{1}{1 + T_2 s} \cdot \exp(-T_1 s)$$

$$- \frac{q}{Q} \frac{T_2}{(1 + T_2 s)^2} \cdot \exp(-T_1 s)$$

therefore $$\tau = T_1 + \frac{T_2 q}{Q} = T_1 + \frac{V_2}{Q} \qquad (44.1)$$

and similarly $$\overline{T^2} = \frac{1}{Q}((Q - q)\, T_1^2 + q T_1^2 + 2q T_1 T_2 + 2q T_2^2)$$

therefore $$\sigma^2 = \overline{T^2} - \tau^2$$

$$= (2 - \frac{q}{Q}) \frac{q}{Q} T_2^2$$

$$= (2\frac{Q}{q} - 1)(\frac{q}{Q} T_2)^2$$

$$= (2 \frac{Q}{q} - 1) (\frac{V_2}{Q})^2 \qquad (44.2)$$

FIGURE 15 (a) MIXED MODEL FLOW DIAGRAM

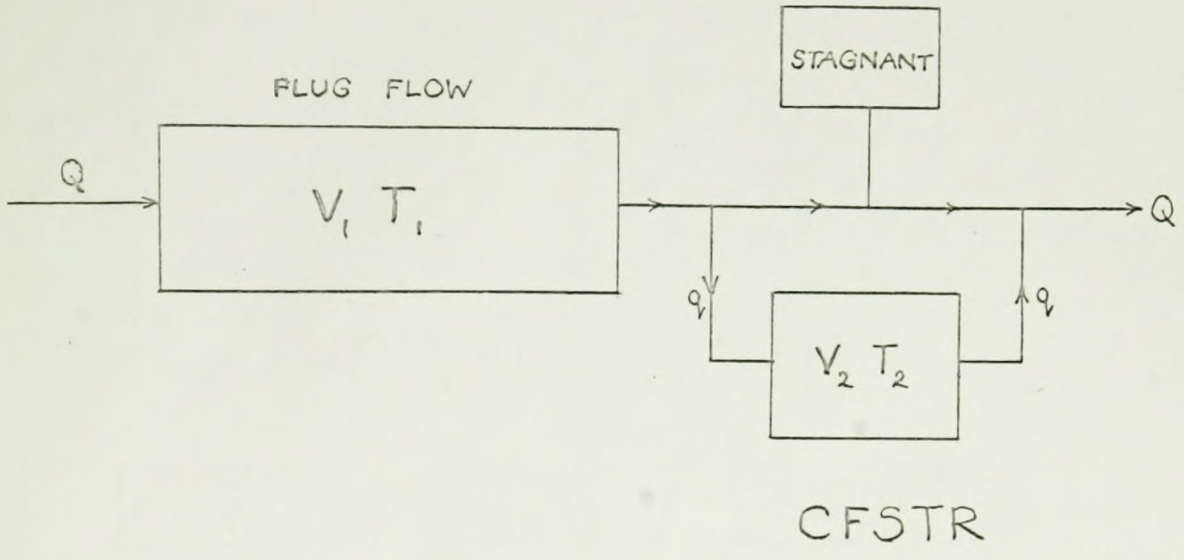

CFSTR

(b) RESIDENCE TIME DISTRIBUTION CURVE FOR ABOVE MODEL

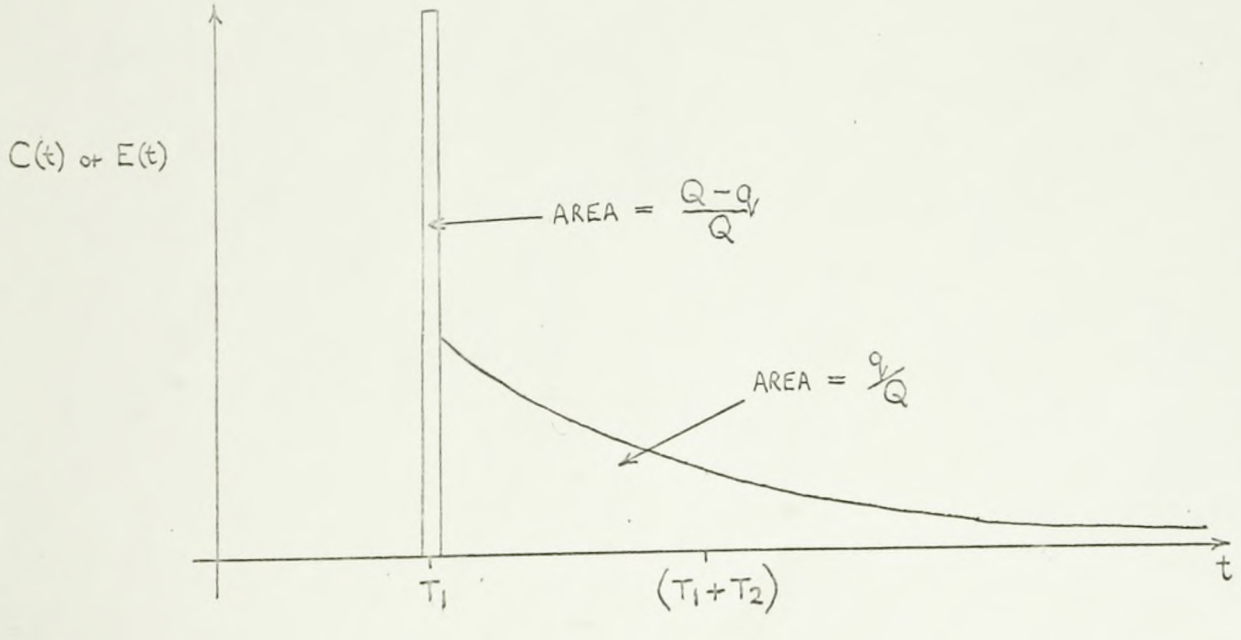

It is clear that T_1 corresponds to t_1, the time for bubbles to rise through the tank, which can be obtained from equation 31.1 by multiplying through by H (in inches):

$$T_1 = 0.0172H + 0.00081\frac{H}{Q}$$

from which $$\Upsilon = 0.0172H + 0.00081\frac{H}{Q} + \frac{V_2}{Q}$$

From equation 44.2, $$\sigma = (2\frac{Q}{q} - 1)^{\frac{1}{2}}\ \frac{V_2}{Q} \qquad (44.3)$$

The experimentally determined equations for Υ and σ (35.4 and 35.6) were:

$$\Upsilon = 0.0187H + 0.00172\frac{H}{Q} + 0.320 \text{ (seconds)}$$

and $$\sigma = 0.00223\frac{H}{Q} + 0.750 \text{ (seconds)} \qquad (44.4)$$

Comparison between experimental and theoretical equations for Υ suggests that the term in H is essentially the same in both equations and hence the required expression for V_2 is:

$$V_2 = .00091H + 0.320Q \text{ (cu.ft.)} \qquad (44.5)$$

Similarly, a comparison of the equations for σ shows that if $(2\frac{Q}{q} - 1)^{\frac{1}{2}}$ is assumed to be constant, this expression for V_2 gives the same form of σ in both equations. By substituting for V_2 in equation 44.3, and from equation 44.4, the following identity for σ is obtained:

$$\sigma = (2\frac{Q}{q} - 1)^{\frac{1}{2}}\ (.00091\frac{H}{Q} + 0.320)$$

$$\equiv 0.00233\frac{H}{Q} + 0.750$$

From this identity, the equation of terms in $\frac{H}{Q}$ gives

$$(2\frac{Q}{q} - 1)^{\frac{1}{2}} = \frac{223}{91} = 2.45 \qquad (44.6)$$

and the equation of the constant terms gives

$$(2\frac{Q}{q} - 1)^{\frac{1}{2}} = \frac{75}{32} = 2.34 \qquad (44.7)$$

The close agreement of these two values for $(2\frac{Q}{q} - 1)^{\frac{1}{2}}$ shows that the same expression for V_2 gives exact correspondence between experimental and theoretical equations for both Υ and $\bar{\sigma}$. This expression for V_2 is

$$V_2 = 0.0009H + 0.3Q$$

The mean value of $\frac{Q}{q}$, from equations 44.6 and 44.7, is 3.4.

The assumption that $(2\frac{Q}{q} - 1)^{\frac{1}{2}}$ is constant can be checked by reference to table III, since $(2\frac{Q}{q} - 1)^{\frac{1}{2}} = R$. There is a possible tendency for R to decrease with increasing air flow rate particularly at the lower tank heights, but in general the variation of R is fairly random and justifies the assumption.

It is therefore suggested that the proposed composite model can be used to represent the system over the range of the parameters covered by the experimental work, though it is possible that at the lowest air flow rate the model may not be a very good fit.

The parameters for this model are summarised below.

	Plug Flow Region	CFSTR
Flow through region (cu.ft./sec.)	Q	0.3 Q
Volume of region (cu.ft.)	0.018.H.Q. + 0.008H	0.0009H + 0.3Q
Mean residence time of contents of region (secs)	$0.018H + 0.008\frac{H}{Q}$	$0.003\frac{H}{Q} + 1.1$

3. Other Work

This part contains the results of work performed subsequently to that reported in part 2, partly to substantiate the findings therein, and partly to investigate further aspects of the system.

The first section deals with the effects of inhibited coalescence and liquid viscosity changes, using tracer methods as in part 2. The second section is a report of photographic work performed in an attempt to elucidate the mechanism of bubble removal from the system, and the third section is a report of experiments performed to obtain some measure of the rate of coalescence between bubbles within the system.

3.1 Effects on the System of Certain Liquid Properties

In this section are reported the results of investigations concerning the effects on the system of two liquid properties. These were (i) the effects of additives such as to inhibit coalescence and (ii) liquid viscosity effects.

The methods used were those previously mentioned (see part 2) and results were obtained for the voidage and for the residence time distribution parameters.

3.1.1. Effects of Coalescence

The effects on the system of inhibiting coalescence between gas bubbles were investigated by mixing minute quantities of acetic acid with the water in the tank. Pattle (12) has recorded that aqueous solutions of acetic acid stronger than .0005 parts acetic acid by weight, effectively prevent coalescence and consequently a dilution of approximately .0006 parts by weight was used.

The most noticeable effect was an increase in the voidage. The 25¼ - inch high tank was used throughout these experiments and values of the voidage fraction for various air flow rates are shown below.

Air flow rate (cu.ft./sec.)	.045	.063	.090	.135
Voidage fraction (%)	5.7	8.7	13.5	21.0

These results are also shown plotted on figure 16, which shows the line obtained previously for the voidage

FIGURE 16 VOIDAGE FRACTIONS FOR VARIOUS LIQUIDS

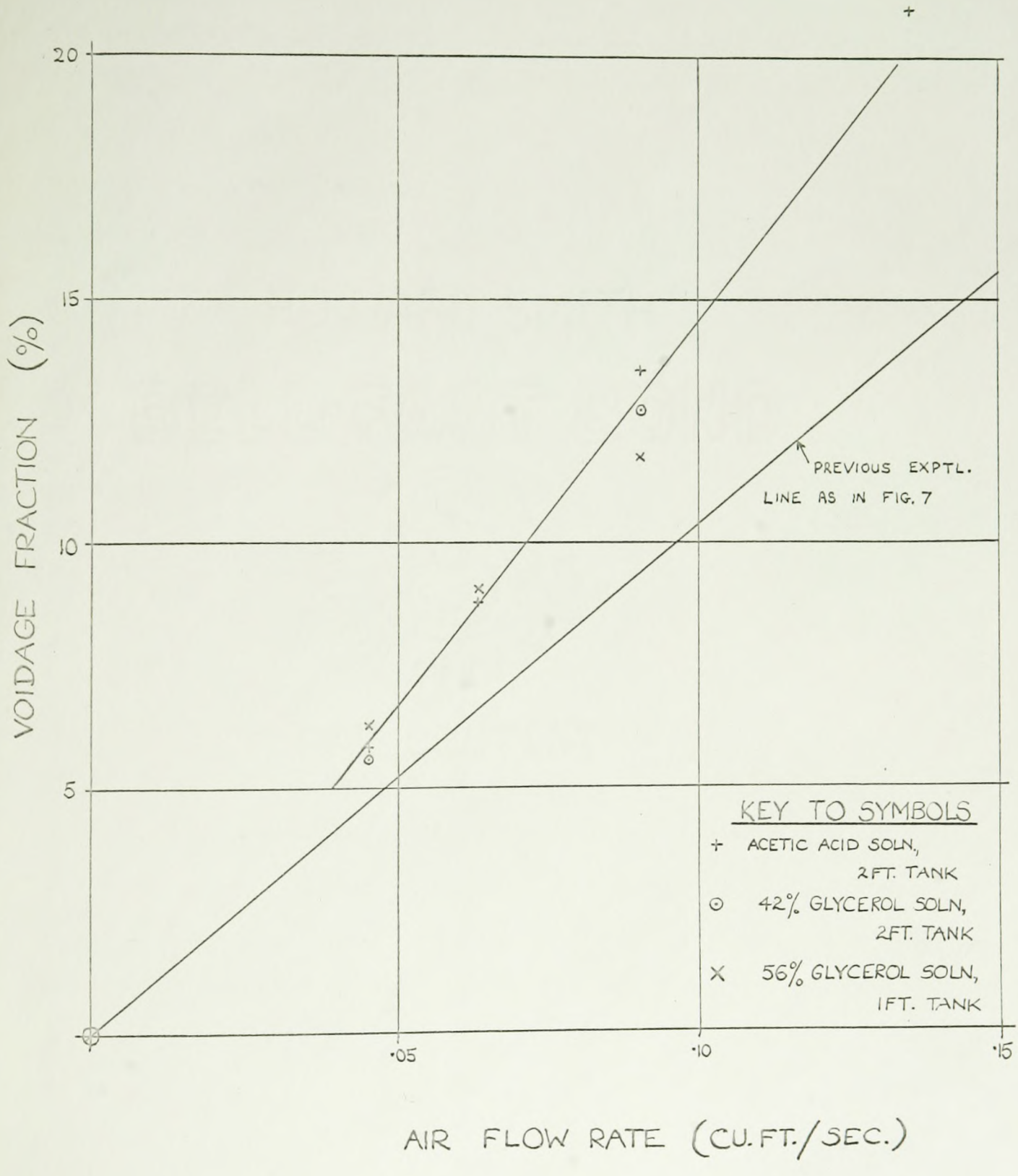

fraction under normal coalescence conditions. As can be seen, the voidage fraction in this case is increased by 20-50%, the fractional increase being greater at the higher air flow rates.

Visual observation showed that the bubbling liquid had become milky and almost opaque in appearance and this change was due to the presence of large quantities of very small bubbles. Normally small bubbles are removed from the system by coalescence with larger bubbles since their terminal velocities in the liquid are too small to allow them to reach the surface at all quickly. (This point has been more fully discussed in subsection 2.3.5.). In this case, this means of removal was no longer available and hence a large steady state concentration of them accumulated.

Tracer experiments showed that the residence time distribution curve parameters were not affected by the inhibition of coalescence nor by the associated increase in voidage. Thus the increased voidage under these conditions only contributes to an increase in the stagnant volume.

These results substantiate the arguments presented in subsection 2.3.5. that the stagnant volume corresponds to the smaller bubbles within the system.

3.1.2. Effects of Liquid Viscosity

To determine the effects of the liquid viscosity on the system, glycerol solutions of varying strengths were used. The results obtained from tracer experiments and other

work are shown in table IV, which also includes the corresponding results for pure water.

Table IV

Results for glycerol solutions

Liquid Viscosity (c.poise)	Tank Ht. (ins)	Air flow rate cu.ft./sec.	τ (secs)	Variance (sec^2)	Voidage fraction %	No. of Readings in Sample
7.0 (55% glycerol)	13.25	0.045	1.06	3.76	6.2	16
		0.063	0.95	1.53	9.0	13
		0.090	0.86	0.75	11.6	15
4.4 (43% glycerol)	25.25	0.045	1.78	3.6	5.6	15
		0.063	1.53	3.0	-	15
		0.090	1.25	-	12.8	12
Comparable readings for water						
1.0	13.25	0.045	1.02	2.76	4.8	10
		0.063	0.92	1.27	7.6	32
		0.090	0.82	0.69	9.7	13
1.0	25.25	0.045	1.65	3.29	4.3	25
		0.063	1.49	2.31	6.6	33
		0.090	1.25	2.24	8.8	18

The results for the voidage fractions are shown plotted on figure 16, and it can be seen that they are again higher than the results for water but correspond closely to those obtained with the dilute acetic acid solution. Visual observation showed there to be a large increase in the number of smaller size bubbles formed and, with the agreement of these voidage fractions with those for the acetic acid solutions, it seems likely that the voidage increase is again predominantly caused by these smaller bubbles. In this case it is assumed

that coalescence is hindered by the higher viscosity of the liquid, since Pattle (12) mentions that high viscosity organic liquids do not inhibit coalescence by surface activation.

The effects of viscosity on the mean residence time do not appear to be significant and the slight differences between these data and those for water lie well within the estimated errors of the experiment. This result suggests that the increased voidage is due entirely to an increase in the stagnant or deadwater regions - more specifically the smaller bubbles, which agrees with the observations above.

That the gas-phase mean residence time is unchanged by liquid viscosity increases of the order of 7 times, is perhaps surprising. However the report by Haberman and Morton (9), on the motion of bubbles in various liquids, shows that for bubble radii in excess of 0.25 cms., the terminal velocity of the bubbles in 42% and 56% glycerol-water solutions is no less than in pure water. Since the initial bubble size at the orifice is 0.68 cms. radius, it would appear that the velocities of all but the smaller bubbles in these glycerol solutions would be much the same as those in water. The smaller bubbles are considered to be stagnant in any case, so that the effective residence time distribution would not be altered.

The effect of liquid viscosity on the variance of the residence time distribution is more pronounced, the values being higher in all cases than those for water. Again the increase is sufficiently small that it can be accounted for by the estimated experimental error, and in the case of the values

obtained from the 25½ in. high tank, the corresponding values for water were rather low in any case.

However it is possible, since all the values are increased that a definite effect exists. In terms of the mixed flow model (subsection 2.4.4.) the effect of increasing the variance is either an increase in volume V_2 or an increase of the ratio $\frac{Q}{q}$. Since an increase in V_2 would also affect the value of the mean residence time, it seems more probable that the effect is an increase in $\frac{Q}{q}$ i.e. a decrease in flow rate q. This is feasible if flow q is considered to consist of the bubbles that tend to be at the smaller end of the size range, such that their velocities are just starting to be affected by the increased viscosity.

In summary, these results show that liquid viscosity changes in the range investigated tend to have little effect other than increasing the stagnant volume of the gas phase. A slight effect on the variance of the residence time distribution curve may exist and suggests changes in the model as mentioned.

3.2. Bubble Removal at the Surface

As an aid to understanding the mechanism of bubble removal from the system, and possibly to shed further light on the proposed model, a series of studies was made which involved the high speed filming of the changes occurring in the system when the air supply was cut off.

The experimental procedure was as follows. Initially the tank was bubbling in a steady state with a certain constant air flow rate. The camera was started and when it had reached the correct filming speed, the air supply to the lower chamber was cut off and simultaneously the lower chamber was vented to the atmosphere. This had the effect of abruptly cutting off the flow of bubbles, and the subsequent changes in the system were recorded on film. A little water drained through the orifice holes during this period but this flow was too small to appreciably affect the liquid height.

A quantitative measurement that could be obtained from the film was of the total height of the bubbling liquid. This was a very difficult measurement to make because the surface of the liquid was very broken and many waves made a consistent determination of its exact position impossible. Also, since the camera's optical axis was below the level of the surface, the picture was often confused and the rest of the surface obscured by wave crests on the side of the tank nearest to the camera. For these reasons the experimental scatter is quite

large, as can be seen from figure 17 which shows the change in liquid height with time for a typical run.

As can be seen from this figure, it is possible to split the curve into two roughly linear segments, and most of the curves show this feature.

In terms of the mixed flow model of subsection 2.4.4. and the tank flow regions of figure 5, these curves may be interpreted as follows: The first segment, A, may be considered as corresponding to the period during which the air in the plug flow region 2 is coming up and out of the tank. At the same time air from the CFSTR region 3 is also leaving the tank and thus the initial rate of change of gas-liquid volume with respect to time should equal the sum of these two flows, i.e. the total air flow rate. The table below gives the data from all the curves that could be evaluated, and it will be seen that there is reasonable agreement between the rate of change of volume calculated from the slope of segment A, and the total air flow rate before shut-off.

Run Number	1	2	3	4	5
Initial Air Flow rate (cu.ft./sec)	0.090	0.090	0.135	0.135	0.135
Slope A (cu.ft./sec)	0.080	0.088	0.109	0.140	0.122
Time to end of plug flow (sec)	0.85	0.55	0.90	0.85	-
Slope B (cu.ft./sec)	0.043	0.040	0.060	0.036	.060
$\left[\frac{\text{Slope B}}{\text{Initial Air flow}}\right]$	0.48	0.44	0.44	0.26	0.44

FIGURE 17 GRAPH OF CHANGE OF HEIGHT OF SURFACE WITH TIME WHEN AIR FLOW WAS CUT OFF.

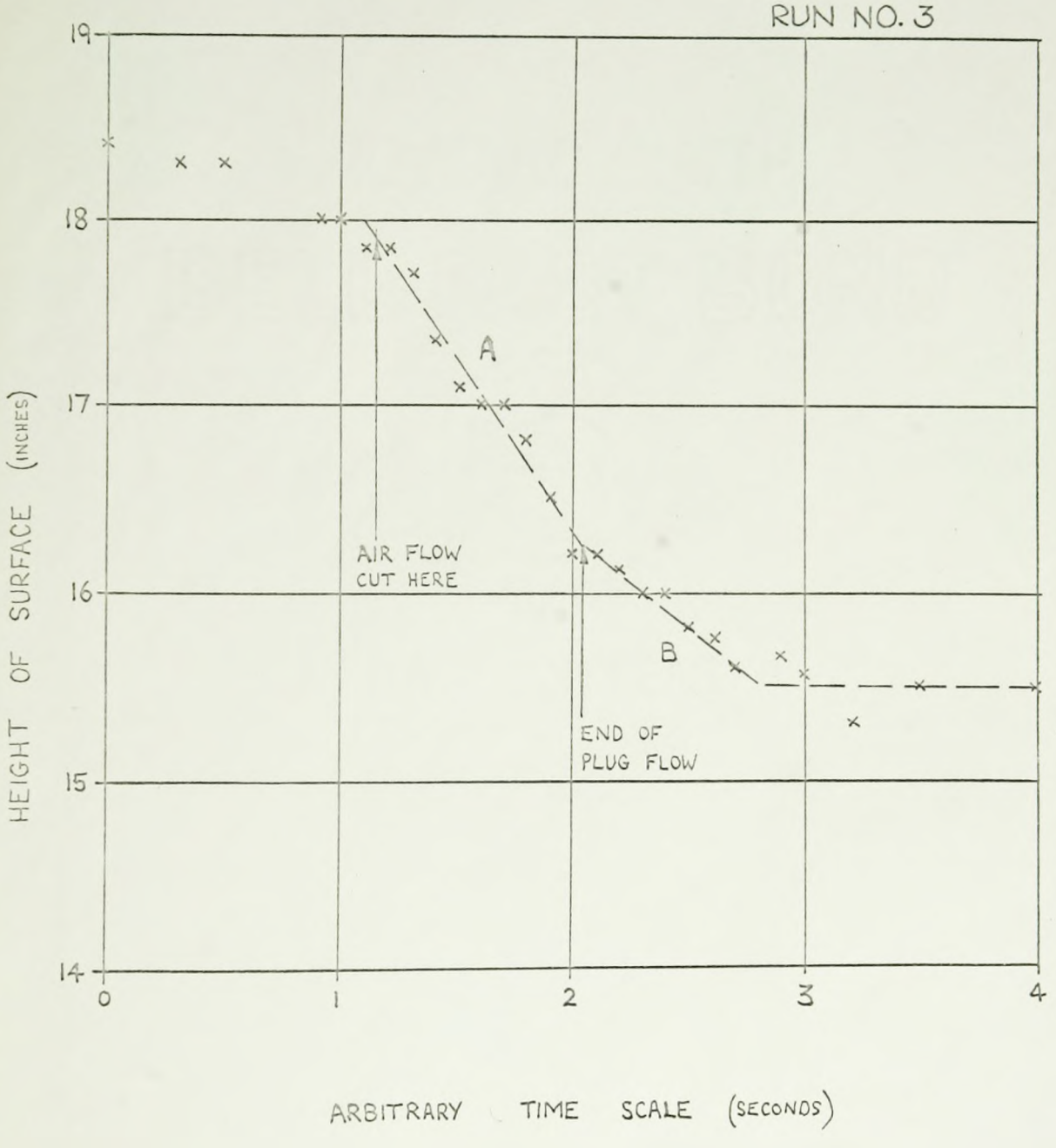

From the films it was possible to see approximately when the last of the plug flow bubbles reached the surface, and this point is marked on figure 17. At this time the circular motion of the liquid was greatly reduced and the bubbles previously swept downwards by it were beginning to rise.

The second segment of the curve, B, is again nearly linear and from the film it could be seen that this segment corresponded to the rise and loss of these bubbles from the system. The rate of loss of gas bubbles at the surface at this stage seemed to be controlled solely by the rate at which the bubbles reached the surface. Since they were fairly equally distributed in the tank the rate at which they reached the surface was constant, giving a constant slope to the segment.

In terms of the mixed flow model the slope of segment B should correspond to the sum of the flow out of CFSTR region 3, plus a certain amount of stagnant volume that flows out of the tank through the space vacated by the plug flow. If it is assumed that initially for this segment, this stagnant flow is about 1/4 to 1/3 of the total flow, since this is about the fraction of cross-sectional area previously occupied by the plug flow, a rough estimate of the magnitude of q can be made.

From the table the ratio $\frac{\text{Flow (slope B)}}{\text{Actual Initial Flow}}$ has a mean value of about 0.41, hence

$$\frac{q}{Q} \simeq 0.27 - 0.31$$

This result is in agreement with the value of 0.3 obtained for $\frac{q}{Q}$ in the previous studies.

Thus this work shows that the rate of loss of bubbles at the surface at lower rates and under less disturbed conditions seems to be determined solely by the rate at which they reach the surface. At the higher rates of loss the system was too disturbed to yield results. These loss rates may be interpreted in terms of the mixed model with good agreement as previously shown.

3.3. Rate of Bubble Coalescence

In this section is reported the investigation made into the frequency of bubble coalescence within the system. The method used is described in the following subsection, and makes use of the almost instantaneous gas phase reaction between nitric oxide and oxygen to yield nitrogen dioxide, together with the fact that nitric oxide is almost insoluble in water whereas nitrogen dioxide is very soluble.

The analysis required to evaluate the data and its results are covered in a further subsection.

3.3.1. Experimental Method, Principles, and Results

Nitric oxide was injected into the tank through the usual tracer injection system and care was taken to prevent it coming into contact with any air before it was injected. The exact amount of nitric oxide injected each time was determined by recording the reservoir pressure before and after injection.

Bubbles of pure nitric oxide did not tend to dissolve but as soon as they coalesced with air bubbles, nitrogen dioxide was formed and this dissolved rapidly to give a mixture of nitrous and nitric acids. The nitrous acid rapidly decomposes to give nitric oxide and more nitric acid and thus the net reaction for the dissolution of the nitrogen dioxide in water may be written:

$$3NO_2 + H_2O \rightarrow 2HNO_3 + NO$$

The implications of this reaction are discussed in the next subsection.

The quantity of nitric acid formed in the water, after each injection of nitric oxide was determined by means of a pH meter, which sampled a side stream of liquid taken from one drain hole and returned via another. The output of the pH meter was recorded on a chart recorder for ease in evaluating the results.

The one disadvantage of this method was that the pH of the water was buffered to some extent by dissolved carbon dioxide. Consequently a calibration between the change of pH and the amount of equivalent acid or base absorbed by the system was obtained immediately before and after the nitric oxide injection runs, by adding successive measured quantities of standardised sulphuric acid and standardised potassium hydroxide solution and recording the subsequent change of pH.

These experiments were performed with a tank height of 25¼ in., at two different air flow rates and the results were as follows:

Air flow rate (cu.ft./sec)	0.063	0.090
Mean Volume of nitric oxide injected (ccs)	57	57
Therefore Gm. moles of nitric oxide injected	2.74×10^{-3}	2.74×10^{-3}
Mean gm. moles of nitric acid formed in the water	$4.7 \pm 1.5 \times 10^{-4}$	$6.7 \pm 1.7 \times 10^{-4}$

The last line of results - gm. moles of nitric acid

formed in the water - was obtained from the changes in pH of the solution using the calibration obtained by adding standardised acid, as mentioned previously. These results were quite scattered, as is indicated by the quoted error which was estimated from the variance at the 95% confidence limits.

3.3.2. Analysis of the Results using a Model for the Coalescence Behaviour

For the coalescence model presented here, the following basic assumptions are made: (1) There is a uniform bubble size. (volume of a bubble = Vb)

(2) When coalescence occurs between two bubbles, their contents are completely mixed and this mixture then splits into two identical bubbles. This whole process is instantaneous.

(3) The probability of coalescence is constant, under constant experimental conditions, and independent of the gas composition of the bubbles, and of their position in the tank.

The reaction between oxygen (or air) and nitric oxide is practically instantaneous at room temperature (13) in the gas phase and is given by the following equation

$$2NO + O_2 \rightarrow 2\,NO_2$$

In the case of coalescence in the tank between a bubble of pure nitric oxide and one of air, since both bubbles are assumed to have the same volume, the equation must be

written $2N_2 + \frac{1}{2}O_2 + 2\frac{1}{2}NO \rightarrow 1\frac{1}{2}NO + NO_2 + 2N_2$

If the change in volume is neglected and it is assumed that the right hand mixture splits into two equal volumes (bubbles), a further coalescence gives:

$$2N_2 + \frac{1}{2}O_2 + \frac{3}{4}NO + \frac{1}{2}NO_2 + N_2 \rightarrow 1\frac{1}{4}NO_2 + \frac{1}{8}O_2 + 3N_2$$

Hence it can be seen that two coalescences are necessary to achieve complete oxidation of the nitric oxide and that an intermediate bubble composition exists containing thirty-three per cent nitric oxide, twenty-two percent nitrogen dioxide and the remainder nitrogen.

Further coalescences beyond this stage of complete oxidation only serve to dilute the concentration of nitrogen dioxide in the bubbles but at the same time the interfacial area exposed to nitrogen dioxide is increased. However it can be shown that the absorption of nitrogen dioxide is sufficiently rapid that, under the prevailing experimental conditions, 70-75% of the nitrogen dioxide formed will be dissolved. (see appendix V)

The derivation for the amount of nitrogen dioxide formed is as follows. Let m be the rate of coalescence per bubble per second, N' be the number of bubbles containing pure nitric oxide initially injected, and N the number of those bubbles remaining at time t. Also let n be the number of bubbles of nitric oxide which have only undergone one coalescence at time t, and contain thirty-three percent nitric oxide.

Therefore $$-\frac{dN}{dt} = mN \qquad (33.1)$$

and $$-\frac{dn}{dt} = mn + 2\frac{dN}{dt} = mn - 2mN \qquad (33.2)$$

Equation 33.1 assumes that all the coalescences of the nitric oxide bubbles will be with air bubbles, and does not allow for the fact that some of the coalescences will be between bubbles which each contain nitric oxide and that for these coalescences $\frac{dN}{dt} = 0$. The same argument applies to equation 33.2. However since the tracer flow rate during the period of injection is forty times less than the air flow rate, and conditions at the orifice plate tend to mix the tracer bubbles directly in with the air bubbles, these effects will only be slight and corrections for them are probably not worthwhile in view of the rather low accuracy of the experimental results.

By taking Laplace transforms in both equations 33.1 and 33.2, the following transformed equations are obtained

$$-(s\bar{N} - N') = m\bar{N}$$

$$-s\bar{n} = m\bar{n} - 2m\bar{N}$$

therefore $$\bar{N} = \frac{N'}{s + m}$$

therefore $$\bar{n} = \frac{2mN'}{(s + m)^2}$$

Inversion of these equations yields N and n:

$$N = N'\exp(-mt)$$

$$n = 2mN't.\exp(-mt)$$

The volume of nitric oxide initially injected = $N'Vb$

The volume of nitric oxide left after time t = $(N + \frac{1}{3}n)Vb$

Therefore the fraction of nitric oxide remaining after time t

$$= \frac{N + \frac{1}{3}n}{N'}$$

$$= (1 + \frac{2}{3}mt).\exp(-mt) \qquad (33.3)$$

This fraction of nitric oxide remaining, as calculated from the model, may now be equated to the experimental results, to yield a value of m, as follows.

The net reaction for the dissolution of nitrogen dioxide in water is, as mentioned previously,

$$H_2O + 3NO_2 \rightarrow 2HNO_3 + NO$$

Thus for every three moles of nitrogen dioxide dissolving, a further mole of nitric oxide is formed. Under the prevailing experimental conditions this would tend to return to the gas phase where it could be oxidised to form more nitrogen dioxide which in turn would dissolve to give nitric acid and nitric oxide. Therefore, depending on the rates at which these various steps took place, between 0.67 and 1.0 moles of nitric acid would be formed for every original mole of nitrogen dioxide dissolving. From the analysis and arguments presented in appendix V, 75% of the nitrogen dioxide formed is considered to dissolve during the mean residence time of the gas phase and consequently, for the purposes of this calculation, it is assumed that 0.55 moles of nitric acid are formed for every mole of NO_2 formed from the original nitric

oxide injected.

Thus the number of moles of nitrogen dioxide formed may be calculated from the results for the number of moles of nitric acid formed, and hence the fraction of nitric oxide not reacted may be evaluated. By equating this to expression 33.3, and using the mean residence time as a value for t, the following values of m for the two experimental cases were evaluated:

at Q = 0.063 cu.ft./sec, m = 0.53

at Q = 0.090 cu.ft./sec, m = 0.93

So far in this analysis m has been considered merely as the average coalescence rate per bubble under the conditions existing in the tank and therefore its value depends on the degree and thoroughness of mixing as well as the concentration of bubbles. This latter effect may be allowed for by considering that m is proportional to the mean concentration of bubbles in the tank,

i.e. $m = m'.c$

where $c = \frac{\text{Voidage fraction}}{\text{mean bubble volume}}$

Value of m' obtained by applying these equations are as follows:

at Q = 0.063 cu.ft./sec, $m' = 3.8 \times 10^{-4}$ cu.ft./sec and

at Q = 0.090 cu.ft./sec, $m' = 4.6 \times 10^{-4}$ cu.ft./sec

(Note that m' is the rate of coalescence per bubble per unit bubble concentration, per second, or alternatively the rate of coalescence per unit volume, per (bubble concentration)^2 per second).

From these results it is seen that m' appears to be greater at increased flow rates which is to be expected from the higher bubble velocities and degree of mixing. This increase though is not significant when compared to the estimated error in the experimental measurements and may be purely coincidental.

In view of these experimental errors, the simplicity of the model and the assumptions made, the values of m and m' should be regarded only as estimates of the order of magnitude of the true values, rather than as accurate results. The magnitude of m is such that for the higher flow rate it predicts that on the average every bubble can be expected to undergo at least one coalescence whilst in the tank, and for the lower flow rate the expectation of coalescence of each bubble whilst in the tank drops to about 3/4.

4. Summary and Conclusions

This thesis has reported the investigations made into the use of tracer methods to determine the residence time distribution of the gas phase existing in a bubbling reactor. Other work has been performed to obtain a more complete picture of the mixing patterns occurring within the gas phase, and the results of the whole work may be summarised as follows.

(a) The bubble and liquid flow within the tank had a pronounced circular pattern which tended to give high upward bubble velocities. Consequently a large proportion of the air flow passed through the tank in a very short time.

(b) The mean residence time and the standard deviation of the residence time distribution could be related to the tank height and the air flow rate by the following equations:

$$\tau = 0.0187H + 0.00172\frac{H}{Q} + 0.320 \quad \text{(secs)}$$

$$\sigma = 0.00223\frac{H}{Q} + 0.750 \quad \text{(secs)}$$

These equations could be represented by a composite region model, composed of a plug flow reactor followed by a CFSTR with by-pass flow.

(c) The voidage fraction increased linearly with the air flow rate.

(d) At the higher air flow rates, the mean residence time was far smaller than would be predicted from the ratio of the total gas volume to the air flow rate. This indicates that

an increasing proportion of the gas volume acted as stagnant volume which has been identified with the small gas bubbles.

(e) The decrease in the standard deviation of the residence time distribution suggests that the flow through the system approached plug flow at the higher air flow rates.

(f) Liquid viscosity changes in the range 1 - 7 centipoise affected only the voidage fraction, and this effect was thought to be due to the inhibition of coalescence.

(g) The bubble coalescence rate within the system was quite high and suggested that most bubbles undergo at least one coalescence whilst in the system.

The practical applications of this work are discussed in appendix VI.

As an extension of this work, the following suggestions are made.

(i) Further work could be done using higher air flow rates, though this would require changes in the sampling system at least. In the present work, it was found that at air flow rates above those used, the surface of the liquid became so disturbed that its position was difficult to determine and attempts to sample the gas flow as it emerged from the surface resulted in flooding of the sampling system. As an alternative to redesigning the sampling system, a different type of tracer and detection system could be used, which would not be affected by the presence of liquid. An example that may be cited, is the method of Calderbank et al.(3) who used

mercury vapour as the tracer and U.V. absorption for its detection.

(ii) The effects of different methods of air injection, to give different flow patterns within the system, could be investigated. This might require a different method of tracer injection, or more modifications as mentioned above might be considered.

(iii) The behaviour of the system as a gas-liquid contacting device could be studied, using a standard reaction such as the oxidation of sodium sulphite solution, and this would test the results contained herein. In this connection further information would also be required on the mixing occurring in the liquid phase and the gas-liquid interfacial area or the mean bubble size.

(iv) Further investigations could also be made of the effects of liquid properties, particularly of the effects of liquid viscosities higher than the range covered in the present work.

APPENDICES

Appendix I - Literature Survey

This survey has been divided into three sections. The first deals with papers on the subject of bubbling at single or multiple orifices, and the second with papers on the determination of reactor flow patterns and related behaviour. The few papers covering both topics are included in the latter section. The third section indicates the relevant findings that influenced the design and operation in this work.

(i) Much work has been done on the formation of bubbles at single orifices (5, 6, 12, 15, 16, 17, 18, 19). This has shown that as the rate of gas flow through an orifice is increased, there are three distinct regimes of bubble formation.

In the first regime, at very low gas flow rates, bubble formation is determined by the static equilibrium of surface tension and buoyancy forces. From a balance of these forces, an equation for the bubble volume is obtained which depends on the diameter of the orifice and the physical properties of the system,

$$Vb = \frac{2\pi r.\gamma}{\Delta\rho.g}$$

(The symbols in this section will be found with the rest of the nomenclature at the end of the thesis).

This formula has been tested experimentally by many

of the early workers in this field, whose results are listed by Datta, Napier and Hewitt (16), as well as by Davidson and Amick (5) and by Van Krevelen and Hoftijzer (18). These workers confirm that for a given system with constant orifice size, the bubble size is constant for varying flow rate. This regime can be conveniently called the constant volume regime.

At higher gas flow rates, the bubbling frequency stops increasing and remains fairly constant while the bubble volume increases instead. This regime, the constant frequency regime, has been investigated by Van Krevelen and Hoftijzer (18), Davidson and Amick (5), and by Leibson et al. (6). Van Krevelen and Hoftijzer (18), using orifices less than 0.02 inches in diameter, claimed that in this regime bubble size is independent of orifice size, but work by Davidson and Amick (5), and Leibson et al. (6) using larger size orifices, has shown a relationship between bubble size and the square root of the orifice diameter. Their equations are:

$$Vb = 0.189\ (Qr^{\frac{1}{2}})^{0.95}$$

and $D = 0.18\ d^{\frac{1}{2}}Re^{1/3}$, respectively and these show very good agreement when reduced to a similar form (6). Davidson and Amick (5) also derive the equation for the constant bubble frequency and show it to be:

$$f = 9.09Q^{0.133}\ r^{-0.434}$$

Thus the bubble frequency is not quite constant but increases slightly with the gas flow rate.

The third regime of bubbling occurs at higher gas flows, when turbulence develops in the gas flow through the orifice. This regime was investigated by Leibson et al.(6), who showed that bubble formation was very non-uniform, and that the distribution of bubbles sizes was close to a logarithmic normal probability distribution.

The effect of the volume of the gas chamber immediately below the orifice (V_c) has been studied by Hughes et al.(17) and by Davidson and Amick (5). The former workers found that bubble formation depended on a dimensionless group

$$\left(Nc = \frac{\Delta\rho . Vc . g}{\pi + 2 . \rho . c_s^2}\right),$$

for which a critical value was about 0.85. For subcritical values of this group (i.e. smaller chamber volumes), bubble formation was found to be independent of the chamber volume and to occur by a mechanism of delayed release. Bubble growth is accompanied by a rise in the chamber pressure until a point is reached at which the bubble detaches itself and the chamber pressure drops abruptly. For values of this group, Nc, greater than 0.85, bubble formation depends on the size of chamber volume and, under identical conditions, the bubble volume increases as the chamber volume increases. The chamber pressure remains constant during bubble growth and release, which is a faster process than in the previous case. Davidson and Amick (5) also investigated these effects and confirmed the above results.

The effects of liquid properties and hydrostatic

pressure have been investigated by several of the workers mentioned above (15, 16, 12). In general it has been found that viscosity and hydrostatic pressure have little effect on bubble size, but that with surface tension variations, bubble volumes were found to increase linearly as might be expected from the simple hydrostatic formula previously quoted. The motion of single bubbles in liquids, after formation, has been extensively reviewed and studied at the David W. Taylor Model Basin, and reports of this work are given by Rosenberg (29) and by Haberman and Morton (9).

The performance of multiple orifices has not received as much investigation to date as that of single orifices.

An early paper by Verschoor (7) describes work done with fairly narrow columns, at the bottom of which the gas was introduced into the liquid through a porous glass filter. Using a number of different liquids, he found that at the lower gas flow rates, the voidage increased linearly with gas flow up to a critical point. At this point the voidage decreased with increasing gas flow, but then at even higher gas flow rates, the voidage increased again. For these measurements, a range of gas superficial velocities of 0 - 160 cms/sec. was used. He also calculated the mean ascending bubble velocities which showed an irregular behaviour.

Similar work is reported by Siemes and co-workers (20, 21, 22) who used gas distributors made of sintered glass and sintered metal. By photographing bubble swarms, they obtained bubble size distributions and observed the effects o.

these of distributor pore size and gas flow rate.

Calderbank (4) has investigated the performance of multiple slots and orifices under conditions similar to common industrial practice. He found that under a very wide range of conditions, the frequency of bubbling remains constant at about 16 - 20 bubbles/sec., and showed this to be consistent with the results obtained with single orifices by other workers. In a later paper Calderbank and Rennie (23) studied the properties of foams formed on sieve plates with cocurrent liquid flow. From flash photographs, using a unique statistical method, they determined the Sauter mean bubble size and found their results to compare very well with those of Leibson et al. (6) for single orifices.

The contacting efficiencies of single and multiple orifice plates in a one inch pipe, with cocurrent gas-liquid flow was investigated by Ottmers and Rase (24). They found the contacting efficiency to be fairly insensitive to the type of orifice plate used, whether single orifice or multiple orifice, but to be far more dependent on the total gas flow rate and the plate spacing.

(ii) There have been very many papers published on reactor flow patterns and residence time distributions of reactors and for a complete review and bibliography the reader is referred to the review on the subject by Levenspiel and Bischoff (8). The selection of papers here will be confined to those with a bearing on the present work and more

specifically to those dealing with stirred tanks.

The mixing efficiency of stirred tanks containing miscible liquids has been studied by Cholette and Cloutier (25), and also by Van de Vusse (26). The former workers studied the changes in outlet concentration for a step change in the inlet concentration and found their results could be interpreted by considering the actual stirred tank to be a combination of an ideal CFSTR, a bypass stream which did not mix with any of the tank contents, and a further volume that did not contribute at all to the mixing and could be considered as stagnant. The apparent volume of the CFSTR they named the active volume and they found that the size of this depended on the agitator speed, the type of impeller, and the location of the feed inlet.

Van de Vusse (26), using a "Schlieren" technique, studied the time required to completely mix two layers of miscible liquids in a stirred tank, and he found this time to be approximately the time required for the impeller to circulate the total volume of the tank once. In a later paper (27), he proposed a model for this system in terms of circulating streams of liquid within the tank which are pumped around by the impeller, and he correlated the performance of this model with experimental findings.

In the field of bubbling reactors, the only residence time studies on the gas phase so far reported are by Westerterp et al.(1) and by Calderbank, Moo-Young, and Bibby (3), though Gal-Or and Resnick (28) have mentioned that work on

this topic is in progress.

Westerterp and co-workers (1) studied the response to a step change in composition of the gas input to a gas-liquid stirred tank reactor, and found the behaviour of the gas phase to be intermediate between one CFSTR and two CFSTR's in series. They explained this by considering that the impeller divided the tank flow patterns to give two perfectly mixed volumes. Their equipment and techniques were similar to those used in the present work and are further discussed in the following subsection.

Calderbank and co-workers (3) investigated the residence time distribution and the rate of coalescence for clouds of uniform bubbles rising vertically in a deep column of liquid. They found that coalescence occurred in their system by a mechanism of a larger spherical cap bubble, once formed, rising rapidly and sweeping smaller elliptical bubbles from its path. Under these conditions they found that coalescence rates increased rapidly as the viscosity was increased and this was due to "wake effects" of the spherical cap bubble. From their residence time distribution curves it was deduced that the flow within their system was close to plug flow.

Other work on coalescence in two-phase systems has been done by Madden and Damerell (30), who studied the rate of coalescence between drops in a two-phase liquid-liquid system in a stirred tank reactor. They found that the coalescence rate was increased both by the impeller speed, and by the volume of the dispersed phase.

(iii) The work reported in the first section of this literature survey shows that, by suitable design and operation, bubble formation can be in one of three regimes with respect to gas flow rate, and in one of two regimes according to the volume of the lower gas chamber. In this study it was decided to work in the constant frequency regime with larger chamber volumes, since these are the conditions that prevail in industrial plants. The orifice size and spacing on the plate were determined such that the bubbles would not interfere with one another at the plate during formation.

The selection of papers in the second section indicates methods and findings of other workers in this field and provides a comparison with the findings of the present work. The work of Westerterp et al.(1) may be directly compared with the present study and the following similarities and differences may be enumerated:

(a) The physical dimensions of the equipment were much the same for the two cases, though theirs was a stirred tank reactor.

(b) In their work, the step change in tracer concentration was introduced into the gas flow before it entered the tank through a ring-shaped distributor. This could not be done in the present work since ideal plug flow could not occur in the bottom chamber.

(c) The top of their tank was conical to allow the whole of the gas flow to be collected, and the volume of the gas space in the cone was reduced by having the liquid level

well above the base of the cone. This was investigated in the present work, but it was found that the presence of the cone greatly affected the liquid and bubble flow patterns. Thus it would not be possible to relate the results so obtained to the behaviour of a normal, flat-topped, cylindrical tank.

(d) The gas space in the cone above the liquid was well stirred to allow them to assume ideal CFSTR flow for this region. In the present work, this was not considered necessary because of the small cone volume.

(e) A conventional method of using packing to demist the gas was used, through which they assumed that plug flow occurred. Packing was not used in the present work because complex flow patterns might be associated with it, and in any case it was not needed.

(f) A similar method of detection was used; a side stream was drawn off through an orifice to a gas thermal conductivity detector operating under partial vacuum. Their detector consisted of electrical filaments mounted directly in the wall of the tube through which the sample stream passed; this configuration gave a fast response time.

Appendix II

II (a) The Operation of the Analogue Computer

A Pace TR-10 computer was used, with a computing circuit as shown in figure 18. The signal voltages were kept as high as possible throughout the circuit to ensure the best possible accuracy and for this reason potentiometers were used extensively. The settings of these potentiometers shown on the diagram were for when helium was used as the tracer gas. When carbon dioxide was used, more sensitivity was required and the settings given in brackets were used.

The integrators were switched on just before the timer was triggered, but their outputs remained at zero because the input signal was zero for $t < o$. At $t = o$, the timer momentarily closed the circuit of the two wires fed to it, which switched the comparator. This in turn switched on the input to the time ramp generating integrator, which generated a time signal until its value became 12.V. This is the maximum operational signal allowed on this computer and at this point the comparator switched the time ramp off. The total time for which the ramp was generated depended on the setting of potentiometer 9 and was adjusted to suit the experimental conditions. Thus, the time ramp was made as steep as possible without it being switched off before the cut-off point on the experimental residence time distribution curve was reached. Typical settings of potentiometer 9 were

FIGURE 18 ANALOGUE COMPUTER CIRCUIT

(MODEL : PACE TR-10)

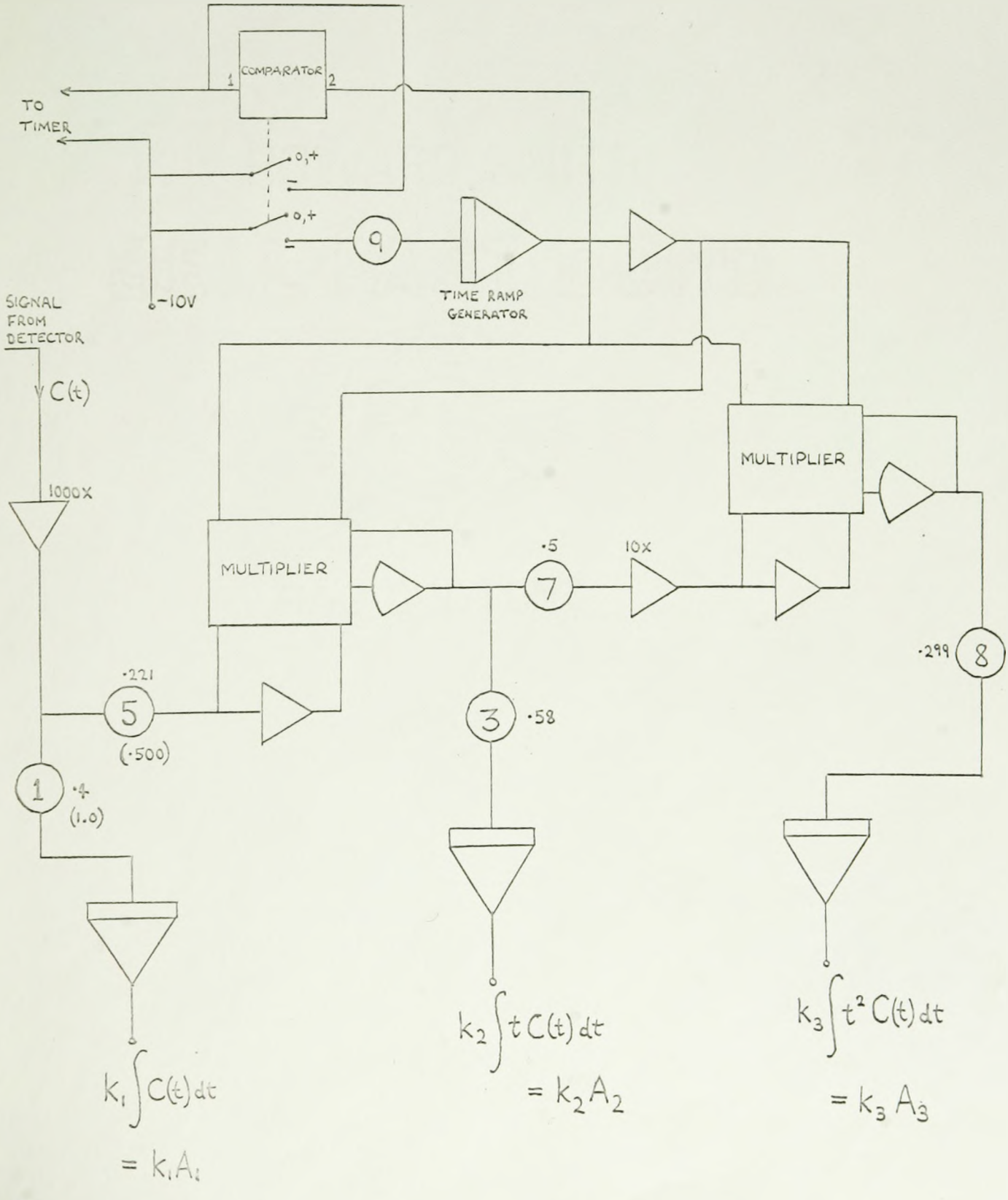

0.1 and 0.08 giving duration times of 12 secs. and 15 secs. respectively.

The constants k_1, k_2, and k_3, which had to be used in converting the computed figures to the required integrals could be calculated from the potentiometer settings. When helium was used as the tracer gas and the time ramp was generated at 1V/sec., the values of these constants were:

$$\frac{k_1}{k_2} = 2.9$$

$$\frac{k_1}{k_3} = 12.1$$

II (b) The Operation of the Detector

The circuit diagram of the hot-wire detector (Gow-Mac model 9285) is shown in figure 19 (a). The principle of its operation as an instrument for measuring gas thermal conductivities is as follows.

Four tungsten filaments (S1, S2, R1, and R2) are electrically connected as a standard Wheatstone bridge circuit, and are set into small holes in a solid metal block. The reference and sample gas streams pass through the holes and can diffuse around the filaments in the order indicated in fig. 19 (a). When thermal equilibrium is attained, the rate of heat loss by the filaments through the surrounding gas to the block equals the rate of heat gained electrically by the filaments. As the temperature of the filaments is constant,

FIGURE 19 (a) HOT WIRE DETECTOR CIRCUIT DIAGRAM

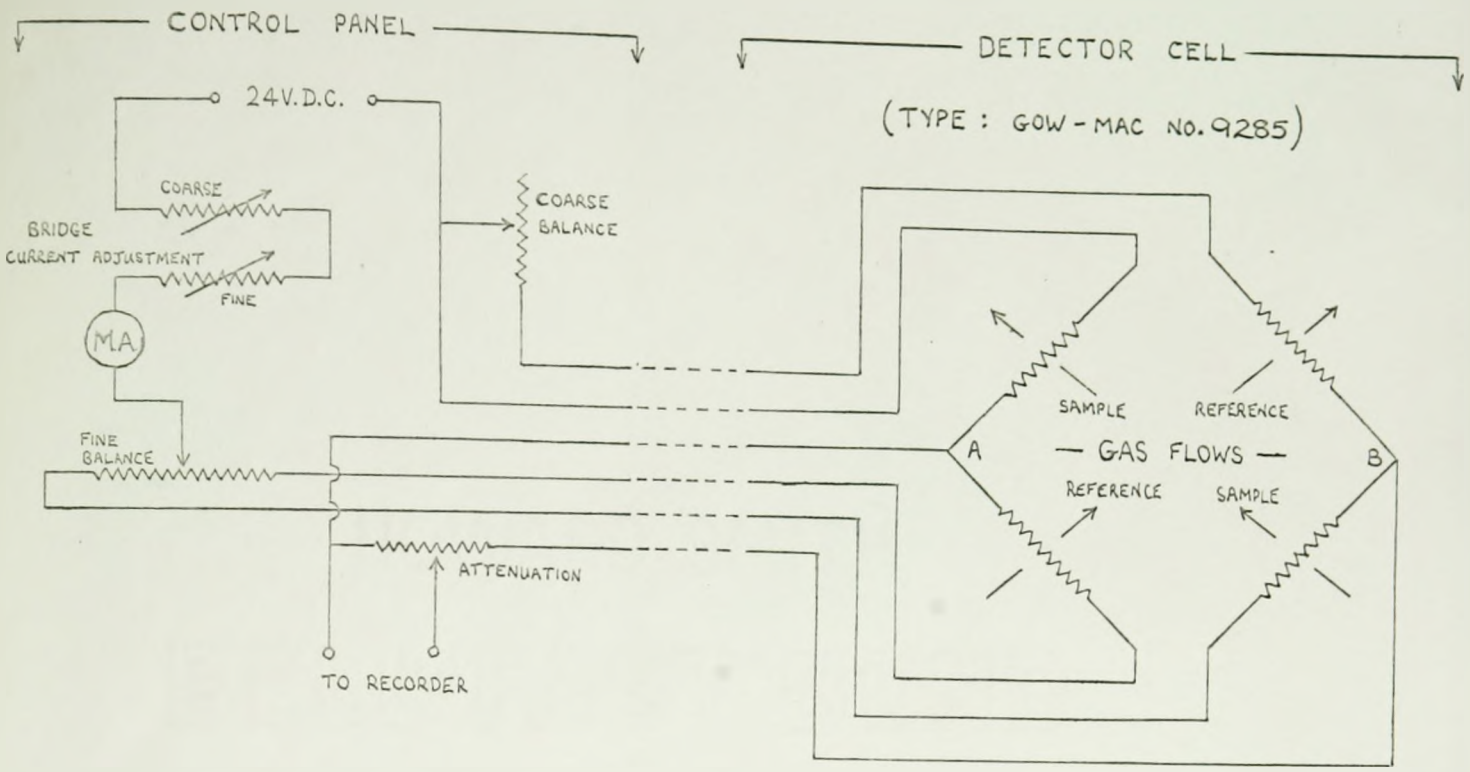

(b) EXPERIMENTAL CALIBRATION CURVE FOR DETECTOR

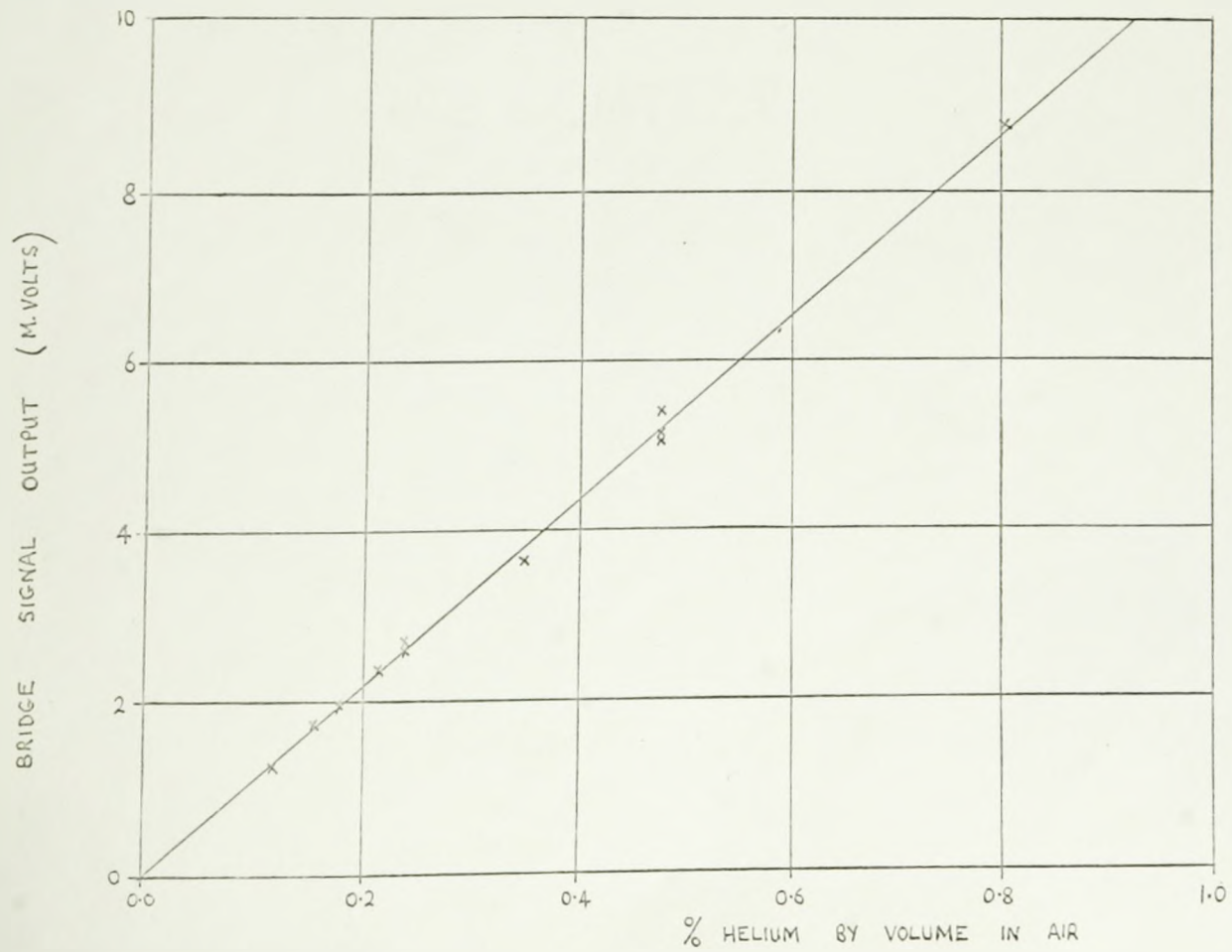

their electrical resistance will also be constant. This allows the bridge to be balanced electrically such that no current flows through the recording circuit connected between A and B.

If now the composition of the sample stream changes, such that its thermal conductivity rises, for example, the heat loss from S1 and S2 will increase, and their temperatures and also their electrical resistance will be lowered. This means that the bridge is no longer electrically balanced, and a voltage exists across the recording circuit linked between A and B. By suitable design, the magnitude of this voltage can be made proportional to the concentration of one component in the sample stream, and this is illustrated in figure 19 (b) which shows the experimental response of the detector for sample stream concentration changes.

A reference gas stream is used to minimise the effects of external conditions, such as the temperature of the block and flow variations, on the output signal.

The normal operating conditions for the detector when helium was used as the tracer gas were:

Total Bridge current	= 145 m.Amps.
Attenuation	= 1
Recorder input sensitivity	= 10 mV. for full scale
Gas Sample stream flow rate	= 350 cc/min.
Absolute pressure of gas	= 6.2 cms. of mercury
Gas reference stream flow rate	= 150 cc/min.

When using carbon dioxide as the tracer gas, more sensitivity was required and the following changes were made in the operating conditions:

Total Bridge current = 185 m.Amps.

Recorder input sensitivity = 1 mV. for full scale

It should be noted that although this sensitivity allowed carbon dioxide to be used as a tracer gas, the signal to noise ratio was much lower in this case, and the optimum signal to noise ratio was only achieved using helium tracer gas under the conditions specified.

The response of the detector with respect to time was determined experimentally as follows. The detector cell was set to the normal operating conditions and the probe was placed so that it sampled an air stream, in which a small concentration of helium was maintained by a flow of helium from a nozzle immediately upstream from the probe. The relative flow rates were arranged such that the signal output from the detector remained steady. The flow of helium could be cut off by the action of a solenoid valve, thus introducing a step change in concentration of the air stream. The resulting F curve, obtained from the detector, was recorded on an oscillograph which also recorded the shutting of the solenoid valve.

These F curves showed first a time delay of $\frac{1}{100} - \frac{1}{50}$ of a second and then an exponential decay curve. The time constant for this exponential was found to be 0.35 secs.

Thus in terms of ideal flow units the detector can be represented by a CFSTR of mean residence time 0.35 seconds in series with a time delay of about 0.02 seconds.

This response time is faster than that quoted by the manufacturers, who quote (31) a range of 1 - 1.5 secs. However this range refers to different cell conditions, namely atmospheric pressure and a flow rate of 60 cc/min., both of which factors would be expected to decrease the response time of the diffusion cell.

II (c) Photographic Details

The set-up for the photographic studies was as shown in figure 20. Back-lighting was used exclusively; the effect was that the bubbles showed up in silhouette against the bright background of the translucent opal glass screen.

A Fastax 16 m.m., high-speed camera was used with film speeds of 170-300 frames/sec.

FIGURE 20 PLAN VIEW OF PHOTOGRAPHIC ARRANGEMENTS

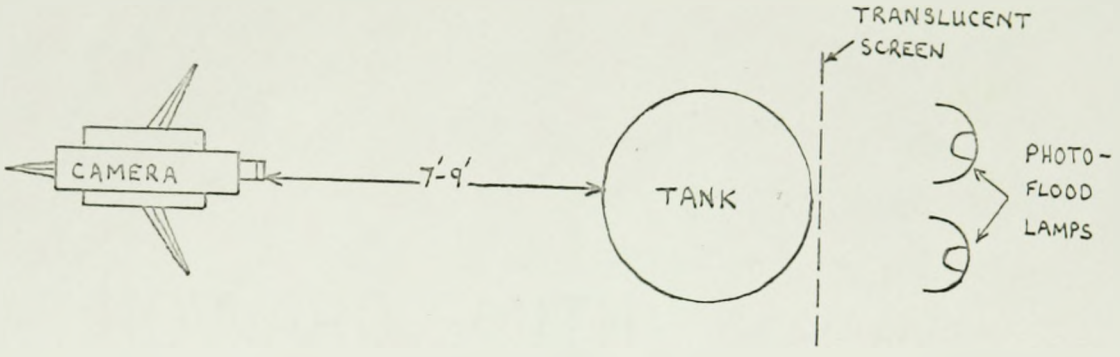

FIGURE 21 TAIL PART OF DETECTOR RESPONSE CURVE

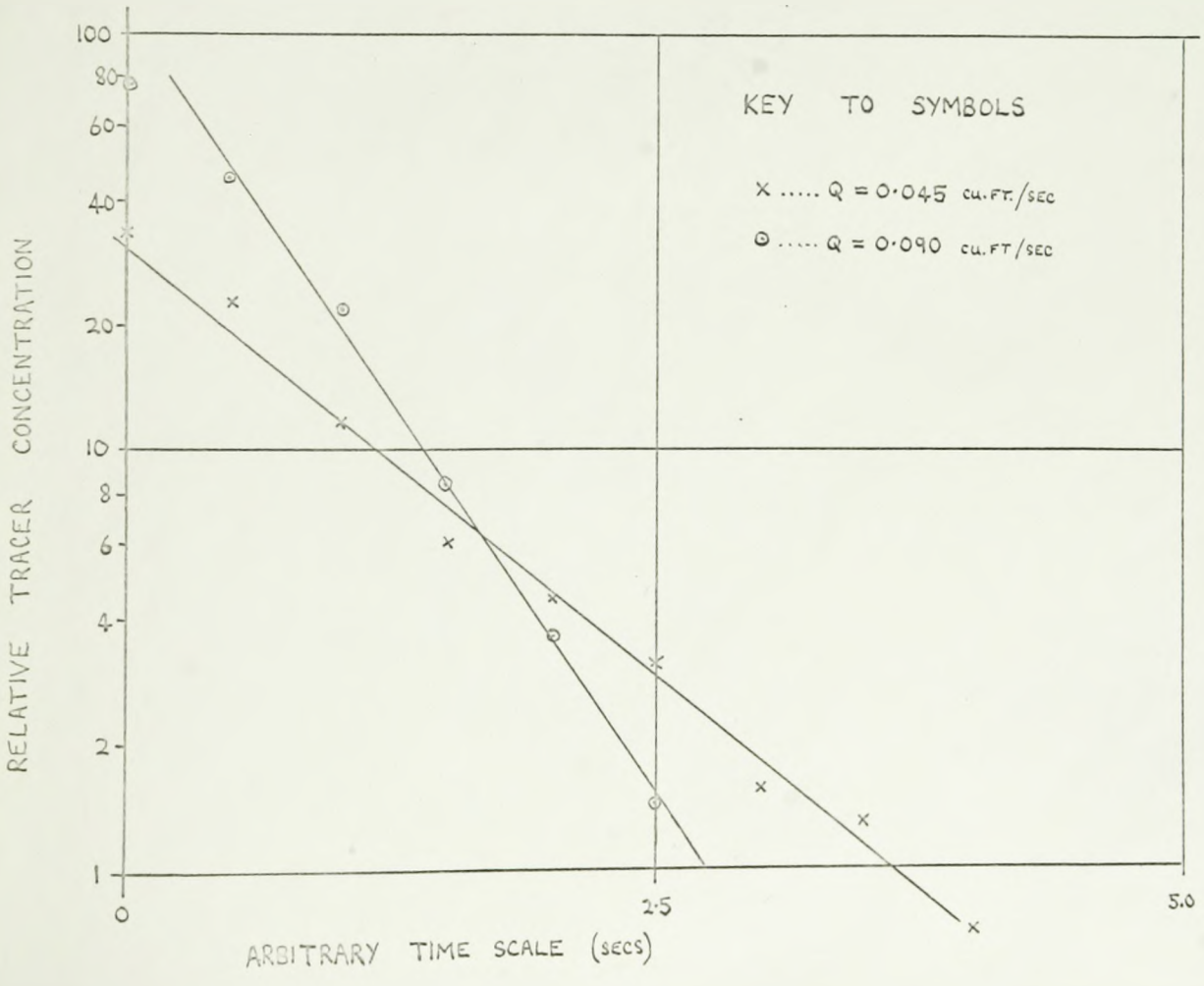

Appendix III

III (a) Measurement of ascending bubble velocities

The velocities of ascending bubbles were obtained from the motion pictures by the technique of observing the change in position on the screen of the projected picture of a bubble for a number of successive film frames. Since a reference height scale and a stop watch were included in the total picture, this technique enabled the velocity of the bubble to be calculated. This procedure was followed for ascending bubbles in the main stream (region 2) at different heights within the tank to allow a mean rising bubble velocity to be obtained.

The results obtained showed considerable scatter, even within samples taken under the same experimental conditions, and analyses of variance were performed between the samples to determine whether the two variable parameters - the overall tank height and the air flow rate - affected the bubble velocities. It was found from these analyses that the effect of the overall tank height was not significant, but that the effect of air flow rate was significant.

To take account of the effects of the air flow rate on the ascending bubble velocities, a correlation was performed on the data of $\frac{1}{v}$ against $\frac{1}{Q}$. $\frac{1}{v}$ was used as the dependent variable, instead of the velocity (v) itself, because a more useful expression for the time of rise of a bubble up through

the tank could thereby be obtained.

The result of this correlation was:

$$\frac{1}{v} = 0.0097\frac{1}{Q} + 0.207 \text{ (sec./ft.)} \qquad \text{(A3.1)}$$

and the standard deviation of this line was 0.063 sec./ft.

III (b) The Response Characteristics of the Sampling System

In this section, both the experimentally obtained response and the theoretically predicted response of the sampling system are analysed and found to give good agreement.

(i) Experimental Response

This was obtained by injecting a pulse of tracer into the gas flow as it emerged from the bubbling liquid immediately underneath the sampling cone. The direction of injection was side-ways, as shown in figure 4, and the position of the injection nozzle was varied from the centre to the side of the cone without any noticeable change in the response.

From the results obtained, the average values of the mean residence time at the following air flow rates were:

Air flow rate (Q) (cu.ft./sec)	Value of mean residence time (from analogue computer) (secs.)
0.045	1.65
0.063	1.33
0.090	1.12

These points lie on a straight line given by the equation:

$$\text{Mean residence time} = 0.048\frac{1}{Q} + 0.59 \qquad \text{(A3.2)}$$

The tail part of the response curve was found to have the shape of an exponential. This was verified, and the time constant of the exponential obtained, by plotting the tail of the response curve on a semi-logarithmic graph as shown in figure 21.

This type of response would be obtained from a CFSTR having a mean residence time equal to the reciprocal of the time constant of the exponential. The average of the equivalent CFSTR mean residence times for the following flow rates is shown below:

Air flow rate (Q) Cu.ft./sec.	Equivalent mean residence time of CFSTR (from graphs) (secs.)
0.045	1.06
0.063	0.70
0.090	0.58

These results show the mean residence time to be directly proportional to $\frac{1}{Q}$, the relationship being:

$$\text{Equivalent M.R.T. of CFSTR} = .049\frac{1}{Q}$$

A comparison of this result with equation A3.2, suggests that the mean residence time of the overall sampling system may be represented by a CFSTR in series with a plug flow section. The mean residence time of the CFSTR varies inversely with the air flow while the time delay due to the plug flow section has a constant value.

These results were used to correct the experimental response curve as described in subsection 2.3.4. and shown in

figure 8. The mean values of the variance obtained by the tracer studies are given at the end of the following sub-section.

(ii) Theoretical Response

The dimensions of the sampling system are shown in figure 4. The system may be divided into two parts; that part between the liquid surface and the probe in which the air flow varies with the main air flow rate through the tank, and that part including the probe and the detection cell where the flow is constant.

For the first part, the total volume,

V = vol. under cone
+ vol. of cone
+ vol. of cone neck up to the probe.
= 11.9 + 11.9 + 0.8
= 24.6 cu. ins.
= 0.014 cu. ft.

The air flow through this first part is one quarter of the total air flow = 1/4 Q cu.ft./sec.

Therefore the mean residence time of this part

$$= 0.056\frac{1}{Q} \text{ secs.}$$

This assumes that the flow uses the whole volume and that there are no stagnant regions.

The response time of the second part has already been mentioned, (appendix II(b)), and was found to be equivalent to a CFSTR in series with a time delay, with mean residence times of 0.35 secs. and 0.02 secs. respectively. Consequently

the total mean residence time of the sampling system is given by

$$\tau_s = 0.056\frac{1}{Q} + 0.37$$

However, before comparing this expression with equation A3.2, the effect of using a non-ideal pulse to determine the experimental mean residence time must be allowed for. It is shown later (appendix III (e)) that this has the effect of adding about 0.3 secs. to the measured mean residence time.

Thus the measured mean residence time should be

$$\tau_s = 0.056\frac{1}{Q} + 0.67 \qquad \text{(A3.3)}$$

A comparison shows that equations A3.3 and A3.2 are in good agreement and suggests that the whole of the sampling system below the probe behaves as a CFSTR. This is possibly due to the mixing action of the bursting bubbles and the general movement of the top surface of the liquid.

The theoretical variance of the residence time distribution for the sampling system may be easily obtained, since the standard deviation of the residence time distribution equals the mean residence time for a CFSTR and is zero for a time delay. Hence the total variance of the sampling system assuming the whole system below the probe to act as a CFSTR, at various air flow rates, is as follows:-

Air Flow Rate cu.ft./sec.	Theoretical variance sec^2	Experimental Variance sec^2
0.045	1.67	1.2
0.063	0.92	0.7
0.090	0.52	0.5

The experimental values are also tabulated and it can be seen that agreement is good at the high air flow rate but gets rapidly worse at the lower air flow rates. Two possible causes may account for this:

(1) The cut-off point on the experimental curve will reduce the experimental value below the true value.

(2) The assumption of CFSTR flow below the probe is not completely correct, and any proportion of plug flow in this region will decrease the variance.

III (c) Position of the Sampling System

As the flow of liquid and gas bubbles within the tank is non-symmetrical, it was thought possible that the position of the collector cone might influence the residence time distribution curve obtained. This would happen if gas having certain residence times consistently appeared at a certain part of the surface, relative to the position of main bubble flow.

Normally the collector was positioned in the centre of the grid, and all the results quoted were obtained with it in this position. However, as the radius of the lower rim of the cone was only half that of the tank, the collector could be moved from one side of the tank to the other. To check the effect of this, two sets of runs were made with the collector positioned directly above the rising bubble region (position A in figure 5). These runs were made in the shortest tank (H = 13¼ inches), at the lower air flow rates, because

the circular flow was most stable and pronounced under these conditions, and region 3 had least effect. Therefore it was to be expected that any effects of cone position would be most noticeable under these conditions.

The results of these runs were as follows:

Tank Height (ins.)	Air Flow Rate (cu.ft./sec.)	Mean Residence Time (secs.)	Variance: σ^2 (sec^2)	No. of readings in sample
13.25	0.045	0.95	1.45	29
13.25	0.063	0.95	1.85	23

The values of the mean residence time are close to the previous values and well within the estimated experimental error. The values of the variance though not close to previous values, are still well within the estimated experimental error. However, no trend appears from these figures, since they are higher than those previously obtained for Q = 0.063 cu.ft./sec., but lower for Q = 0.045 cu.ft./sec.

It was therefore concluded that the position of the collector had no distinct detectable influence on the results as obtained under the existing experimental conditions.

III (d) Effects of Tracer Gas Solubility

In the present set of experiments, using a delta function pulse input of tracer gas, it is possible for the solubility of the tracer gas to distort the residence time distribution curve. This would happen by absorption of tracer gas into the water from bubbles carrying the pulse,

in which the tracer concentration is high, with subsequent desorption into bubbles low in tracer. Thus the effective residence times of the tracer gas would be longer than the true residence times of the air stream as a whole.

The magnitude of this effect would naturally depend on the solubility of the tracer gas, and therefore some runs were made in which carbon dioxide was used as the tracer gas instead of helium. The relative solubilities of these gases may be seen from their Henry's law coefficients which are 9.5 x 10^7 atm./mole fraction for helium and 1.07 x 10^6 atm./ mole fraction for carbon dioxide, and thus carbon dioxide is about 100 times more soluble than the very insoluble helium.

The comparison was made by doing a set of runs using one gas as tracer, and then without changing any of the experimental conditions, except the sensitivity of the detection equipment, doing a further set of runs using the other gas as tracer. These runs were made with a tank height of 25¼ inches for a range of air flow rates. Each pair of sets of results was then tested by an analysis of variance but in no case could any significant difference be found between results obtained with different tracers.

It was therefore concluded that the absorption and desorption of tracer gas by the liquid had no effect on the measured residence time distribution curve, even with a relatively soluble gas such as carbon dioxide.

III (e) Effects of Using a Non-ideal Pulse

In this section, the possible errors in using a non-

ideal pulse are investigated. The actual pulse used was a burst of tracer bubbles of 0.6 secs. duration. This duration time was kept constant throughout the work for reasons which will become apparent in this section. The volume of tracer gas injected during this time depended on the pressure in the tracer system reservoir, and was in the range of 20 - 50 cc. for normal injection. Smaller pressures and volumes were used when determining the response of the sampling system.

In this analysis the form of the non-ideal pulse is considered to be a square pulse, f(t), such that f(t) = 0 for $t < o$ and $t > T$, and $f(t) = \frac{1}{T}$ for $0 < t < T$. Now instead of considering this non-ideal pulse being fed into the actual system, consider an ideal pulse being fed into the following system which contains a first unit which has a residence time distribution curve in the shape of the non-ideal pulse.

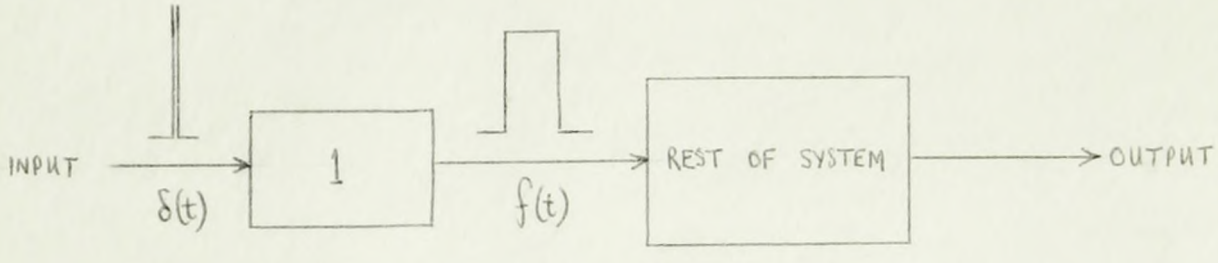

For the overall mean residence time of this system,

$$\tau_t = \tau_1 + (\tau \text{ for the rest of system})$$

Hence the difference in mean residence time of the overall system, and the system after the first unit, is $\tau_1 = \frac{T}{2}$

Therefore, the effect of using a non-ideal pulse of

length T is to increase the mean residence time of the system, calculated assuming an ideal pulse input, by $\frac{T}{2}$. Similarly the effect on the variance is to increase the measured variance by the variance of a square wave of duration T, $= \frac{T^2}{12}$.

It is therefore possible to correct the values of the parameters obtained for these errors, but in this work an explicit correction was not necessary because the correction was inherent in the corrections made for the sampling system.

III (f) Sample Set of Readings, Illustrating Calculating Procedures

Reproduced below is a sample set of experimental readings, with the associated calculations used to obtain results for the mean residence time and the variance of the residence time distribution function, under the conditions stated.

Tank height: nominal 1 ft., air flow rate = 0.045 cu.ft./sec.

Run* No.	Values from analogue computer A'_1	A'_2	A'_3	Mean Residence time (secs.)	$\overline{T^2}$ (sec^2)
1	2.95	1.95	1.0	1.9	4.7
2	4.0	2.5	1.2	1.8	3.75
3	3.2	2.1	1.2	1.9	4.7
4	2.75	1.6	0.85	1.7	3.9
5	2.8	1.8	1.0	1.9	4.5
6	2.8	1.9	1.1	2.0	4.9
7	2.6	1.7	1.0	1.9	4.8
8	2.8	1.7	0.8	1.8	3.6
9	3.0	2.05	1.25	2.0	5.2
10	2.25	2.3	2.3	3.0	12.8
11	3.0	2.9	2.4	2.8	10.0
12	2.25	2.5	2.75	3.2	15.3
13	2.6	2.25	1.7	2.5	8.2
14	3.8	3.6	3.0	2.8	9.9
15	1.8	1.8	1.4	2.9	9.7
16	2.75	2.75	2.3	2.9	10.05
17	4.3	4.0	2.95	2.7	8.6
18	3.3	3.4	3.7	3.0	14.0
19	2.7	3.05	3.3	3.2	15.3

* Runs 1 - 9 were made on the sampling system alone, runs 10 - 19 were made on the overall system.

The mean residence time, and $\overline{T^2}$ are computed from:-

$$MRT = 2.9\ A_2'/A_1'$$

$$\overline{T^2} = 12.1\ A_3'/A_1'$$

For the 9 sampling system runs

$$\Sigma MRT = 16.9$$

$$\Sigma (MRT)^2 = 31.81$$

$$\Sigma \overline{T^2} = 40.1$$

$$\frac{(\Sigma MRT)^2}{9} = 31.77$$

Therefore mean value of MRT $= \frac{16.9}{9} = 1.88$ seconds

Variance of sample values of MRT $= \frac{1}{8}(31.81 - 31.77) = .005\ sec^2$

Mean value of the variance of the residence time distribution $= \frac{1}{9}(\Sigma \overline{T^2} - \frac{(\Sigma MRT)^2}{9})$

$= 0.92\ sec^2$

For the 10 overall runs

$$\Sigma MRT = 29.0$$

$$\Sigma (MRT)^2 = 84.52$$

$$\Sigma \overline{T^2} = 120.9$$

$$\frac{(\Sigma MRT)^2}{10} = 84.10$$

Therefore mean value of MRT $= \frac{29.0}{10} = 2.90$ secs.

Variance of sample values of MRT $= \frac{1}{9}(84.52 - 84.10) = .052 \text{ sec}^2$

Mean value of Variance of residence time distribution $= \frac{1}{10}(120.9 - 84.10) = 3.68 \text{ sec}^2$

Results for the gas phase in the tank

$$\Upsilon = 2.90 - 1.88 = \underline{1.02}$$

(Standard deviation of distribution for $\Upsilon = (0.052 + 0.005)^{\frac{1}{2}}$

$= 0.24$

or since the standard deviation of a mean of a sample of size n, for a distribution having a standard deviation of s, is $s.n^{-\frac{1}{2}}$ The standard deviation of $\Upsilon = 0.08$)

Variance of residence time distribution $= 3.68 - 0.92$

$$\sigma^2 = \underline{2.76 \text{ sec}^2}$$

III (g) Regression Analysis Details

The correlations for Υ and σ, reported in subsection 2.3.5. were obtained by multiple regression analyses on an IBM 7040 computer, as outline below.

The Mean Residence Time

As it was seen that Υ was proportional to both H and $\frac{1}{Q}$, it was thought that a relationship might exist of the form $\Upsilon = (H + \alpha)(\frac{1}{Q} + k)$. Consequently a regression analysis was made of Υ versus H, $\frac{H}{Q}$ and $\frac{1}{Q}$. The fit in this case was

$$\Upsilon = 0.0146H + 0.0020\frac{H}{Q} + 0.0061\frac{1}{Q} + 0.421 \text{ (secs.)}$$

with an estimated standard deviation about the line of 0.092 secs.

However the significant confidence level of the $\frac{1}{Q}$ term was very low (25%), as measured by the t test, and so a second analysis was made without this term. This gave a fit:

$$\Upsilon = 0.0187H + 0.00172\frac{H}{Q} + 0.320 \quad \text{(secs.)}$$

with an estimated standard deviation about the line of 0.089 secs., and both variables significant at the 99% confidence level. This was therefore considered to be the best obtainable correlation.

The standard deviation of the residence time distribution function

A regression analysis was run, initially on the same three independent variables as above, but using a limited number of data points as mentioned in subsection 2.3.5. The result showed that the $\frac{H}{Q}$ term was the least significant (91%) and an analysis was run with this term deleted, but as a check an analysis was also run using the $\frac{H}{Q}$ term alone.

The two fits obtained were:

(i) $\sigma = 0.0307H + 0.0574\frac{1}{Q} - 0.0432$ (secs.)

with a standard deviation about the line of 0.18 secs. and

(ii) $\sigma = 0.00223\frac{H}{Q} + 0.750$ (secs.)

with a standard deviation about the line of 0.20 secs.

In both cases the variables are significant at the 99.9% confidence level. Thus these two correlations fit the data almost equally well, and either or both may be used.

Regression analyses were also made using the variance (σ^2),

and the coefficient of variation ($\frac{\sigma}{\bar{T}}$), as dependent variables but neither gave results as good as those obtained using the standard deviation as the dependent variable.

Appendix IV

IV (a) Derivation of Υ and σ^2 from transfer functions

Let F(s) be the transfer function of a given system and f(t) the corresponding exit residence time distribution function.

Therefore from the definition of Laplace transforms

$$F(s) = \int_0^\infty \exp(-st).f(t).dt$$

therefore $$\frac{dF(s)}{ds} = \int_0^\infty -t.\exp(-st).f(t).dt$$

(Differentiating inside the integral without evaluating the integral is permissable if the function is considered continuous over the range of integration. For a more rigourous treatment see Aris (32))

therefore as $s \to 0$, $\frac{dF(s)}{ds} \longrightarrow \int_0^\infty -t.f(t).dt = -\Upsilon$

since $f(t) = 0$ for $t < 0$.

Similarly $$\frac{d^2F(s)}{ds^2} = \int_0^\infty t^2.\exp(-st).f(t).dt$$

$$\to \overline{T^2} \text{ as } s \to 0$$

IV (b) The Additive Property of Υ and σ^2

Let F(s) be the transfer function for the overall

system and $F_1(s)$ and $F_2(s)$ be those for the two units in series that comprise the overall system, then

$$F(s) = F_1(s).F_2(s)$$

For the overall system, $\gamma = - \lim_{s \to 0} \left(\frac{dF(s)}{ds}\right)$

$$= - \lim_{s \to 0} F'(s)$$

(where $F'(s)$ denotes $\frac{dF(s)}{ds}$)

therefore $\gamma = - \lim_{s \to 0} (F_1(s).F_2'(s) + F_2(s).F_1'(s))$

But $F_1(0) = F_2(0) = 1$

therefore $\gamma = - \lim_{s \to 0} (F_1'(s) + F_2'(s))$

$$= \gamma_1 + \gamma_2$$

Similarly for the overall system, $\sigma^2 = \overline{T^2} - \gamma^2$

therefore $\sigma^2 = \lim_{s \to 0} (F''(s) - (F'(s))^2)$

where $F''(s) = \frac{d^2F(s)}{ds^2}$

$$= F_1(s).F_2''(s) + 2F_1'(s).F_2'(s) + F_1''(s).F_2(s)$$

therefore $\sigma^2 = \lim_{s \to 0} (F_1(s).F_2''(s) + F_1''(s).F_2(s) - F_1'(s)^2 - F_2'(s)^2)$

$$= \sigma_1^2 + \sigma_2^2$$

Appendix V - Absorption of Nitrogen Dioxide

In this section is derived the amount of nitrogen dioxide that dissolves during a given residence time in the tank. The basic assumptions are, as before in subsection 3.3.2;

(a) There is a constant bubble volume (Vb)

(b) On coalescence, the contents of the two bubbles are completely mixed, and then split to give two identical bubbles. This happens instantaneously.

(c) The rate of coalescence per bubble (m) is constant.

Let N be the number of bubbles that contain some nitrogen dioxide at time t, then:

$$\frac{dN}{dt} = m.N \qquad (A5.0)$$

The same arguments that applied to equation 33.1, apply to equation A5.0, but again the implied assumptions are valid while N remains small. Provided that the initial value of N, (Ni), is small, and m is small, this holds true.

Therefore $N = Ni.\exp(mt)$ (A5.1)

If x and y are respectively the number of moles in the system of nitrogen dioxide and nitrogen tetroxide (N_2O_4), and V is the total volume of the bubbles containing these gases, the mean concentration of nitrogen dioxide (C) is given by:

$$C = \frac{x}{V}$$

where $V = N.Vb$

It will be assumed that this mean concentration is uniform for all the bubbles containing nitrogen dioxide.

It has been shown (33) that the equilibrium $2NO_2 \rightleftharpoons N_2O_4$ is rapidly established

therefore $$K = \frac{[N_2O_4]}{[NO_2]^2} = \frac{y.V}{x^2} \qquad (A5.2)$$

therefore $$\frac{dy}{dt} = \frac{K.x}{V} \cdot \left(2\frac{dx}{dt} - \frac{x}{V}\frac{dV}{dt}\right) \qquad (A5.3)$$

The total change in x = number of moles converted from N_2O_4

- (number of moles absorbed by water)

Caudle and Denbigh (14) have shown that the rate of absorption of nitrogen dioxide into water, per unit interfacial area, is directly proportional to the concentration of N_2O_4 in the gas phase.

Therefore $$\frac{dx}{dt} = -Ak''.\frac{y}{V} - 2\frac{dy}{dt}$$

$$= -AkC^2 - 2\frac{dy}{dt} \qquad (A5.4)$$

where $k = K.k''$

and A = total interfacial area available for absorption

$= N.a$

Total change in volume containing NO_2 and N_2O_4 = change due to coalescence + change due to absorption

therefore $$\frac{dV}{dt} = Vb.\frac{dN}{dt} + k'\left(\frac{dx}{dt} + \frac{dy}{dt}\right)$$

$$= Vb.m.N + k'\left(\frac{dx}{dt} + \frac{dy}{dt}\right) \qquad (A5.5)$$

By the elimination of $\frac{dy}{dt}$ from equations A5.3, A5.4, and A5.5, the following equations are obtained:

$$K.C^2 \frac{dV}{dt} = 2K.C \frac{dx}{dt} + \frac{1}{2}A.kC^2 + \frac{1}{2}\frac{dx}{dt} \qquad (A5.6)$$

and
$$\frac{dV}{dt} = Vb.m.N + k'\left(\frac{1}{2}\frac{dx}{dt} - \frac{1}{2}A.k.C\right) \qquad (A5.7)$$

therefore
$$\frac{dx}{dt} = \frac{K.C^2Vb.m.N - \frac{1}{2}A.kC^2 - \frac{1}{2}Ak'.KkC^4}{2KC + \frac{1}{2} - \frac{1}{2}k'KC^2} \qquad (A5.8)$$

Since N is known in terms of t from equation A5.1, equations A5.6 and A5.8 can be solved numerically, simultaneously, using x and V, or C, as the dependent variable, and t as the independent variable. This was done on an IBM 7040 computer using a Runga-Kutta-Gill method, and the following data.

k' = 22,400 ccs/mole - gas molal volume at S.T.P.

K = 1.7×10^5 ccs/mole - reaction equilibrium const. as quoted in (34)

k'' = 2.0 cm/sec. - from Caudle and Denbigh (14),

- the lowest of their range of values.

For the other data, it was assumed that 60 cc. of nitric oxide was injected, which immediately coalesced with twice its volume of air to form 60 bubbles, of volume 3 cc. each, containing a molal concentration of equivalent nitrogen dioxide

of 33%. Thus:

$$\text{initial } (x + 2y) = \frac{Vi}{3.k'}$$

$Ni = 60$, $Vb = 3cc.$, $a = 10\ cm^2$

and the initial value of V, $Vi = Ni.Vb = 180$ cc.

hence the initial value of x can be calculated using equation A5.2.

The effect of these initial assumptions is probably to over-estimate the bubble size and thus underestimate the interfacial absorption area and the amount of nitrogen dioxide absorbed. In this model, the value of Ni did not greatly affect the fraction of nitrogen dioxide absorbed.

Solutions for x and V were obtained for different values of m, at increasing values of t, and from these, the total equivalent nitrogen dioxide dissolving over any period of time could be calculated. This proved to be very insensitive to the value of m, over a range from 0.1 to 1.0, and consequently, the solution with respect to time is the only one that requires consideration.

This solution is shown on figure 22, which is plotted so as to show the percentage of nitrogen dioxide which dissolves, if the gas bubbles spend a total time of 1.5 secs. in the system and all the nitrogen dioxide is formed at a time after injection given by the abscissa. Since, in fact, from the analysis given in subsection 3.3.2, the formation of nitrogen dioxide occurs throughout this period, the actual percentage dissolving will be some weighted average value of the curve.

FIGURE 22 GRAPH SHOWING PERCENTAGE OF NITROGEN DISSOLVING AS A FUNCTION OF THE TIME IT SPENDS IN THE SYSTEM

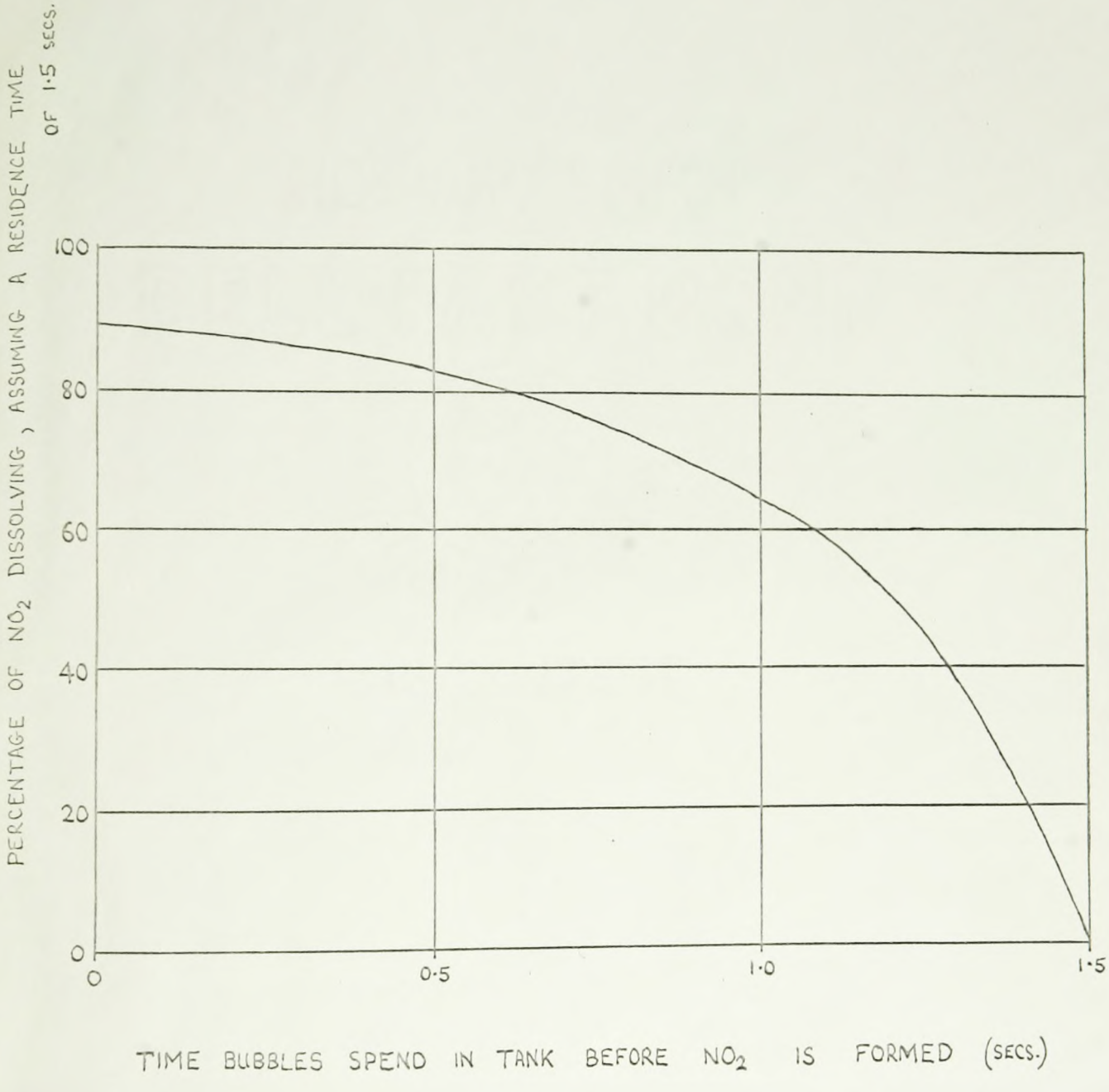

This averaging should be weighted more at the lower end of the time scale, since more nitrogen dioxide is formed initially, according to the model of subsection 3.3.2, and consequently a mean value of 75% is probably a close approximation. A more accurate value could be obtained by actually numerically integrating the curve, using weighting factors supplied by equation 33.3, but in view of the simplicity of the model and the lack of accuracy in the experimental results, this approach is probably not worthwhile.

The mean residence time of 1.5 secs. assumed for this solution corresponds to the air flow rate of 0.063 cu.ft./sec; for the higher flow rate a shorter mean residence time (1.25 sec.) applies, but this would not alter the mean value of the curve very much and the above value was used.

Appendix VI - Practical Application of this Work

In using the results of this study as a basis for design, the method of use would to some extent depend on the application. In addition, other information about the system would be required.

Equipment of this type is commonly used for gas-liquid contacting where mass transfer occurs between the phases. In this case the area of the gas-liquid interface would need to be known, as well as the mass transfer mechanism and rate controlling step. The mixing occurring in the liquid phase is also unknown but probably if the liquid flow rate was not large enough to affect the flow patterns, complete mixing could be assumed.

With this information a first approximation for the design could be to consider the flow of the gas phase to be plug flow with a mean residence time given by equation 35. This would probably be quite accurate enough for a process that was of low order with respect to a constituent in the gas phase, since as the order of a reaction approaches zero, the amount of conversion occurring in the reactor becomes independent of the type of flow within the reactor and depends only on the mean residence time.

For higher order processes, the deviation from plug flow on the gas side should be taken into account, and this is best done by means of the mixed region model proposed in

subsection 2.4.4. Thus the gas flow would be treated as a combination of an ideal plug flow region and an ideal CFSTR, and the mass transfer occurring in each region could be evaluated.

If the mass transfer is accompanied by chemical reaction, information concerning its kinetics would be required, but again the same approximations for the flow patterns, as given above, could be used. The accuracy of design in this case would depend on how accurately known are the flow pattern of the phase in which the reaction occurred and the order of the reaction. The lower the order (or apparent order) of reaction, the better would be the accuracy.

In some cases the plug flow character of the gas phase would be an advantage, as, for example, for reactions of high order with respect to the constituents of the gas phase. CFSTR characteristics would be advantageous where the optimum operating conditions require the composition of the reactor contents to stay within certain limits. Examples of this are when the reaction is autocatalytic and a concentration of product should be maintained, or if complex reactions occur and an optimum ratio of reactants or products is maintained to give the required products. In these cases it would, of course, probably be better to use a system where more complete mixing occurs, such as in a stirred tank.

As a method of liquid-gas contacting alone, this type of reactor is not as efficient as those where other methods

of gas dispersion are employed, such as those using a sparger or a turbine impeller. This is due to the large bubble size and the small mean residence time of the present equipment. This equipment would, however, approximate the conditions existing in a sieve tray column where the liquid hold-up is large and the orifice sizes are comparable to the present case.

In considering the use of these results to predict behaviour in different sized equipment the following points should be borne in mind:

(i) The equations obtained can be made more general by replacing the air flow rate, Q, by its superficial velocity (vs). These are related by: $Q = 0.656.(vs)$ in ft.-sec. units.

(ii) The correlations are probably less accurate if the ratio of tank height to diameter is outside the range (1 - 3) covered in this work.

(iii) "Wall effects" and "end effects" will become more apparent if the dimensions are much reduced though moderate scaling up, by factors up to 5 or so, are less likely to meet the same problems.

References

1. J. Hanhart, H. Kramers, and K. R. Westerterp; Chem. Eng. Sci. 18, 503 (1963)

2. P. V. Danckwerts; Chem. Eng. Sci. 2, 1 (1953)

3. P. H. Calderbank, M. B. Moo-Young, and R. Bibby; Third European Symposium on Chem. Reaction Engineering, Amsterdam, (1964)

4. P. H. Calderbank; Trans. Inst. Chem. Engrs. 34, 79 (1956)

5. L. Davidson and E. H. Amick; A.I.Ch.E. Journ. 2, 337 (1956)

6. I. Leibson, E. G. Holcomb, A. G. Cacoso, J. J. Jacmic; A.I.Ch.E. Journ. 2, 296 (1956)

7. H. Verschoor; Trans. Inst. Chem. Engrs. 28, 52 (1950)

8. O. Levenspiel and K. B. Bischoff; Advances in Chemical Engineering 4, Academic Press (1963)

9. W. L. Haberman and R. K. Morton; U.S. Navy Dept., Taylor Model Basin Report No. 802 (1953)

10. P. V. Danckwerts; Chem. Eng. Sci. 8, 93 (1958)

11. R. V. Churchill; Operational Mathematics, McGraw-Hill (1958)

12. R. E. Pattle; Trans. Inst. Chem. Engrs. 28, 32 (1950)

13. S. Y. Tyree and K. Knox; Textbook of Inorganic Chemistry, p. 223, MacMillan (1961)

14. P. G. Caudle and K. G. Denbigh; Trans. Faraday Soc. 49, 39 (1953)

15. W. B. Hayes, B. W. Hardy, and C. D. Holland; A.I.Ch.E. Journ., 5, 319 (1959)

16. R. L. Datta, D. H. Napier, and D. M. Hewitt; Trans. Inst. Chem. Engrs. 28, 14 (1950)

17. R. R. Hughes, A. E. Handlos, H. D. Evans, and R. L. Maycock; Chem. Eng. Prog. 51, 557 (1955)

18. D. W. Van Krevelen and P. J. Hoftijzer; Chem. Eng. Prog. 46, 29 (1950)

19. A. A. Poutanen and A. I. Johnson; Can. J. Chem. Eng. 38, 93 (1960)

20. W. Siemes; Chem.-Ing.-Tech. 26 614 (1954)

21. W. Siemes and E. Borchers; Chem.-Ing.-Tech. 28 783 (1956)

22. W. Siemes and E. Borchers; Chem. Eng. Sci. 12 77 (1960)

23. P. H. Calderbank and J. Rennie; Trans. Inst. Chem. Engrs. 40, 3 (1962)

24. D. M. Ottmers and H. F. Rase; Ind. and Eng. Chem. Fund. 3 106 (1964)

25. A. Cholette and L. Cloutier ; Can. J. Chem. Eng. 37 105 (1959)

26. J. G. Van de Vusse; Chem. Eng. Sci. 4 178,209, (1955)

27. J. G. Van de Vusse; Chem. Eng. Sci. 17 507 (1962)

28. B. Gal-Or and W. Resnick; Chem. Eng. Sci. 19, 653 (1964)

29. B. Rosenberg; U.S. Navy Dept., Taylor Model Basin Report No. 727 (1950)

30. A. J. Madden and G. L. Damerell; A.I.Ch.E. Journ. 8, 233 (1962)

31. Gow-Mac Instrument Company Bulletin, TCTH-4-61

32. R. Aris; Proc. Roy.Soc. A245 268 (1958)

33. P. D. Brass and R. Tolman; J. Amer. Chem. Soc. 54, 1003 (1932)

34. K. G. Denbigh and A. J. Prince; J. Chem. Soc. 1947, 790

Nomenclature

I(t), E(t)	- Residence time distribution curves	)
F(t), C(t)	- Tracer response curves	) as defined
δ(t)	- Delta function	) in section 2.1
A_1, A_2, A_3	- Zeroth, 1st, and 2nd moments of f(t)	
c, c', ce, co, Ci, Co	- tracer concentrations	
c_s	- velocity of sound in the gas	
D	- diameter of bubble	
d	- diameter of orifice	
f	- frequency of bubbling	
f(t)	- tracer exit concentration curve	
g	- acceleration due to gravity	
H	- tank height (inches)	
N, N', n	- numbers of bubbles containing certain gases as defined in section 3.3	
Nc	- dimensionless group defined in appendix I	
Q	- air flow rate into tank (cu.ft./sec)	
q, qo	- flow rates within models (see figs. 14 and 15)	
R	- derived parameter, $= \frac{\sigma}{t_2}$	
r	- radius of orifice	
Re	- Reynolds Number $\left(= \frac{4.Q.\rho}{\pi.d.\mu} \right)$	
T	- duration of input pulse (appendix III (e))	
T_1, T_2	- residence times in model (figure 15)	
$\overline{T^2}$	- mean square residence time	
t	- time (secs)	

t_1 - rise time of bubbles in tank

t_2 - derived parameter (= Υ - t_1)

$\bar{U}$, u - flow velocities in circular model (figure 14)

V - volume of gas phase (cu.ft.)

V_1, V_2 - volumes in model (figure 15)

Vb - mean bubble volume

Vc - chamber volume

v - ascending bubble velocity in tank

vs - superficial gas velocity in tank

x - distance (figure 14)

Υ - mean residence time of gas phase in tank (secs.)

σ^2 - variance of residence time distribution function of gas phase in tank (sec^2)

σ - standard deviation as above (secs)

(For Υ and σ^2, subscript s denotes the sampling system and subscript t denotes the overall system)

θ - reduced time scale (= $\frac{t}{\Upsilon}$)

γ - surface tension of liquid

ρ - gas density

$\Delta\rho$ - difference gas-liquid densities

(In appendix V the nomenclature is different, in part, to that listed above, and is defined within the appendix)